

Thesis presented to the Instituto Tecnológico de Aeronáutica, in partial fulfillment of the requirements for the degree of Doctor of Science in the Graduate Program of Physics, Field of Nuclear Physics.

**Sílvia Pereira Nunes**

**THE STRUCTURE AND STABILITY OF MASSIVE  
HOT WHITE DWARFS: COMPARISONS WITH  
OBSERVATIONAL DATA AND CHARGE-POLARIZED  
MATTER EFFECTS**

Thesis approved in its final version by signatories below:

*Manuel Malheiro*

Prof. Dr. Manuel M. B. Malheiro de Oliveira

Advisor



Prof. Dr. José Domingo Arbañil Vela

Co-advisor

Prof. Emília Villani

Pro-Rector of Graduate Courses

Campo Montenegro  
São José dos Campos, SP - Brazil  
2021

**Cataloging-in Publication Data**  
**Documentation and Information Division**

Nunes, Sílvia Pereira

The structure and stability of massive hot white dwarfs: comparisons with observational data and charge-polarized matter effects / Sílvia Pereira Nunes.

São José dos Campos, 2021.

94f.

Thesis of Doctor of Science – Course of Physics. Area of Nuclear Physics – Instituto Tecnológico de Aeronáutica, 2021. Advisor: Prof. Dr. Manuel M. B. Malheiro de Oliveira. Co-advisor: Prof. Dr. José Domingo Arbañil Vela.

1. Estrelas anãs. 2. Campos magnéticos. 3. Equações de estado. 4. Densidade de energia. 5. Relatividade. 6. Astrofísica. 7. Física nuclear. I. Instituto Tecnológico de Aeronáutica. II. Title.

**BIBLIOGRAPHIC REFERENCE**

NUNES, Sílvia Pereira. **The structure and stability of massive hot white dwarfs: comparisons with observational data and charge-polarized matter effects.** 2021. 94f. Thesis of Doctor of Science – Instituto Tecnológico de Aeronáutica, São José dos Campos.

**CESSION OF RIGHTS**

AUTHOR'S NAME: Sílvia Pereira Nunes

PUBLICATION TITLE: The structure and stability of massive hot white dwarfs: comparisons with observational data and charge-polarized matter effects.

PUBLICATION KIND/YEAR: Thesis / 2021

It is granted to Instituto Tecnológico de Aeronáutica permission to reproduce copies of this thesis and to only loan or to sell copies for academic and scientific purposes. The author reserves other publication rights and no part of this thesis can be reproduced without the authorization of the author.



Sílvia Pereira Nunes

Praça Marechal Eduardo Gomes, 50  
12.228-900 – São José dos Campos–SP

# THE STRUCTURE AND STABILITY OF MASSIVE HOT WHITE DWARFS: COMPARISONS WITH OBSERVATIONAL DATA AND CHARGE-POLARIZED MATTER EFFECTS

**Sílvia Pereira Nunes**

Thesis Committee Composition:

Prof. Dr. César Henrique Lenzi	Chairman	-	ITA
Prof. Dr. Manuel M. B. Malheiro de Oliveira	Advisor	-	ITA
Prof. Dr. José Domingo Arbañil Vela	Co-advisor	-	UPN/UNMSM
Prof. Dr. Nadja Simão Magalhães	Internal member	-	UNIFESP
Prof. Dr. Rodolfo Valentim da Costa Lima	External member	-	UNIFESP
Prof. Dr. Rodrigo Picanço Negreiros	External member	-	UFF

To my mother Sueli, my sister Lília and  
my brother Luiz Sérgio

# Acknowledgments

I would like to thank the people without whom this work would not have happened beforehand; my advisor Professor Manuel Malheiro and my co-advisor Professor José D. V. Arbañil. I express all my gratitude to my advisor and co-advisor for all the extensive and tireless meetings we have done during this thesis. To Professor Malheiro for providing me with a tiny fraction of his immense knowledge and experience in doing physics. He changed my way of doing and understanding Astrophysics. To Professor José D. V. Arbañil my gratitude for passing on a bit of all your motivation for doing correct and understandable physics. It was four years of a lot of learning with these two scientists for whom I can not express my strong admiration.

I also would like to thank my base during these four years, my family. To my mother, Sueli Pereira Nunes, and my siblings Lília Pereira Nunes and Luiz Sérgio Pereira Nunes. My gratitude for being with me during these four hard years supporting, encouraging, and celebrating every tiny accomplishment. As a base, they were impeccable and I have my deep appreciation not barely for this doctoral period but also for everything that brought me here. I would have no words to declare the depth of my gratitude for being all that they are in my life.

Reflecting on the trajectory, I would also like to thank all the professors and employees who in some way have contributed to my formation and this final thesis. To Professor Joel Medeiros for having encouraged me to this career in Physics, which brought me here. To Professor Marcelo Chiapparini, whom I have great admiration and appreciation for. Due to his invitation to scientific initiation made during my graduation, I learned so much about computing in Nuclear Astrophysics. The program originated under the supervision of Professor Marcelo Chiapparini was the base for all the others produced during this thesis, so my acknowledgments are immeasurable. To professors César Lenzi and Odilon Lourenço for the discussions on the radial oscillations and for providing me their codes. In addition, I would also like to thank professor Edson Otoniel for the discussions in a cooling part that ended up not being placed in the final version of this thesis. I also thank the no less important teachers who in some way contributed to my formation and being such an inspiration: José Roberto Pinheiro Mahon, Maria de Fátima Alves, and Hilário Rodrigues.

To the friends that have accompanied me during these four years or more. My gratitude to the women who were deeply encouraging and inspiring me by being such an example. To Sarah Borges Villanova for all her confidence that I admire and get inspired. Thanks for the discussions you contribute so much to the structure and stability work of hot white dwarfs. Additionally, thanks to my big friend, Flávia Rocha, for all the companionship we had and for being such an immeasurable example of determination and resilience. I also thank Taiana Ferreira for accompanying me at all times, encouraging me, and being the special person she is. To Beatriz Alvarenga and Carolina Mandarino, friends of more than a decade that I have and who have followed all my formation so far. To the no less important Laís Imbelloni and Michael Aleixo who were always with me at all times, supporting and encouraging me. I also thank Leonardo Moreira for the discussions we had on various parts of the work. To all the other friends I did not mention but somehow were present during my doctorate.

*“Vivemos para o estudo  
Soldados da ciência  
O livro é o nosso escudo  
E a arma a inteligência”*

— STUDENTS ANTHEM OF COLÉGIO PEDRO II

# Resumo

Neste trabalho, analisamos a estrutura e a estabilidade de anãs brancas com temperatura, fazendo comparações com dados observacionais e a análise da inserção de uma carga elétrica devido à polarização da matéria em seu envelope. Ao que confere o fluido estelar, nós o definimos como sendo uma composição de elétrons e nucleons em uma célula de Wigner-Seitz, além de fótons livres. Devido à essas anãs brancas serem formadas por um caroço degenerado quente com transporte condutivo, a temperatura é aproximadamente constante nessa região. No envelope não degenerado, porém, há transporte de energia devido a convecção e radiação, o que cria uma distribuição de temperatura. Por considerarmos apenas anãs brancas massivas em todas as análises, a determinação desse envelope não altera a estrutura da estrela (apesar de ser necessário para garantir o equilíbrio hidrostático). Utilizando as equações de Tolman-Oppheimer-Volkoff (TOV), nós obtemos numericamente a estrutura de anãs brancas quentes. Através de algumas estrelas observacionais presentes em catálogos do Sloan Digital Sky Survey e Extreme Ultraviolet Sky Survey, observamos que algumas delas tinham massas e raios compatíveis com nossas curvas de temperaturas centrais bastante elevadas. Então, realizamos um ajuste aos dados observacionais de gravidade superficial e temperatura efetiva para encontrar a massa, raio e temperatura centrais dessas estrelas. Obtemos que devido à relatividade geral, essas estrelas com gravidade superficial muito alta apresentam massas e raios menores do que os reportados anteriormente. A fim de facilitar a obtenção da massa e raio dessas estrelas, criamos uma equação que possibilita obter essas grandezas com a temperatura efetiva e a gravidade superficial. Além disso, analisamos também a estabilidade destas anãs brancas massivas e quentes investigando reações pycnonucleares,  $\beta$ -inverso e oscilações radiais. Obtemos que anãs brancas com temperatura central a partir de  $10^8$ [K] devem ter sua estabilidade analisada segundo oscilações radiais. Adicionalmente, também fazemos um estudo de uma possível matéria com carga polarizada no envelope de anãs brancas quentes. Nós investigamos essa polarização introduzindo condições para a localização da carga, o que garante uma neutralização total da estrela. Por analisarmos casos extremos, consideramos que a temperatura central seria da ordem de  $10^8$ [K], na qual os efeitos de interação de rede podem ser negligenciados. Resolvemos as equações de Maxwell-Einstein e obtemos estrelas maiores e mais massivas (massas de aproximadamente  $2.4M_{\odot}$  para carga

polarizada de  $Q = 5 \times 10^{19}$  [C]). Ao analisarmos a estabilidade dessas estrelas, encontramos que as reações pycnonucleares devem ser usadas para estabelecer um limite para a densidade central da estrela. Considerando efeitos devidos à rotação da estrela encontramos campos magnéticos máximos da ordem de  $10^8$ [G]. Pela primeira vez fornecemos estruturas de anãs brancas com massas além do limite de Chandrasekhar, com campo elétrico nulo no exterior.

# Abstract

In this work, we analyze the structure and stability of white dwarfs at finite temperature, making comparisons with observational data and analyzing the insertion of an electric charge due to a polarization of the matter on their envelopes. Regarding the stellar fluid, we define it as being a composition of electrons and nucleons in a Wigner-Seitz cell, as well as free photons. Because a hot degenerate lump with conductive transport forms these white dwarfs, the temperature is approximately constant in this region. In the non-degenerate envelope, however, there is energy transport due to convection and radiation, which creates a temperature distribution. As we only considered massive white dwarfs in all analyses, the determination of this envelope does not change the structure of the star (although it is necessary to guarantee hydrostatic balance). Using the Tolman-Oppenheimer-Volkoff (TOV) equations, we numerically obtain the structure of hot white dwarfs. Through some observational stars present in the Sloan Digital Sky Survey and Extreme Ultraviolet Sky Survey catalogs, we observed that some of them had masses and radii compatible with very high core temperature curves. We then fit the observational surface gravity and effective temperature data to find the core mass, radius and temperature of these stars. We find that due to general relativity, these stars with very high surface gravity have smaller masses and radii than those previously reported. In order to improve the next estimates of the mass and radius of these stars, we obtain an equation for these quantities as a function of the effective temperature and surface gravity. We also analyzed the stability of very massive hot white dwarfs by pycnonuclear reactions,  $\beta$ -inverse and radial oscillations. We obtain that white dwarfs with core temperature from  $10^8$ [K] have their stability analyzed according to radial oscillations. Additionally, we also study a possible electric charge due to a polarized matter in the envelope of hot white dwarfs. We investigate this polarization by introducing conditions to the charge location, which ensures a global charge neutralization. By analyzing extreme cases, we consider that the core temperature would be in the order of  $10^8$ [K], in which lattice interaction effects can be neglected. We solve the Maxwell-Einstein equations obtaining bigger and more massive stars (masses of approximately  $2.4M_{\odot}$  for polarized charge of  $Q = 1.5 \times 10^{19}$  [C]). When analyzing these stars stability, we found that pycnonuclear reactions may be used to settle a limit for the star central density. Considering effects due

to the star rotation we found maximum magnetic fields of the order of  $10^8$ [G]. For the first time we provide white dwarf structures with masses beyond the Chandrasekhar limit, with zero external electric field.

# List of Figures

FIGURE 2.1 – The tridimensional models for the internal structure of DA, DO and DB white dwarfs. . . . .	25
FIGURE 2.2 – Hystogram from the SDSS and EUVE surveys reported in (TREMBLAY <i>et al.</i> , 2011; NALÉŻYTY; MADEJ, 2004; MADEJ <i>et al.</i> , 2004; VENNES <i>et al.</i> , 1997; KOESTER; KEPLER, 2019) . . . . .	27
FIGURE 4.1 – Uni-dimensional spherical star. . . . .	37
FIGURE 4.2 – Pycnonuclear reaction C+C fusion time as against the mass density for $T = 0$ [K] and $T_c = 10^8$ [K]. . . . .	47
FIGURE 4.3 – An illustration for mass-central density curve . . . . .	47
FIGURE 5.1 – Fluid pressure compared against the energy density for some different central temperatures. . . . .	61
FIGURE 5.2 – Mass, normalized in solar masses $M_\odot$ , as a function of the radial coordinate for five central temperature values and a total mass $M = 1.37M_\odot$ . . . . .	62
FIGURE 5.3 – Mass of the star, normalized to the Sun mass $M_\odot$ , as a function of central energy density for four different central temperature values. The filled triangles over the curves represent the maximum–mass points. The box within the figure shows the region where the maximum mass values are found. . . . .	63
FIGURE 5.4 – Mass–radius curves for different central temperatures. The filled triangles represent maximum–mass points. Observational data extracted from the catalogs (TREMBLAY <i>et al.</i> , 2011), (NALÉŻYTY; MADEJ, 2004), (KOESTER; KEPLER, 2019), (VENNES <i>et al.</i> , 1997) and (MADEJ <i>et al.</i> , 2004) are, respectively marked with gray triangles, purple circles, green diamonds, orange squares, and blue hexagons. . . . .	64

- FIGURE 5.5 – The surface gravity of the white dwarf against its total gravitational mass, for some central temperatures. The filled triangles over the curves mark the maximum–mass points. Observational results obtained from the catalogs in (TREMBLAY *et al.*, 2011), (NALEŻYTY; MADEJ, 2004), (KOESTER; KEPLER, 2019), (VENNES *et al.*, 1997) and (MADEJ *et al.*, 2004) are, respectively indicated by gray triangles, purple circles, green diamonds, orange squares, and blue hexagons. . . . . 65
- FIGURE 5.6 – The mass against the total radius for some temperatures according to general relativity (solid lines) and Newtonian formulations (full lines). The green points represent WD 1659 + 440 with a helium envelope and the pink ones represent WD 0346 – 011 with a helium and hydrogen envelope. The unfilled points are obtained according to (VENNES *et al.*, 1997) and the filled ones are obtained with our fitting. . . . . 70
- FIGURE 5.7 – Square of eigenfrequency  $\omega^2$  as a function of the central energy  $\varepsilon_c$  and of the total mass are shown on the panels on top and bottom, respectively, for some central temperatures. . . . . 71
- FIGURE 5.8 – Total mass against the central energy density for some central temperatures. The gray shaded regions indicate the places where the instabilities against pycnonuclear reactions and inverse  $\beta$ -decay take place, and the filled triangles in pink mark the onset of the radial instability. . . . . 73
- FIGURE 6.1 – A charge-polarized matter in a white dwarf star. . . . . 78
- FIGURE 6.2 – The electric field as a function of radial coordinate for stars with  $\varepsilon_c = 5 \times 10^9$  [g/cm<sup>3</sup>] and several charges. The gray region represents the space between the two charges  $R^+$  and  $R^-$ . . . . . 79
- FIGURE 6.3 – The pressure as a function of radial coordinate for stars with  $\varepsilon_c = 5 \times 10^9$  [g/cm<sup>3</sup>] and several charges. . . . . 80
- FIGURE 6.4 – Mass as a function of central energy density for several charges. The pink triangles represents the maximum mass. . . . . 81
- FIGURE 6.5 – Mass as a function of radius for several charges. The pink triangles represents the maximum mass. . . . . 81
- FIGURE 6.6 – Magnetic field as a function of mass for  $T_c = 10^8$ [K] and several charge-polarized matter. The red curves represents instabilities due to pycnonuclear reactions. . . . . 83

# List of Tables

TABLE 2.1 – Spectral classification of white dwarfs. Source: (SION, 2011) . . . . .	25
TABLE 3.1 – Melting limits according to (TREMBLAY, 2019; GARCÍA-BERRO; OSWALT, 2016; MONTGOMERY <i>et al.</i> , 1999; MESTEL; RUDERMAN, 1967) . . . . .	33
TABLE 4.1 – Dimensionless parameter values for the static approximations. . . . .	45
TABLE 5.1 – The central temperature employed with the maximum masses with their respective total radii and central energy density . . . . .	66
TABLE 5.2 – Comparison between the data reported by (VENNES <i>et al.</i> , 1997) and the results derived in this work for a helium surface. . . . .	68
TABLE 5.3 – Comparison between the data reported by (VENNES <i>et al.</i> , 1997) and the results derived in this work for a helium surface. . . . .	68
TABLE 5.4 – Central temperatures and the parameter values appearing in Eq. (5.23). . . . .	70
TABLE 5.5 – Threshold energy density values for instability against pycnonuclear reactions, inverse $\beta$ -decay, and radial oscillations for some central temperature values. . . . .	72
TABLE 6.1 – The values of the maximum mass $M^{\max}$ for radius and energy density for different values of a charge-polarized matter $Q$ . . . . .	82

# List of Symbols

$a$	Radiative constant
$A$	Mass weight
$B$	Magnetic field
$c$	Speed of light
$e$	Electrons index
$\varepsilon$	Energy density
$\varepsilon_c$	Central energy density
$E$	Energy
$\Gamma$	Coulomb coupling parameter
$\gamma$	Photons index
$n$	number density
$N$	Nucleons index
$k_B$	Boltzmann constant
$L$	Lattice index
$t$	Time coordinate
$T$	Temperature
$T_m$	Melting temperature
$T_c$	Central temperature
$m(r)$	mass within Schwarzschild radial coordinate $r$
$\rho_{ch}$	charge density
$M_\odot$	Solar mass
$L_\odot$	Solar luminosity
$g_\odot$	Solar surface gravity
$G$	Gravitational constant
$P$	pressure
$P_c$	central pressure
$\omega$	oscillation frequency
	rotation frequency
$r$	Radial coordinate
$\rho$	barionic density

---

$\rho_c$	central mass-energy density
$s$	Line element
$S$	Entropy
	Surface
$Z$	atomic weight

# Contents

1	INTRODUCTION . . . . .	20
2	WHITE DWARF PROPERTIES . . . . .	23
2.1	<b>Evolution</b> . . . . .	23
2.2	<b>Classification</b> . . . . .	24
2.3	<b>History and observation</b> . . . . .	25
3	THE EQUATION OF STATE . . . . .	28
3.1	<b>The electron pressure and energy density</b> . . . . .	29
3.2	<b>The nucleons pressure and energy density</b> . . . . .	31
3.3	<b>The radiation pressure and energy density</b> . . . . .	32
3.3.1	The crystallization . . . . .	32
3.3.2	Wigner-Seitz cell . . . . .	33
3.3.3	The threshold of degeneracy and temperature distribution . . . . .	34
4	EQUILIBRIUM CONFIGURATIONS AND STABILITY . . . . .	36
4.1	<b>Hydrostatic Equilibrium – Uncharged star</b> . . . . .	37
4.2	<b>Newton’s framework</b> . . . . .	37
4.2.1	The Schwarzschild solution . . . . .	38
4.2.2	The Tolman-Oppheimer-Volkoff equation . . . . .	40
4.2.3	Reissner-Nordstrom solution . . . . .	42
4.2.4	Bekenstein equations: charged Tolman-Oppheimer-Volkoff equations . . . . .	43
4.3	<b>The Instabilities</b> . . . . .	44
4.3.1	Pycnonuclear reactions . . . . .	44

---

4.3.2	Inverse $\beta$ -decay . . . . .	46
4.3.3	The turning-point . . . . .	47
4.3.4	The radial oscillations . . . . .	48
5	<b>THE STRUCTURE AND STABILITY OF HOT WHITE DWARFS . . . . .</b>	51
5.1	<b>Introduction . . . . .</b>	51
5.1.1	Equilibrium configuration of white dwarfs . . . . .	51
5.1.2	On the stability of white dwarfs . . . . .	52
5.1.3	Our aim . . . . .	54
5.2	<b>The EOS . . . . .</b>	55
5.3	<b>Stellar equilibrium equations and radial perturbation equations . . . . .</b>	56
5.3.1	The energy momentum tensor and the background line element . . . . .	56
5.3.2	Stellar equilibrium equations . . . . .	57
5.3.3	Radial perturbation equations . . . . .	58
5.4	<b>Pycnonuclear reactions and inverse <math>\beta</math>-decay . . . . .</b>	59
5.4.1	Pycnonuclear reactions . . . . .	59
5.4.2	Inverse $\beta$ -decay . . . . .	59
5.5	<b>Equilibrium and stability of hot white dwarfs . . . . .</b>	60
5.5.1	Numerical method . . . . .	60
5.5.2	Influence of temperature on the fluid pressure, energy density, and mass of the star . . . . .	60
5.5.3	Equilibrium configurations of hot white dwarfs . . . . .	62
5.5.4	Stability of hot white dwarfs . . . . .	70
6	<b>CHARGE-POLARIZED MATTER IN HOT DQ WHITE DWARFS AS A POSSIBLE SOURCE OF TYPE IA SUPERNOVAE . . . . .</b>	74
6.1	<b>The equation of state . . . . .</b>	76
6.2	<b>Equilibrium Configuration . . . . .</b>	77
6.2.1	The electric charge density . . . . .	77
6.3	<b>Equilibrium of charge-polarized matter in hot white dwarfs . . . . .</b>	78
6.3.1	Numerical method . . . . .	78

CONTENTS	19
<b>6.4 Results</b> . . . . .	79
6.4.1 The magnetic field . . . . .	82
<b>7 CONCLUSION</b> . . . . .	84
<b>BIBLIOGRAPHY</b> . . . . .	87

# 1 Introduction

We initiate this thesis with a short introduction since at the beginning of each chapter we will present a more detailed explanation of the topics covered in each of them.

White dwarfs are the last evolutionary stage of around 98% stars in the Universe (SION, 2011). When a Red Giant (RG) star nuclear fuel exhausts and collapses, it forms a white dwarf. Indeed, when the RG fuel is completely consumed, it radiates the external layer and the remaining core transforms itself into a white dwarf (CAMENZIND, 2007). Due to the radius decrease, white dwarfs have (as a heritage) a high central temperature inside, which makes that some of them are the hottest objects in the Hertzsprung-Russell diagram (ROSE, 1998). In this work, we study the structure and stability of white dwarfs considering temperature effects. Besides, we are going to make a comparison with observational data, and also consider electric charge effects due to polarized matter in the star envelope.

To determine both the structure and stability of white dwarfs, we primarily need to set up the equation of state. The equation of state determines the relation between density and pressure. For cold white dwarfs, this equation of state is well-known in the literature (SHAPIRO; TEUKOLSKY, 2004); the low temperature makes pressure be due only to electrons, and energy density due to nucleons. Additionally, interactions between electrons or nucleons-electrons also can contribute to the EoS (OTONIEL *et al.*, 2019). However, since the white dwarf temperatures in the core can be three times their surface temperatures, more detailed comparisons with observational data need an equation of state including the temperature effects.

Regarding the equation of state for white dwarfs with temperature, the complete degeneracy state is not valid. The Fermi-Dirac integrals need to be considered in the electrons' terms of the energy density and pressure. Timmes and collaborators (TIMMES; ARNETT, 1999) discussed the equation of state for the stellar matter with temperature. In their work, they explicit each contribution from electrons, nucleons, and photons, disregarding interactions. The lattice interaction has to be considered when we have temperature, as mentioned recently by de Carvalho and collaborators' work (CARVALHO *et al.*, 2014). A reasonable approach to regard these interactions is with the Wigner-Seitz

cell (SALPETER, 1961). Once the equation of state is well-established, the temperature distribution in the stellar interior has to be analyzed.

Conduction, radiation, and convection are the processes that produce a white dwarf's temperature distribution. Conduction is a process particularly present in solid materials, while convection is in fluids. The radiation (opposite these last two), does not have these restrictions. In fact, due to the high core degeneracy, radiation is present only in the envelope. Due to the white dwarf structure being a solid core with a fluid envelope, the conduction is mainly in the center and the convection in the envelope. Besides, the radiation in the center is very small and neglected. Thus, in the stellar core, the transport is mainly due to conduction and generates an isothermal environment. In the stellar envelope, the energy settles due to radiation and convection (HORN, 1970; FONTAINE; HORN, 1976; KRITCHER, 2020). This transport creates a temperature distribution that assists stellar cooling, and it is crucial to define with precision the stellar structure.

To study the hydrostatic equilibrium of carbon white dwarfs with masses  $M < 1.37M_{\odot}$ , it is enough to consider Newtonian physics (NUNES *et al.*, 2021). For masses above this limit, the general relativity effects are present. In a static and spherical symmetric configuration the hydrostatic equilibrium is obtained in general relativity (GR) by solving the Tolman-Oppenheimer-Volkoff equations (TOLMAN, 1939; OPPENHEIMER; VOLKOFF, 1939). The pressure and matter-energy density in GR contribute to gravity, which is not the case in the Newtonian formalism, and as a consequence, we obtain a very small change of star mass comparing to classical physics but the star radius becomes smaller. Since the energy momentum tensor curves the space-time in Einstein gravity theory the electromagnetic energy will also play a role in GR. For the case of static, spherical and electric charged configurations the hydrostatic equilibrium equations are different since we need to solve Einstein-Maxwell equations of general relativity (BEKENSTEIN, 1971).

The hydrostatic equilibrium is not enough to obtain a stable star configuration. A study of radial oscillations to analyze the dynamical instability is also necessary (CHANDRASEKHAR, 1964a; CHANDRASEKHAR, 1964b). Furthermore, due to high density at the star core, nuclear fusion processes can play an important role destabilizing the star. In white dwarfs, these nuclear processes are pycnonuclear reactions and inverse  $\beta$ -decay (CARVALHO *et al.*, 2014; OTONIEL *et al.*, 2019). These conditions are sufficient to ensure carbon white dwarfs stability studied in this thesis with temperature.

If a white dwarf has a mass above Chandrasekhar's limit, it can produce a type Ia Supernovae. The associated mechanisms to provide the increase in mass for isolated white dwarfs are rotation, magnetic, and electric fields. Electric fields effects in white dwarfs have already been investigated as an isolate (LIU *et al.*, 2014) or conductor (CARVALHO *et al.*, 2018b). These previous works imply a very strong and positive electric field outside the white dwarf capable of attracting negative particles and discharging the star. The electric

charge due to a strange matter polarization inside quark stars has been considered in (NEGREIROS *et al.*, 2010). There, the authors avoid the existence of a strong external field and allow stable charged quark stars configurations.

In this thesis, we analyze the structure and stability of white dwarfs with a finite temperature. We compare our results with observational data to analyze the central temperature and stability of these stars. Besides, to associate with Type Ia Supernovae events, we investigate electric charge effects due to polarized matter in the white dwarf envelop to obtain super-Chandrasekhar configurations. This thesis is divide as follows: in Chapter 2 we revisit a common white dwarf evolution, classification, history, and observation in order to establish the study field. In Chapter 3 we detail each term of the equation of state we consider. In Chapter 4 we deduce Newtonian scenario, the Tolman-Oppenheimer-Volkoff (TOLMAN, 1939; OPPENHEIMER; VOLKOFF, 1939) equations, and obtain solutions for Einstein-Maxwell equations (BEKENSTEIN, 1971) in the case of charged configurations. Besides, in this Chapter we also detail the instabilities we obtain due to pycnonuclear reactions, inverse  $\beta$ -decay, GR turning-point, and radial oscillations. In Chapter 5, we discussed previous works on white dwarfs with finite temperature. Additionally, we make a study of the structure and stability of massive hot white dwarfs, which is is a copy of the published article in the Astrophysical Journal. In Chapter 6, we revisit the charge compact stars theory and make, the first time, an investigation of charge effects due to the electrically polarized matter in the white dwarfs' surface, maintaining the global charge neutrality outside the star. Finally, we present our conclusions.

We highlight that the first four chapters of the thesis are for a reader that is not familiar with the physics of white dwarfs. In order to present more details to the essence of this thesis, in the next two chapters are two articles, one already published. Thus, some parts may seem repetitive due to our choice to include these previous chapters with a didactic perspective, and not only the two chapters with the thesis articles, and the conclusions.

## 2 White dwarf properties

In what concerns the stellar evolution, stars have a life as any else. They are born, leave the life evolving and end up dying. Indeed, there is three possible faith of stars: white dwarfs, neutron stars, and black holes. In this order, these objects are from the less to the most compact objects. In this thesis, we are going to investigate the white dwarfs in the beginning of their lives, when they have high central temperatures.

White dwarfs are what the vast majority of stars (around 98%) will become (SION, 2011), including our Sun. Even though white dwarfs can have a mass similar to neutron stars, their greater radius (around  $10^3$  to  $10^5$  [km]) implies smaller central densities (around  $10^9$  to  $10^5$  [g/cm<sup>3</sup>]). In this chapter, we analyze the evolutionary track of a star to become a white dwarf. Besides, we discuss the history and discovery of such stars. Finally, we discuss some observational data used for the following chapters.

### 2.1 Evolution

In the Universe, white dwarfs are the final evolutionary stage of stars whose mass is not high enough to become a neutron star or black hole. The evolution of any star begins with a cloud of dust with hydrogen predominance. Due to Jeans' instability, this cloud begins a contraction originating an object called protostar (HORVATH, 2011). This contraction continues until the protostar has enough self-gravitational pressure to counterbalance the inward pressure. At this time, the protostar heats up and becomes a star.

Once there is the formation of a star, its mass determines the evolutionary track. The stars with masses above  $0.08M_{\odot}$  carry enough energy to begin the hydrogen-burning phase, which affords the entrance in the main sequence of the Hertzsprung-Russel (HR) diagram (HOYNG, 2006). Specifically, hydrogen-burning is the process that two molecules of hydrogen fuse to produce a helium one. This process, in brief, begins the formation of a shell structure in the star, providing the heavier atoms to be closer to the stellar core.

During the stellar hydrogen-burning phase, the star supports itself against self-grav-

itation collapse with nuclear processes. As a consequence, the hydrostatic equilibrium could be in distress due to a central pressure possible decrease (due to the increase of the stellar mean molecular weight). Thus, for the hydrostatic equilibrium to be supported, the star heats and contracts creating degenerate electrons. These degenerate electrons are the most responsible for the star hydrostatic equilibrium hereafter. Besides, in contrast to what occurs in the core, the outer layers expand and increases the stellar radius creating a Red Giant (HOYNG, 2006).

After the helium-burning phase, the transition from the giant branch to a white dwarf sets in. The low-mass stars convert the helium into heavy elements such as carbon and oxygen. The creation of an additional shell in the stellar structure due to heavier elements is settling. For effective temperature of around  $3 \times 10^4$  [K] in the star (MACDONALD, 2015), the circumstellar material (produced by mass loss) is excited by the photons' ultra-violet flux (that can be seen as a planetary nebula). Finally, the remainder core of this process is what becomes a white dwarf.

## 2.2 Classification

As already mentioned, the white dwarf presents a shell model. Due to the shell structure of white dwarfs, Schatzman (SCHATZMAN, 1950) concluded that these stars have very pure surfaces that can include even hydrogen or helium. It was discovered that the purity of these zones is not complete afterward, and there can be metallic elements including calcium, magnesium, and iron (KAWALER *et al.*, 1996). The white dwarfs are classified according to their shell structures.

In table 2.1, the spectral type and characteristics are showed. The DA star has spectra with Balmer lines dominancy, while the DB and DO present lines of helium. Besides, DC has a continuous spectrum, DZ has only metals, and DQ has carbon features. The discovery of carbon atmosphere white dwarfs with a little or no trace of hydrogen or helium was recently done by Dufour and collaborators (DUFOUR *et al.*, 2007; DUFOUR *et al.*, 2008).

In Fig. 2.1, we present tridimensional models for the shell structures of DA, DO, and DB white dwarfs. We can note that the heaviest elements are orderly from core to surface. We have to highlight some aspects of this surface. Since the surface corresponds to a substantial region in low-mass white dwarfs, envelope determination which uninfluenced the total mass affects the stellar radius. For near-Chandrasekhar's limit stars, the mass and the radius are unaffected by the surface.

Spectral type	Characteristics
DA	Only Balmer lines with no He I nor metals present
DB	He I lines; no H nor metals present
DC	Continuous spectrum, no lines deeper than 5% in any part of the electromagnetic spectrum
DO	He II strong, He I or H present
DZ	Metal lines only, no H nor He lines
DQ	Carbon features, either atomic or molecular in any part of the electromagnetic spectrum

TABLE 2.1 – Spectral classification of white dwarfs. Source: (SION, 2011)

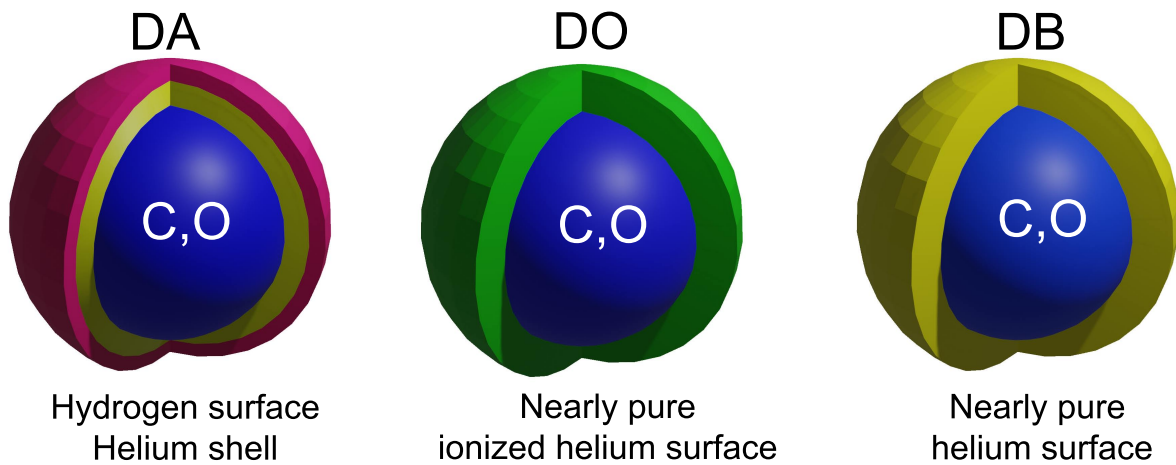


FIGURE 2.1 – The tridimensional models for the internal structure of DA, DO and DB white dwarfs.

### 2.3 History and observation

The history of white dwarfs begins with Friedrich Bessel's first observation in 1844. At the time, he noticed an irregular back and forth movement of Sirius, indicating a gravitational attraction of a nearby unseen companion (CAMENZIND, 2007). After years, in 1862, Alvan Clark finally solved this mystery. This American astronomer and telescope maker detected the companion, a white dwarf named Sirius B. Indeed, after Sirius B was discovered, Sirius was named as Sirius A.

After some more years, in 1915, Walter S. Adams performed another discovery regarding white dwarf, the 40 Eridani B. The movement of Eridani, in contrast to Sirius, was not responsible for its detection. The detection became possible by its luminosity, albeit it is a member of the triple star system 40 Eridani. According to the spectral type, Adams assigned a disk temperature of around  $1 \times 10^4$  [K] (LANG, 2013). Besides, the flux of white dwarf is a necessary parameter for detection even in more recent works (VENNES *et al.*, 1997).

Recently, it has been reported observations from different sky surveys. For instance, there is the Sloan Digital Sky Survey (SDSS) and the Extreme Ultraviolet Explorer (EUVE). These surveys provide a flux analysis to determine parameters as effective temperature and surface gravity. Equally important, the comparison of flux patterns enables the findings of elements in the stars (VENNES *et al.*, 1997). With the observational surface gravity and effective temperature, works associate mass and radius according to some models. The models used were the Hamada-Salpeter (HAMADA; SALPETER, 1961), or an evolutionary grid as (ALTHAUS *et al.*, 2005).

In Fig. 2.2 we illustrate in histograms the white dwarfs found in some catalogs. The first left and right histogram report the data from Vennes and collaborators (VENNES *et al.*, 1997). These authors analyzed a sample of hot DA white dwarfs from the EUVE all-sky survey. Additionally, they used a mass relation of white dwarfs following Wood (WOOD, 1995) for a carbon interior and  $10^{-4}M_{\star}$  helium envelope and  $10^{-2}M_{\star}$  helium and  $10^{-4}M_{\star}$  hydrogen envelope. Besides, Madej and collaborators (MADEJ *et al.*, 2004) analyzed the first data release of SDSS and used Bergeron (BERGERON *et al.*, 1992) method to obtain mass-radius values for DAs. Nalezyty and Madej (NALEŻYTY; MADEJ, 2004) reported several massive white dwarfs, including (VENNES *et al.*, 1997) findings. Tremblay, Bergeron, and Gianninas (TREMBLAY *et al.*, 2011), using the SDSS data release 4 (DR4), improved spectroscopy and photometric analysis of the hydrogen-line DA white dwarfs. Their gravity values were converted to stellar masses using Wood (WOOD, 1995) models. Koester and Kepler (KOESTER; KEPLER, 2019) recently analyzed DQ white dwarfs from the Sloan Digital Sky survey. They used for gravity values  $g \geq 10^9 [\text{cm s}^{-2}]$  Hamada and Salpeter model (HAMADA; SALPETER, 1961), and for low gravity values a Montreal mass-radius relation. From Fig. 2.2 we can see that the catalogs differ in mass and radius data, according to their atmosphere consideration and method used to determine mass. Besides, it is important to note that only the data in (VENNES *et al.*, 1997) and (NALEŻYTY; MADEJ, 2004) report very massive white dwarfs, with masses above  $1.3M_{\odot}$ . These stars, due to be in the near Chandrasekhar mass limit, will be investigated using general relativity corrections in section 5. These corrections are important in order to provide exact values for the radii of these very massive stars.

In Fig. 2.2 we can note that most of white dwarfs are located in the range of mass  $0.3 \leq M/M_{\odot} \leq 1.2$  and radius of  $5 \times 10^3 < R \leq 14 \times 10^3$  [km]. Thus, the vast majority of white dwarfs in this range are not affected by general relativity effects.

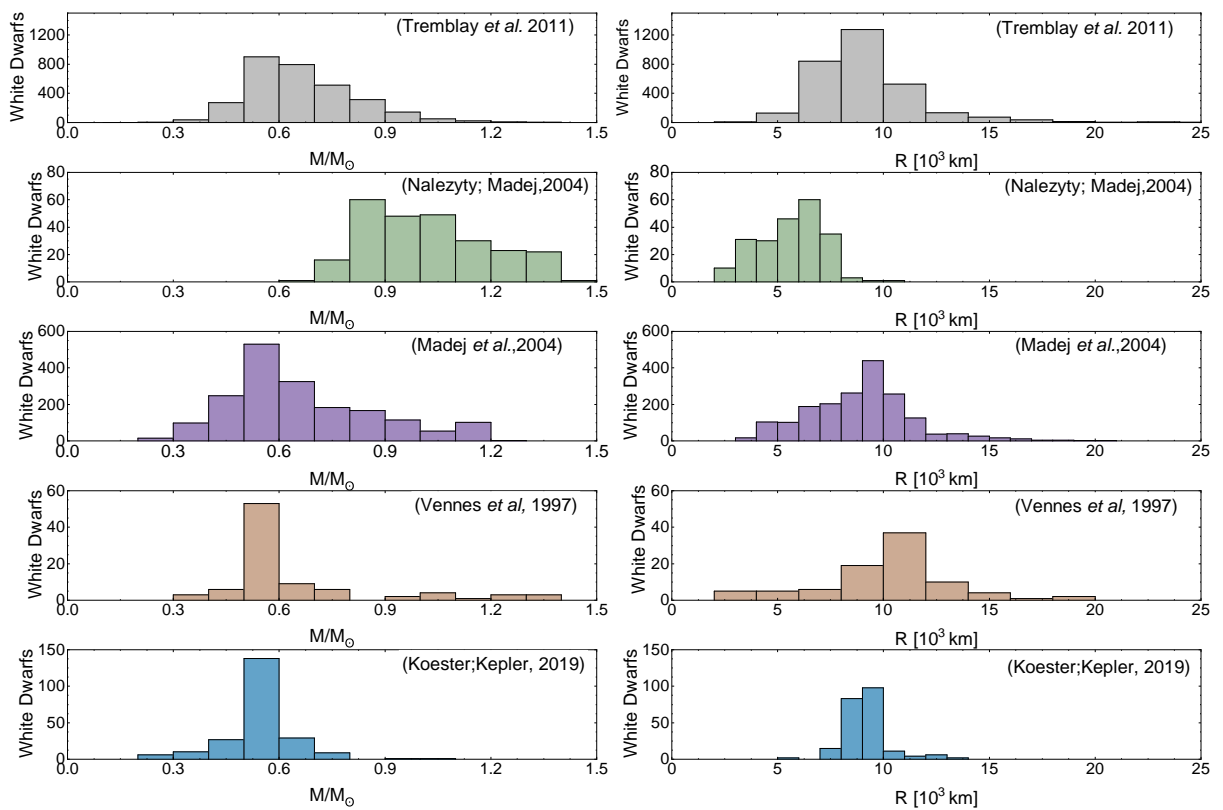


FIGURE 2.2 – Histogram from the SDSS and EUVE surveys reported in (TREMBLAY *et al.*, 2011; NALEŻYTY; MADEJ, 2004; MADEJ *et al.*, 2004; VENNES *et al.*, 1997; KOESTER; KEPLER, 2019)

### 3 The Equation of State

To define the structure of white dwarfs, first, we have to define the stellar matter composition. In these stars, the main responsible force to support the self-gravitational collapse comes from the degenerate electrons (SHAPIRO; TEUKOLSKY, 2004; CAMENZIND, 2007). This degeneracy has its origin in the Pauli exclusion principle that demands each fermion to occupy a single quantum level below the Fermi energy.

Complete degeneracy is a condition reached when the environment has zero temperature or the chemical fermion potential is much larger than its temperature. The observable white dwarfs have temperatures in their core, proven by their effective temperature, that can be near or even at the order of the chemical electron potential. Consequently, models that want to be accurate when compare theory with observations have to consider the temperature influence. The effective temperature is related to the black-body emission. Thus, the stellar opacity influences its measurement. This effective temperature is usually much smaller than central ones, which implies the use of an equation of state (EOS) with temperature to study with high accuracy the white dwarf structure.

In order to obtain the real equations that describe the white dwarf interior, we will deduce some contributions considering the temperature dependence. The stellar matter is neutral and composed of ions with their nuclei formed by nucleons imbedded in a gas of electrons. The electrons contribution are deduced in the section 3.1, using Dirac (DIRAC, 1926) and Fermi (FERMI, 1926) calculations. Besides, due to nucleons' low velocity, they are related to an ideal classical gas. A complete equation of state, needs to consider the radiation pressure due to the thermal photons, that can contribute to the star for high temperatures. Another contribution we are going to consider is the lattice in the star interior. The stellar crystallization (with interactions) depends on the temperature considered and melting limit. Thus, we calculate lattice interactions by approximating them as a Wigner-Seitz cell.

With all the assumptions described, the fluid inside our white dwarf has contributions from nucleons, electrons, photons, and considering the lattice interactions, the energy

density inside these stars can be written as

$$\varepsilon = \varepsilon_e + \varepsilon_N + \varepsilon_\gamma + \varepsilon_L, \quad (3.1)$$

and the pressure

$$P = P_e + P_N + P_\gamma + P_L, \quad (3.2)$$

being the index  $e$ ,  $N$ ,  $R$ ,  $L$  relative to electrons, nucleons (ions contribution), radiation and lattice respectively. These terms are going to be analyzed in the next sections.

### 3.1 The electron pressure and energy density

The following deduction of the equation of state contributions from a electron gas will follow Dirac (DIRAC, 1926) and Fermi (FERMI, 1926) calculations. Considering a system of  $N$  non-interacting and indistinguishable particles. The  $N_1, N_2, \dots, N_s$  particles are distributed in  $E_1, E_2, \dots, E_s$  energy levels with  $A_1, A_2, \dots, A_s$  the respective number of quantum states. The total number of possibilities the particles can be distributed is

$$W = \prod_s \frac{A_s!}{N_s!(A_s - N_s)!}. \quad (3.3)$$

The entropy associated with this system is related to the number of accessible states (equation (3.3)) as

$$S = k_B \log W \quad (3.4)$$

$$= k_B \sum_s \{A_s (\log A_s - 1) - N_s (\log N_s - 1) - (A_s - N_s) [\log(A_s - N_s) - 1]\}, \quad (3.5)$$

being  $k_B$  the Boltzmann constant. Considering an equilibrium system and an unchanged entropy, i.e.,  $\delta S = 0$ , from Eq. 3.5 we have

$$\delta S = k_B \sum_s \{-\log N_s + \log(A_s - N_s)\} \delta N_s. \quad (3.6)$$

$$= k_B \sum_s \log \left( \frac{A_s}{N_s} - 1 \right) \delta N_s = 0, \quad (3.7)$$

which is valid for any particles fluctuation  $dN_s$ . In addition, the conservation of the total

number of particles and energy can be written as

$$\sum_s dN_s = 0, \quad (3.8)$$

$$\sum_s E_s dN_s = 0. \quad (3.9)$$

With the aim to obtain an equation for the number of the particles, the Eqs. (3.8) and (3.9) are going to be multiplied by an  $\alpha$  and  $\beta$  respectively. Adding these two in Eq. (3.7)

$$\sum_s \left( \log \left( \frac{A_s}{N_s} - 1 \right) + \alpha + \beta E_s \right) \delta N_s = 0, \quad (3.10)$$

which allows us to find the number of particles in a  $s$  state

$$N_s = \frac{A_s}{e^{(\alpha + \beta E_s)} + 1}. \quad (3.11)$$

Now, with the assumption that the  $s$ th state has energy that lies between  $E_s$  and  $E_s + dE_s$ , the number of quantum states  $A_s$  is

$$A_s dE = \frac{8\pi}{(2\pi)^3 \hbar^3} \sqrt{E^2 - m^2} E dE, \quad (3.12)$$

$$= \frac{8\pi}{(2\pi)^3 \hbar^3} p^2 dp, \quad (3.13)$$

where  $V$ ,  $\hbar$ ,  $p$ ,  $m$  corresponds to the total volume, Planck constant over  $2\pi$ , momentum, and particle mass respectively. From now on we will use Geometric units, i.e,  $c=G=1$ . Replacing Eq. (3.13) in Eq. (3.11) and integrating over the energy

$$N = \frac{8\pi}{(2\pi)^3 \hbar^3} V \int_0^\infty \frac{p^2}{e^{\beta(E-\mu)} + 1} dp, \quad (3.14)$$

being  $N$  the total number of particles. It was used that  $\alpha = -\mu/k_B T$  and  $\beta = 1/k_B T$ , being  $\mu$  the chemical potential and  $T$  temperature. Once the number of particles is found, to find the other thermodynamic variables we need to define the partition function  $Z$  with

$$N = \frac{1}{\beta} \frac{\partial}{\partial \mu} \ln Z, \quad (3.15)$$

and consequently,

$$\ln Z = \frac{8\pi V}{(2\pi)^3 \hbar^3} \int_0^\infty \ln(1 + e^{-\beta(E-\mu)}) p^2 dp. \quad (3.16)$$

Thus, fermion energy density  $\varepsilon$  and pressure  $P$  are

$$\varepsilon_F = -\frac{\partial \ln Z}{\partial \beta} = \frac{8\pi}{(2\pi)^3 \hbar^3} \int_0^\infty \frac{\sqrt{p^2 + m^2}}{e^{(\beta(E-\mu))} + 1} p^2 dp, \quad (3.17)$$

$$P_F = P_e = -\frac{1}{\beta} \frac{\partial \ln Z}{\partial \mu} = \frac{8\pi}{3(2\pi)^3 \hbar^3} \int_0^\infty \frac{(p^2 + m^2)^{-1/2}}{e^{(\beta(E-\mu))} + 1} p^4 dp. \quad (3.18)$$

These Eqs. (3.14),(3.17) and (3.18) are valid for any Fermi gas with relativistic velocities. In what concerns to white dwarfs, this description is going to be used to describe the electrons contribution, with  $m = m_e = 0.511[\text{MeV}]$ .

$$\varepsilon_e = \varepsilon_F - n_e m_e. \quad (3.19)$$

## 3.2 The nucleons pressure and energy density

In the classical limit, the Fermi-Dirac partition function become the Maxwell-Boltzmann distribution function (see (ROSE, 1998), which is

$$f(p) = \frac{n \exp\left(\frac{-p^2}{2mk_B T}\right)}{2\pi mk_B T}. \quad (3.20)$$

Considering this distribution the thermal pressure and energy density calculated for these classical particles (the nucleons from ions) are, respectively,

$$P = nkT, \quad (3.21)$$

$$U = \frac{3}{2}nk_B T. \quad (3.22)$$

Despite the thermal contributions, the energy density from nucleons has another contribution from the particles' mass density

$$\varepsilon = \rho_N, \quad (3.23)$$

being  $\rho_N$  the mass density. From Eqs. (3.21), (3.22), (3.23) the pressure and energy density of nucleons can be written as

$$P_N = n_N k_b T, \quad (3.24)$$

$$\varepsilon_N = n_N c_v T + n_N m_u, \quad (3.25)$$

where  $c_v$  is the thermal capacity at constant volume and  $n_N$  the number density of nucleons, and the unified mass  $m_u = 1.6604 \times 10^{-24} \text{g}$ . In order to preserve the charge neutrality

in the star interior, the number of protons has to be equal to the number of electrons in Eq. (3.14)

$$n_e = \frac{N_e}{V} = \frac{Z}{A} n_N, \quad (3.26)$$

being  $Z$  and  $A$  the atomic weight and mass respectively.

### 3.3 The radiation pressure and energy density

In agreement to Timmes and Arnett (TIMMES; ARNETT, 1999) equation for stellar structure, the other term that has to be used is radiation. Since at high temperatures the reaction  $e^+ + e^- \rightleftharpoons \gamma$ , i.e, electrons and positrons combine producing photons. The photons have each the frequency  $\nu$ , and energy  $E = h\nu$ . Using the Bose-Einstein statistics, the occupation index can be written as (MACIEL, 2016)

$$f(E) = \frac{1}{(e^{E/k_B T} - 1)}, \quad (3.27)$$

the photon energy density is

$$\varepsilon_R = \int_0^\infty \varepsilon_\nu = \frac{8\pi}{h^3} \int_0^\infty \frac{\nu^3 d\nu}{e^{h\nu/k_B T} - 1} = aT^4, \quad (3.28)$$

being  $a$  the radiation constant

$$a = \frac{8\pi^5 k^4}{15h^3} = 4\sigma = 7.56 \times 10^{-15} [\text{ergcm}^{-3} \text{K}^{-4} \int_0^\infty \varepsilon_\nu]. \quad (3.29)$$

The **radiation pressure due to the photons** can be integrated as

$$P_R = \frac{1}{3} \int_0^\infty \varepsilon_\nu d\nu = \frac{1}{3} \varepsilon = \frac{1}{3} aT^4. \quad (3.30)$$

#### 3.3.1 The crystallization

Determined conditions are sufficient to make a plasma inside a white dwarf strongly coupled into a repeated configuration also known as lattice. To characterize the plasma properties, it is necessary to determine the Coulomb coupling parameter (GARCÍA-BERRO; OSWALT, 2016; POTEKHIN; CHABRIER, 2000)

$$\Gamma = \langle Z^{5/3} \rangle \Gamma_e, \quad (3.31)$$

being

$$\Gamma_e = \frac{e^2}{a_e k_B T}, \quad (3.32)$$

being  $a_e = \left(\frac{3}{4e}\right)^{1/3}$  the inter-electronic distance. Following (GARCÍA-BERRO; OSWALT, 2016), the coupling parameter  $\Gamma < 179$  represents small Coulomb coupling and at  $\Gamma \approx 179$  the crystallization is sets in. Some authors like (MESTEL; RUDERMAN, 1967) describe the crystallization happening for melting temperatures below

$$T_m < 3 \times 10^5 \left(\frac{\rho}{10^6}\right)^{1/3} Z^{5/3} [\text{K}]. \quad (3.33)$$

In more recent works, the threshold for crystallization in Eq. (3.33) is obtained considering the coupling parameter  $\Gamma$  value. For instance, Eq. (3.33), considering different coupling parameter values can produce different melting limits:  $\Gamma = 175$  according to (TREMBLAY, 2019);  $\Gamma = 179$  according to (GARCÍA-BERRO; OSWALT, 2016);  $\Gamma = 160$  according to (MONTGOMERY *et al.*, 1999). These values reported in (TREMBLAY, 2019; GARCÍA-BERRO; OSWALT, 2016; MONTGOMERY *et al.*, 1999) are very similar among them. Thus, in Table 3.1 we found comparable thresholds for the crystallization. Additionally, we can note that the findings with Eq. (3.33) present smaller values than the obtained by the crystallization in these recent works.

	$\Gamma = 175$	$\Gamma = 179$	$\Gamma = 160$	Eq. 3.33
$T_c = 10^8 [\text{K}]$				
$\frac{\varepsilon}{[\text{g}/\text{cm}^3]}$	$1.2 \times 10^{11}$	$1.3 \times 10^{11}$	$9.3 \times 10^{10}$	$4.9 \times 10^9$
$T_c = 10^7 [\text{K}]$				
$\frac{\varepsilon}{[\text{g}/\text{cm}^3]}$	$1.2 \times 10^8$	$1.3 \times 10^8$	$9.3 \times 10^7$	$5.1 \times 10^6$

TABLE 3.1 – Melting limits according to (TREMBLAY, 2019; GARCÍA-BERRO; OSWALT, 2016; MONTGOMERY *et al.*, 1999; MESTEL; RUDERMAN, 1967)

### 3.3.2 Wigner-Seitz cell

The treatment of compressed atoms inside in a Wigner-Seitz cell has been considered in white dwarfs studies, e.g., review (ROTONDO *et al.*, 2011; CARVALHO *et al.*, 2014). Several historical and seminal papers regarding the development of the white dwarf EOS were written since 1960. We omit here these works since a good description of the equation of states' history is presented in chapter 5. Once the lattice is considered, the interactions between electrons-electrons and electrons-protons, as well as the energy of each cell, are

taken into consideration. Inspired in these articles, we consider the degenerated Fermi gas of non-interacting electrons in Salpeter's model (SALPETER, 1961).

In this case, the lattice pressure can be written of the form (ROTONDO *et al.*, 2011)

$$P_L = \frac{E_{Coul}}{3V_{WS}} + \frac{1}{3} \left( \frac{p_e^F}{\mu_e} \right)^2 \frac{E_{TF}^S}{V_{WS}}, \quad (3.34)$$

with  $p_e^F$ ,  $\mu_e$ ,  $E_{Coul}$  and  $E_{TF}^S$  being the electron Fermi momentum, chemical electron potential, Coulomb energy, and the correction introduced by Salpeter to the Thomas-Fermi model, respectively. The energies  $E_{Coul}$  and  $E_{TF}^S$  are given by

$$E_{Coul} = -\frac{9}{10} \frac{Z^2 e^2}{R_{WS}}, \quad (3.35)$$

$$E_{TF}^S = \frac{162}{175} \left( \frac{4}{9\pi} \right)^{2/3} \alpha^2 Z^{7/3} \mu_e, \quad (3.36)$$

where  $Z$  is the atomic number,  $e$  represents the electron charge,  $\alpha = 1/137$  depicts the fine-structure constant, and  $R_{WS}$  is the Wigner-Seitz radius. In addition, the parameter  $R_{WS}$  is related to the cell density,  $n_{WS}$ , through the equality

$$n_{WS} = \frac{3}{4\pi R_{WS}^3} = \frac{1}{V_{WS}} = \frac{n_e}{Z}, \quad (3.37)$$

being  $V_{WS}$  the cell volume and  $n_e$  the electron number density.

In turn, the lattice energy density is determined as:

$$\varepsilon_L = \frac{E_{Coul}}{V_{WS}} + \frac{E_{TF}^S}{V_{WS}}. \quad (3.38)$$

The first and second term placed on the right-hand side of Eq. (3.38) represent the Colomb energy and the Salpeter's correction to the Thomas-Fermi model (SALPETER, 1961), respectively.

### 3.3.3 The threshold of degeneracy and temperature distribution

At zero temperature the electron gas assume a degeneracy behavior, which makes the distribution of electron be discrete and the partition function will assume a value according to its momentum

$$f(p) = \begin{cases} 1, & p \leq p_F, \\ 0, & p > p_F, \end{cases} \quad (3.39)$$

being  $p_F$  the Fermi momentum. Moreover, in the non-relativistic limit the degenerate pressure according to Eqs. (3.18), and (3.39) is

$$P_d = \frac{3^{2/3} h^2}{20 m_e \pi^{2/3}}. \quad (3.40)$$

In the star, the transition between the non-degenerate ideal gas for the nucleons due to the ions and the degenerate electron gas can be obtained equalizing Eqs. (3.40) and (3.24). The threshold density for degeneracy is

$$\rho_\star = 2.4 \times 10^{-8} \mu_e T_\star^{3/2} \text{ [g/cm}^3\text{]}, \quad (3.41)$$

(BÖHM, 1968). This equation showing a power law expression between the degeneracy threshold density and the temperature is extended to the star envelope. Thus, the temperature distribution in the white dwarf envelope used in the thesis is

$$T(r) = T_c \left( \frac{\rho}{\rho_c} \right)^{2/3}, \quad (3.42)$$

being  $T_c$  and  $\rho_c$  the core temperature and minimum density. In the case of very massive white dwarfs the size of the envelope is too small compared to the star core, and does not contribute to the radius as we explained before, this temperature distribution is well justified in this case, that is the one we are interested in the thesis.

# 4 Equilibrium Configurations and Stability

During the stellar evolution, there are phases in which there are no contracting or expanding stars. These phases are determined when there is the equilibrium of the self-gravitational collapse and the internal pressure. Indeed, we name this condition hydrostatic equilibrium. Typically, white dwarfs' hydrostatic equilibrium is studied since Chandrasekhar (CHANDRASEKHAR, 1931b) using Newton's Second Law. This assumption is reasonable for white dwarfs' masses below  $1.3M_{\odot}$ . Albeit, stars near-Chandrasekhar's limit have to consider general relativity effects (CARVALHO *et al.*, 2018a; MATHEW; NANDY, 2017). The negligence of these effects results in finding a higher radius compared to the real ones (CARVALHO *et al.*, 2018a).

We obtain the hydrostatic equilibrium (in Newton's framework) by analyzing the forces present in the star. Thus, the gravitational force and the internal pressure are balanced to obtain an equilibrium equation. We derive two equations using this method: the pressure distribution and mass conservation. Besides, in the general relativity framework, the hydrostatic equilibrium is also reached solving Einstein's field equation. We obtain, with this method, vacuum solutions (without matter-energy) extended to the stellar interior using Birkoff's theorem. After the calculation, hydrostatic equilibrium equations are obtained according to sphericity, rotation, and charge. In the case of uncharged static spheric stars, Tolman-Oppenheimer-Volkoff equations are obtained (TOLMAN, 1939; OPPENHEIMER; VOLKOFF, 1939). The inclusion of charge by the introduction of Maxwell energy-momentum tensor in Einstein equation aggregate electric field terms in them and also in the metric functions (BEKENSTEIN, 1971).

As already pointed out in the introduction, the condition for hydrostatic equilibrium is not enough to guarantee star stability. Dynamical stability needs to be investigated by solving the radial oscillations equations due to small metric perturbations (CHANDRASEKHAR, 1964a; CHANDRASEKHAR, 1964b). Furthermore, for very dense stars as white dwarfs, nuclear fusion reactions at tiny energies, known as pycnonuclear reactions, can occur in carbon or oxygen white dwarfs at the star center and make the star unstable.

The inverse  $\beta$ -decay reaction - responsible for the decrease of the electron number due to proton capture producing neutrons - can also destabilize the star by diminishing the degeneracy electron pressure that balances the gravitational force (OTONIEL *et al.*, 2019).

## 4.1 Hydrostatic Equilibrium – Uncharged star

The hydrostatic equilibrium of a star depends on some parameters. In this first section, we are considering the star with sphericity and no rotation. We are neglecting effects due to charge and magnetic fields in this first analysis. We are going to deduce the hydrostatic equilibrium in Newtonian physics and in Einstein general relativity.

## 4.2 Newton's framework

To better explain the deduction, we draw Fig. 4.1. We consider a uni-dimensional model due to the assumption of spherical symmetry valid for stars that are not very magnetic and not under strong rotational spin frequency. In this figure,  $r$  represents the radial coordinate,  $R$  total radius, and  $dr$  an infinitesimal radius displacement. As a consequence, the mass laying between  $r$  and  $r + dr$  is

$$dm = m(r + dr) - m(r) = 4\pi r^2 \rho(r) dr, \quad (4.1)$$

being  $\rho(r)$  the mass density. The Eq. 4.1 is known as the mass conservation equation or the continuity equation.

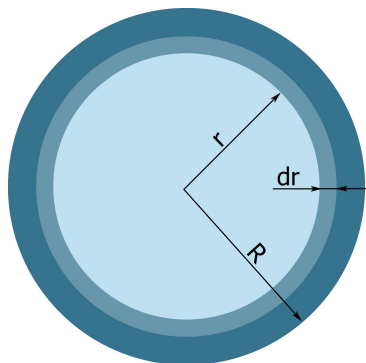


FIGURE 4.1 – Uni-dimensional spherical star.

Intending to obtain an hydrostatic equation, we are going to analyze the forces inside the star. The self-gravitation of the star is obtained by considering Newton's law of universal gravitation. The gravitational force acting in the element  $dm$  due to  $m(r)$ , the

mass inside  $r$ , is

$$d\vec{F}_g = -\frac{m(r)dm}{r^2}\hat{r}, \quad (4.2)$$

where it was considered  $G = 1$ . The gravitational force in Eq. 4.2 is associated to a pressure  $P_g = dF_g/dS$ . To calculate the internal pressure, we have to consider the force pushing outwards between  $r$  and  $dr$  is

$$d\vec{F}_{\text{int}} = \frac{dP}{dr}drdA\hat{r}, \quad (4.3)$$

being  $dA$  the area.

We can note the signs in Eqs. (4.2) and (4.3) are opposite. Thus, replacing Eqs. (4.1) in Eq. (4.2), and using Newton's second law for equilibrium, we have

$$dP(r) = -\frac{Gm(r)\rho(r)}{r^2}dr, \quad (4.4)$$

which is the equation of hydrostatic equilibrium for a static and spherical configuration. The hydrostatic equilibrium involves  $\nabla P = -\rho\nabla\Phi$ , being  $\Phi$ , in this case, the gravitational potential (SHAPIRO; TEUKOLSKY, 2004).

### 4.2.1 The Schwarzschild solution

To describe the vacuum solution in general relativity, we have to consider the object's symmetry. Considering spherical symmetry star, the line element is (D'INVERNO, 1992)

$$ds^2 = e^\nu(dt)^2 - (e^\lambda dr^2 + r^2 d\theta^2 + r^2 \sin^2 \theta d\phi^2), \quad (4.5)$$

being  $\lambda$  and  $\nu$  functions of  $r$ . We have to highlight that in this conditions, since the metric terms only depend on the radial coordinate, we have uni-dimensional models.

Intending to find the values of  $\nu$  and  $\lambda$ , we have to solve the Einstein's field equations (D'INVERNO, 1992)

$$G_{\mu\nu} = R_{\mu\nu} - \frac{1}{2}Rg_{\mu\nu} = 8\pi T_{\mu\nu}, \quad (4.6)$$

where  $R_{\mu\nu}$ ,  $R$  are the Riemann tensor and Ricci scalar, respectively, and  $T_{\mu\nu}$  is the energy-momentum tensor. The  $g_{\mu\nu}$  are the metric elements, according to Eq. (4.5)

$$g_{\mu\nu} = \text{diag}(e^\nu, -e^\lambda, -r^2, -r^2 \sin^2 \theta), \quad (4.7)$$

$$g^{\mu\nu} = \text{diag}(e^{-\nu}, -e^{-\lambda}, -r^{-2}, -r^{-2} \sin^{-2} \theta). \quad (4.8)$$

To obtain the Riemann tensor and Ricci scalar, we have to calculate (D'INVERNO,

1992)

$$R_{\mu\nu} = R_{\mu\lambda\nu}^{\lambda} = g^{\lambda\beta} R_{\beta\mu\lambda\nu}, \quad (4.9)$$

$$R = g^{\mu\nu} R_{\mu\nu}, \quad (4.10)$$

where

$$R_{\mu\lambda\nu}^{\lambda} = -\partial_{\lambda}\Gamma_{\mu\nu}^{\lambda} + \partial_{\nu}\Gamma_{\mu\lambda}^{\lambda} - \Gamma_{\mu\nu}^{\alpha}\Gamma_{\alpha\lambda}^{\lambda} + \Gamma_{\mu\lambda}^{\alpha}\Gamma_{\alpha\nu}^{\lambda}, \quad (4.11)$$

and being  $\Gamma_{\mu\beta}^{\lambda}$  the metric connection given by

$$\Gamma_{\mu\beta}^{\lambda} = \frac{1}{2}g^{\lambda\alpha} (\partial_{\mu}g_{\alpha\beta} + \partial_{\beta}g_{\alpha\mu} - \partial_{\alpha}g_{\mu\beta}). \quad (4.12)$$

Calculating the metric connection terms, the non-vanishing terms are

$$\Gamma_{11}^1 = \frac{\lambda'}{2}, \quad \Gamma_{10}^0 = \Gamma_{01}^0 = \frac{\nu'}{2}, \quad \Gamma_{33}^2 = -\sin(\theta)\cos(\theta), \quad (4.13)$$

$$\Gamma_{22}^1 = -re^{-\lambda}, \quad \Gamma_{00}^1 = \frac{\nu'}{2}e^{\nu-\lambda}, \quad \Gamma_{12}^2 = \Gamma_{21}^2 = \frac{1}{r}, \quad (4.14)$$

$$\Gamma_{13}^3 = \Gamma_{31}^3 = \frac{1}{r}, \quad \Gamma_{23}^3 = \Gamma_{32}^3 = \cot(\theta), \quad \Gamma_{33}^1 = -r\sin^2(\theta)e^{-\lambda}, \quad (4.15)$$

where the notation  $x' = \frac{dx}{dr}$  was used. Beside, the Riemann tensors are

$$R_{\mu\nu} = 0 \quad ; \mu \neq \nu \quad (4.16)$$

$$R_{00} = e^{\nu-\lambda} \left( -\frac{\nu''}{2} - \frac{\nu'^2}{4} + \frac{\nu'\lambda'}{4} - \frac{\nu'}{r} \right), \quad (4.17)$$

$$R_{11} = \left( \frac{\nu'^2}{4} - \frac{\lambda'}{r} + \frac{\nu''}{2} - \frac{\nu'\lambda'}{4} \right), \quad (4.18)$$

$$R_{22} = 1 - e^{-\lambda} + re^{-\lambda} \left( \frac{\lambda'}{2} - \frac{\nu'}{2} \right), \quad (4.19)$$

$$R_{33} = \sin^2(\theta)R_{22}, \quad (4.20)$$

and the Ricci scalar

$$R = \frac{2}{r^2} + e^{-\lambda} \left( -\frac{\nu'^2}{2} - \nu'' + \frac{\nu'\lambda'}{2} - 2\frac{\nu'}{r} + 2\frac{\lambda'}{r} - \frac{2}{r^2} \right). \quad (4.21)$$

To obtain the terms  $G_{00}$ , and  $G_{11}$  of Einstein's tensor, we replace in Eq. (4.6) the Eqs.(4.16)-(4.19), and Eq. (4.21) to obtain

$$G_{00} = -\frac{e^{\nu}}{r^2} + \frac{e^{\nu-\lambda}}{r} \left( \frac{1}{r} - \lambda' \right), \quad (4.22)$$

$$G_{11} = \frac{e^{\lambda}}{r^2} - \frac{1}{r} \left( \nu' + \frac{1}{r} \right). \quad (4.23)$$

In vacuum, the energy-momentum tensor in Eq. (4.6) vanishes. Thus, Eqs. (4.22) and (4.23) become (D'INVERNO, 1992)

$$e^{-\lambda} \left( \frac{\lambda'}{r} - \frac{1}{r^2} \right) + \frac{1}{r^2} = 0, \quad (4.24)$$

$$e^{-\lambda} \left( \frac{\nu'}{r} + \frac{1}{r^2} \right) - \frac{1}{r^2} = 0, \quad (4.25)$$

which can be added to get the dependency in both metric terms

$$\lambda' + \nu' = 0, \quad (4.26)$$

valid for vacuum. In the star surface (i.e.,  $r = R$ ), the interior solution has to match with vacuum solutions, so we can say that the metric terms at this point, according to Eq. (4.26) are

$$\lambda(R) = -\nu(R). \quad (4.27)$$

Now, if we rewrite equation 4.24 as

$$e^{-\lambda} - re^{-\lambda}\lambda' = (re^\lambda)' = 1, \quad (4.28)$$

it can be integrated to get

$$re^{-\lambda} = r + \text{constant}, \quad (4.29)$$

for convenience this constant is defined as  $-2m$ , being  $m$  the mass and using geometric coordinates, i.e.,  $c=G=1$ . Therefore, we obtain the metric term

$$e^\lambda = \left( 1 - \frac{R_s}{r} \right)^{-1}, \quad (4.30)$$

being  $R_s = 2m$  the Schwarzschild radius in geometric coordinates. This relation in Eq. (4.30) is also valid for the stellar interior (see (D'INVERNO, 1992; CARROLL, 2004)).

## 4.2.2 The Tolman-Oppheimer-Volkoff equation

In the star interior, we are looking for non-vacuum solutions. Therefore, the momentum-energy tensor (in Eq. (4.6)) considering the star as a perfect isotropic fluid is (CARROLL, 2004)

$$T_{\mu\nu} = (P + \varepsilon)u_\mu u_\nu - P g_{\mu\nu}, \quad (4.31)$$

being  $u_\mu$  the four-velocity, which we consider to be pointing in the time-like direction. The reason for this is due to our search for static solutions. The normalization of the

four-velocity as  $u^\mu u_\mu = -1$  makes its components

$$u_\mu = (-e^{\nu/2}, 0, 0, 0), \quad (4.32)$$

and the energy-momentum tensor become

$$T_{\mu\nu} = 0, \quad ; \mu \neq \nu, \quad (4.33)$$

$$T_{00} = \varepsilon e^\nu, \quad (4.34)$$

$$T_{11} = P e^\lambda, \quad (4.35)$$

$$T_{22} = P r^2, \quad (4.36)$$

$$T_{33} = P r^2 \sin^2(\theta). \quad (4.37)$$

Intending to find the mass conservation equation, we replace Eq. (4.34) in Eq. (4.6)

$$\frac{-e^\nu}{r^2} + \frac{e^{\nu-\lambda}}{r} \left( \frac{1}{r} - \lambda' \right) = -8\pi\varepsilon e^\nu, \quad (4.38)$$

which can be rearranged to become

$$\frac{dm}{dr} = 4\pi r^2 \varepsilon, \quad (4.39)$$

which is the mass conservation equation. We have to mention that the mass in Eq. (4.39) depends on the energy density, while in Eq. 4.1 it depends on the mass density. This highlights the difference between the baryonic and gravitational mass.

We are going now to look for hydrostatic equilibrium equations in general relativity. Thus, we replace the Eqs. (4.23) and (4.35) in Eq. (4.6) to get

$$\frac{e^\lambda}{r} - \frac{1}{r} \left( \nu' + \frac{1}{r} \right) = -8\pi P e^\lambda, \quad (4.40)$$

from which we rearrange to obtain

$$\frac{d\nu}{dr} = \frac{2}{r^2 (1 - 2m/r)} (4\pi P r^3 + m). \quad (4.41)$$

Once the metric term  $\nu$  is found in Eq. (4.41), to obtain the hydrostatic equilibrium we have to solve the energy-momentum conservations  $\nabla_\mu T^{\mu\nu} = 0$ , being  $T^{\mu\nu} = T_{\alpha\beta} g^{\mu\alpha} g^{\nu\beta}$ , and

$$\nabla_\mu T^{\mu\nu} = \partial_\mu T^{\mu\nu} + \Gamma_{\mu\lambda}^\mu T^{\lambda\nu} + \Gamma_{\mu\lambda}^\nu T^{\mu\lambda} = 0, \quad (4.42)$$

from what we obtain

$$\frac{dP}{dr} = -\frac{(P + \varepsilon)}{2} \frac{d\nu}{dr}. \quad (4.43)$$

Replacing the Eq. (4.43) in Eq. (4.41), we get the Tolman-Oppenheimer-Volkoff (TOLMAN, 1939; OPPENHEIMER; VOLKOFF, 1939) equation, or simply the hydrostatic equilibrium in the general relativity framework

$$\frac{dP}{dr} = -\frac{m\varepsilon}{r^2} \left(1 + \frac{P}{\varepsilon}\right) \left(1 + \frac{4\pi r^3 P}{m}\right) \left(1 - \frac{2m}{r}\right)^{-1}. \quad (4.44)$$

We have to highlight the difference between the Eqs. (4.4) and (4.44). The Eq. (4.4) is reached in Eq. (4.44) when  $\varepsilon \rightarrow \rho$  and the parenthesis terms are equal to one. This situation is reached in a non-relativistic system where the pressure is much smaller than the energy density, and the last term of the r.h.s of Eq. (4.44) due to the curvature of the space-time is equal to 1, situation achieved when Schwarzschild radius  $R_s = 2m$  in geometric coordinates is much smaller than  $r$ .

### 4.2.3 Reissner-Nordstrom solution

In what concerns to charged white dwarfs, some modifications in the deduction presented in the last section have to be done. In contrast to the uncharged case, here we only deduce using general relativity. Due to the spherical symmetry, the Schwarzschild-like line-element (Eq. (4.5)) maintains. The metric terms, although, have a contribution from the charge. The  $\lambda$ , used inside and outside the star is defined as (BEKENSTEIN, 1971)

$$e^\lambda = \left(1 - \frac{2m}{r} + \frac{q^2}{r^2}\right)^{-1}, \quad (4.45)$$

being  $q$  the electric charge.

With the inclusion of charge, Einstein's tensors are going to be different. Therefore, we calculate the stress-energy tensor accounting for the presence of an electric field,

$$T_{\mu\nu} = (\varepsilon + P)u_\mu u_\nu - P g_{\mu\nu} + \frac{1}{4\pi} (-F_\mu^\gamma F_{\nu\gamma}) + \frac{1}{16\pi} g_{\mu\nu} F_{\gamma\alpha} F^{\gamma\alpha}, \quad (4.46)$$

including Maxwell energy-momentum tensor.  $F_{\mu\nu}$  satisfies Maxwell's equations, that in source-free regions (vacuum), are (CARROLL, 2004)

$$\nabla_\mu F^{\mu\nu} = 0, \quad (4.47)$$

$$\partial_{[a} F_{bc]} = 0. \quad (4.48)$$

#### 4.2.4 Bekenstein equations: charged Tolman-Oppheimer-Volkoff equations

Following (BEKENSTEIN, 1971), the Eq. (4.47), considering only a static electric charge density that is the time component of the 4-vector current  $j^\mu = (j^0, 0, 0, 0)$ , becomes

$$(r^3 e^{(\nu+\lambda)/2} F^{01}) = 4\pi j^0 r^2 e^{(\nu+\lambda)/2}, \quad (4.49)$$

which if integrated gives

$$F_{01} = -F_{10} = \frac{e^{(\nu+\lambda)/2} q}{r^2}, \quad (4.50)$$

where

$$\frac{dq}{dr} = 4\pi r^2 e^{(\nu+\lambda)/2} r^2 j^0 = 4\pi r^2 e^{\lambda/2} r^2 \rho_{ch}. \quad (4.51)$$

From the definition, the time component of the current is  $j^0 = u^0 \rho_{ch}$ , being  $u^0$  defined in Eq. (4.32), and  $\rho_{ch}$  the charge density. The energy-momentum tensor contributions from electromagnetic tensor are calculated as

$$(T_{00})^{(EM)} = \frac{1}{8\pi} e^\nu \frac{q^2}{r^4}, \quad (4.52)$$

$$(T_{11})^{(EM)} = -\frac{1}{8\pi} e^\lambda \frac{q^2}{r^4}. \quad (4.53)$$

Thus, the Einstein Eqs. (4.38) and (4.40) are going to add some terms due to electric charge. This inclusion results in

$$\frac{-e^\nu}{r^2} + \frac{e^{\nu-\lambda}}{r} \left( \frac{1}{r} - \lambda' \right) = -8\pi \left( \varepsilon + \frac{1}{8\pi} \frac{q^2}{r^4} \right) e^\nu, \quad (4.54)$$

$$\frac{e^\lambda}{r} - \frac{1}{r} \left( \nu' + \frac{1}{r} \right) = -8\pi \left( P - \frac{1}{8\pi} \frac{q^2}{r^4} \right) e^\lambda. \quad (4.55)$$

To obtain the hydrostatic equilibrium, we do the same replacements for charge and uncharged configurations. Therefore, from the Eqs. (4.54) and (4.55) we derive respectively

$$\frac{dm}{dr} = 4\pi r^2 \varepsilon + \frac{q}{r} \frac{dq}{dr}, \quad (4.56)$$

$$\frac{d\nu}{dr} = \frac{2}{r^2 (1 - 2m/r)} \left( 4\pi P r^3 + m - \frac{q^2}{r} \right). \quad (4.57)$$

The energy-momentum conservation in Eq. (4.42) is also valid and from which we can

derive

$$\frac{dP}{dr} = -\frac{(P + \varepsilon)}{2} \frac{d\nu}{dr} + \frac{q}{4\pi r^4} \frac{dq}{dr}. \quad (4.58)$$

Replacing Eq. (4.57) in Eq. (4.58) an equation such as the Tolman-Oppheimer-Volkoff that describes the hydrostatic equilibrium of charged stars is found

$$\frac{dP}{dr} = -\frac{m\varepsilon}{r^2} \left(1 + \frac{P}{\varepsilon}\right) \left(1 + \frac{4\pi r^3 p}{m} - \frac{q^2}{rm}\right) \left(1 - \frac{2m}{r} + \frac{q^2}{r^2}\right)^{-1} + \frac{q}{4\pi r^4} \frac{dq}{dr} \quad (4.59)$$

### 4.3 The Instabilities

The hydrostatic equilibrium determined in the Newtonian frameworks and with Tolman-Oppheimer-Volkoff equations guarantee forces balance. Albeit, these equations do not ensure stability. The stability for carbon-core white dwarfs is defined by examining either nuclear reactions and dynamical stability. Indeed, nuclear reactions result in instability due to the high densities presented in the star core. These nuclear reactions are restricted (for white dwarf stars) to pycnonuclear reactions and inverse  $\beta$ -decay.

In what concerns dynamical stability, white dwarfs are examined with radial oscillations and the GR turning-point. These two criteria agree for uncharged and unmagnetized cool stars (WHEELER *et al.*, 1968; CHANMUGAM, 1977). However, it is known that they do not coincide for sequences with different total charges (ARBAÑIL; MALHEIRO, 2015). Due to the temperature in the stellar interior, we perform for the first time a complete calculation of radial oscillations, in order to study the stability of hot white dwarfs. Additionally, we associate the fundamental mode, the lower radial oscillation frequency, with observable white dwarfs.

#### 4.3.1 Pycnonuclear reactions

In what concerns the instability due to nuclear reactions, carbon white dwarfs must have the analysis of pycnonuclear reactions and inverse  $\beta$ -decay. Regarding pycnonuclear reactions, they represent the fusion of two atoms in another, a situation that is possible to occur at the star core where the high densities allow very short inter-nuclei distance between the closest pairs that by tunneling effect can penetrate the Coulomb barrier. This barrier becomes lower significantly by screening due to the interaction of a fusing pair with degenerated neutralizing electrons and the surrounding nuclei. Thus, this reaction depends essentially on the density and not on the temperature. In fact, “pycno” means compact, dense, close. In this situation, nuclear fusion rates are higher, and occur at very low energies in nuclear scales, in the order of a few KeV. For further information, see (SON; FISCH, 2005) and references therein.

Pycnonuclear reactions possibility in the dense stellar matter (YAKOVLEV *et al.*, 2005) creates a constraint in the white dwarf's chemical composition. These reactions are almost independent of temperature and appear even at zero temperature. as we already explained. A rigorous approach to calculate these nuclear reactions was realized by Salpeter and Van Horn (SALPETER; HORN, 1969), who established a temperature-dependent pycnonuclear rate for zero-temperature. For a pure carbon core (OTONIEL *et al.*, 2019), where  $^{12}\text{C} + ^{12}\text{C} \rightarrow ^{24}\text{Mg}$ , this reaction rate can be written as (SALPETER; HORN, 1969):

$$\frac{R_{\text{pyc}}(T)}{R_{\text{pyc}}(0)} - 1 = a_1 \lambda^{-1/2} \left[ 1 + a_2 e^{b_1 \beta^{3/2}} \right]^{-1/2} \times \exp \left\{ b_2 \beta^{3/2} + \lambda^{-1/2} a_3 e^{b_1 \beta^{3/2}} \left[ 1 - a_4 e^{b_1 \beta^{3/2}} \right] \right\}, \quad (4.60)$$

where  $R_{\text{pyc}}(0)$  represents the pycnonuclear reaction at zero temperature, and  $a_1$ ,  $a_2$ ,  $a_3$ ,  $a_4$ ,  $b_1$ , and  $b_2$  are model-dependent dimensionless constants. On the right-hand side of Eq. (5.19), the first factor in the principal exponential represents the Boltzmann factor for the contribution from the excited state. The second factor in the main exponential depicts the increase in the rate above its zero-temperature value.

Table 4.1 lists the values of  $a_1$ ,  $a_2$ ,  $a_3$ ,  $a_4$ ,  $b_1$  and  $b_2$  considered in the static lattice model, review (SALPETER; HORN, 1969).

TABLE 4.1 – Dimensionless parameter values for the static approximations.

Parameter	$a_1$	$a_2$	$a_3$	$a_4$	$b_1$	$b_2$
Value	0.0430	1.2624	1.2231	0.6310	-8.7833	-7.2720

Following (SALPETER; HORN, 1969), for the static approximation, the parameters in Latin letters appearing in Eq. (5.19) take the values presented in Table I. The parameters in Greek symbol appearing in the same equation,  $\beta$  and  $\lambda$ , are given by the relations:

$$\lambda = \frac{\hbar^2}{m_u Z^2 e^2} \left( \frac{n_N}{2} \right)^{1/3}, \quad (4.61)$$

$$\beta = 0.18084 \left( \frac{E_{\text{pk}}}{k_B T} \right)^{2/3}, \quad (4.62)$$

where  $E_{\text{pk}}$  represents the zero-point energy and it is given by the relation

$$E_{\text{pk}} = \hbar \omega_p = \hbar \left( \frac{4\pi e^2 Z^2 \rho}{A M_A^2} \right)^{1/2}, \quad (4.63)$$

with  $M_A$  being the atomic nuclei mass. For a  $^{12}\text{C}$ , the parameters  $M_A$  and  $\rho$  are equal to  $A m_u$  and  $10^{10}[\text{g}/\text{cm}^3]$ , respectively, see, e.g., (SHAPIRO; TEUKOLSKY, 2004; OTONIEL *et al.*, 2019).

The pycnonuclear rates for  $T = 0$  [K] can be expressed through the relation:

$$R_{\text{pyc}}(0) = \rho X_i A Z^4 S(E_{\text{pk}}) C_{\text{pyc}} 10^{46} \lambda^{3-C_{\text{pl}}} \times \exp(-C_{\text{exp}}/\sqrt{\lambda}) \text{s}^{-1} \text{cm}^{-3}. \quad (4.64)$$

Following (GASQUES *et al.*, 2005; OTONIEL *et al.*, 2019), we set:  $X_i = 1$ ,  $C_{\text{pyc}} = 3.90$ ,  $C_{\text{pl}} = 1.25$  and  $C_{\text{exp}} = 2.64$ . These are the same dimensionless parameters employed for a regular body-centered cubic lattice at  $T = 0$  [K] (GASQUES *et al.*, 2005; OTONIEL *et al.*, 2019).

The time to complete the atomic nuclei fusion is obtained from (GASQUES *et al.*, 2005; BOSHKAYEV *et al.*, 2013; OTONIEL *et al.*, 2019)

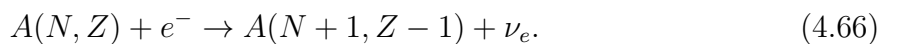
$$\tau_{\text{pyc}} = \frac{n_N}{R_{\text{pyc}}}. \quad (4.65)$$

As considered in (OTONIEL *et al.*, 2019), we employ the pycnonuclear reaction time  $\tau_{\text{pyc}} = 10$  [Gyr], which corresponds to an upper limit where pycnonuclear reactions are extremely slow (CHUGUNOV *et al.*, 2007). It is important to highlight that a lower limit, where this reaction is very fast, is determined by  $\tau = 1$  [s]. For white dwarfs, the limit of  $\rho_{\text{pyc}}(10$  [Gyr]) corresponds to a maximum mass density for stable stars against pycnonuclear reactions. Through these times, it can be estimated the mass density where these reactions appear,  $\rho_{\text{pyc}}(\tau_{\text{pyc}})$ . For white dwarfs, the limit of  $\rho_{\text{pyc}}(10$  [Gyr]) corresponds to a maximum density for stable stars, since from this point pycnonuclear reactions begin to appear.

The pycnonuclear fusion reaction rates against the mass density are plotted in Fig. 4.2 for two different central temperature. The horizontal lines in  $\tau_{\text{pyc}} = 10$  [Gyr] and  $\tau_{\text{pyc}} = 1$  [s] depict the limits where the pycnonuclear reactions are extremely slow and very fast, respectively. The curves traced for  $T_c = 0$  [K] and  $T_c = 10^8$  [K], the lowest and largest central temperature considered throughout this work, exhibit that there is a small difference between the mass densities  $\rho_{\text{pyc}}$  determined for the two central temperatures (CARVALHO *et al.*, 2014).

### 4.3.2 Inverse $\beta$ -decay

It is known that the matter inside white dwarfs may experience instability against the inverse  $\beta$ -decay process,



Due to this process, atomic nuclei turn into more neutron-rich and, as a consequence, the electron energy density and pressure are reduced thus leading to a softer EOS (GAMOW,

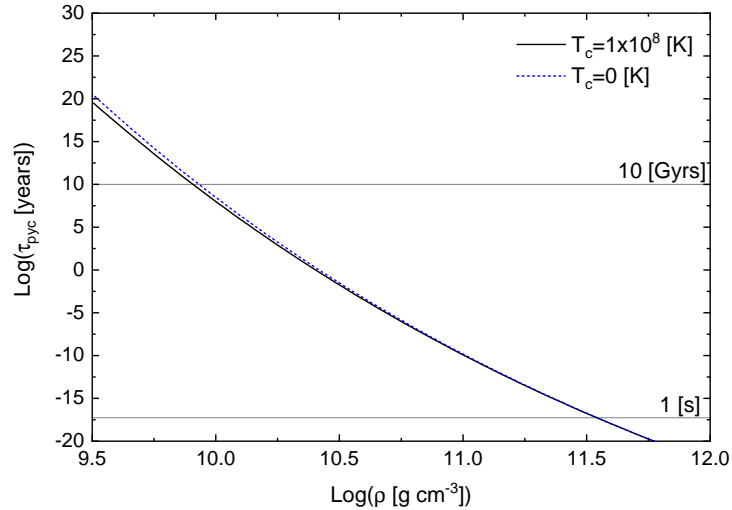


FIGURE 4.2 – Pycnonuclear reaction C+C fusion time as against the mass density for  $T = 0$  [K] and  $T_c = 10^8$  [K].

1939; SHAPIRO; TEUKOLSKY, 2004). Since we are considering a nucleus of  $^{12}\text{C}$ , the instabilities are reached at energies larger than  $\epsilon_Z^\beta = 13.370$  [MeV], see (ROTONDO *et al.*, 2011; CARVALHO *et al.*, 2014; OTONIEL *et al.*, 2019).

### 4.3.3 The turning-point

The turning point is a necessary condition to determine the star's stability (CAMENZIND, 2007; GLENDENNING, 2000). To determine it, the mass-central density curve is interpreted. Thus, we illustrate a common one in Fig. 4.3. Respectively in the y and x-axes are represented gravitational mass and central energy density.

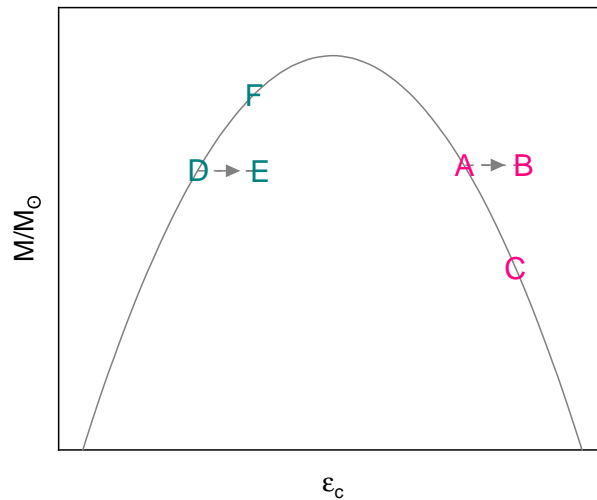


FIGURE 4.3 – An illustration for mass-central density curve

Considering a star in the “A”, a small contraction would lead it to the “B” point. At this point, it has a mass higher than the predicted in the hydrostatic equilibrium for the same central energy density one (at “C”). This means that the self-gravitation pressure is higher than the internal pressure. Thus, the initial contraction continues and generates a collapse.

Instead, a different result occurs if we look for a contraction in “D”. A contraction direct to point “E”, which has a mass smaller than the predicted in hydrostatic equilibrium (at point “F”). In this case, the internal pressure is higher than the self-gravitational. Consequently, the star expands and returns to the fundamental stage in “D”. Using turning point, stability is reached when (CAMENZIND, 2007; GLENDENNING, 2000)

$$\frac{dM}{d\varepsilon_c} > 0. \quad (4.67)$$

#### 4.3.4 The radial oscillations

The contraction we suppose to determine the turning point stability does not consider the sphericity of stars. Now, we are going to investigate carefully perturbations that make stars oscillate radially. According to (WEBER, 1999), these oscillations about their equilibrium configurations are called vibrations, and can be, for instance, torsional or octupole eigenmodes.

To investigate the stability of white dwarf against small radial perturbations, it is necessary to determine the radial oscillation equations. Thus, we will derive the Eulerian perturbations and the non-zero four-velocity. Once the non-zero four-velocity are defined, the fluid and spacetime variables are decomposed into the form presented in Eq. (5.7). Subsequently to these definitions and decomposition in the field equations, the Eulerian perturbations are found just keeping the first-order terms. We will represent the unperturbed terms  $f$ , the perturbation  $\delta f$  and the total  $f_0$  as

$$f_0 = f + \delta f, \quad (4.68)$$

valid for  $P$ ,  $\varepsilon$ ,  $\lambda$ , and  $\nu$ . Returning into the 4-velocity in Eq. (4.32), we will assume that there are additionally non-vanishing terms (CHANDRASEKHAR, 1964b; CHANDRASEKHAR, 1964a)

$$u^1 = e^{-\nu/2}v, \quad u_1 = e^{\lambda-\nu/2}v, \quad (4.69)$$

being  $v = dr/dx^0$ .

With the definition in Eq. (4.69), the energy-momentum tensor described in Eqs. (4.34)-

(4.37) will be related to the total state  $f_0$ . In addition, it will have another component

$$T_{10} = T_{01} = -e^{\lambda-\nu} v (P + \varepsilon), \quad (4.70)$$

and the  $G_{01}$  component

$$G_{10} = \frac{e^{-\lambda}}{r} \frac{\partial \lambda}{\partial x^0}. \quad (4.71)$$

Returning to the Einstein's equation, the perturbed term  $G_{00}$  in Eq. (4.38) becomes

$$\frac{\partial}{\partial r} (r e^{-\lambda} \delta \lambda) = 8\pi r^2 \delta \varepsilon, \quad (4.72)$$

and in  $G_{11}$  in Eq. (4.40)

$$\frac{e^{-\lambda}}{r} \left( \frac{\partial}{\partial r} - \frac{d\nu}{dr} \delta \lambda \right) = \frac{e^{-\lambda}}{r^2} \delta \lambda + \frac{8\pi}{\delta} P. \quad (4.73)$$

In addition, calculating the  $G_{10}$  component and the energy-momentum conservation we find respectively

$$\frac{e^{\lambda}}{r} \frac{\partial}{\partial x^0} \delta \lambda = -8\pi (P + \varepsilon) v, \quad (4.74)$$

and,

$$e^{\lambda-\nu} (P + \varepsilon) \frac{\partial v}{\partial x^0} + \frac{\partial}{\partial r} \delta P + \frac{1}{2} (p + \varepsilon) \frac{\partial}{\partial r} \delta \nu + \frac{1}{2} (\delta P + \delta \varepsilon) \frac{d\nu}{dr} = 0. \quad (4.75)$$

Introducing a "Lagrangian displacement"  $\xi$  that is time dependent as

$$v = \frac{\partial \xi}{\partial x^0}. \quad (4.76)$$

Considering that the Lagrangian displacement  $\xi = \alpha r$ , being  $\alpha$  a constant, and the perturbed quantities have a time dependence  $e^{i\omega t}$ , where  $\omega$  is called as eigenfrequency defined as (CHANDRASEKHAR, 1964a; BAGLIN, 1966)

$$\omega^2 = \frac{\mathcal{Z}}{\mathcal{D}}. \quad (4.77)$$

The functions  $\mathcal{Z}$  and  $\mathcal{D}$  are respectively determined by the equations

$$\begin{aligned} \mathcal{Z} = & 4 \int_0^R e^{\nu+\lambda/2} r^3 \frac{dP}{dr} dr \\ & + 8\pi \int_0^R e^{\nu+3\lambda/2} P(P+\varepsilon) r^4 dr \end{aligned} \quad (4.78)$$

$$\begin{aligned} & + 9 \int_0^R e^{\nu+\lambda/2} r^2 \Gamma P dr - \int_0^R \frac{e^{\nu+\lambda/2} r^4}{(P+\varepsilon)} \left[ \frac{dP}{dr} \right]^2 dr, \\ & \mathcal{D} = \int_0^R e^{3\lambda/2} (P+\varepsilon) r^4 dr, \end{aligned} \quad (4.79)$$

where  $\Gamma$  represents the adiabatic index and it is determined by the condition:

$$\Gamma = \frac{d \log P}{d \log \varepsilon}. \quad (4.80)$$

Equation (4.77) helps us to discriminate stable equilibrium solutions from unstable ones. This is possible by analyzing the eigenfrequency values  $\omega$ .

# 5 The structure and stability of hot white dwarfs

## 5.1 Introduction

This chapter is the article published in the *Astrophysical Journal* “The Structure and Stability of Massive Hot White Dwarfs” (NUNES *et al.*, 2021)

### 5.1.1 Equilibrium configuration of white dwarfs

According to the theory evolution, stars that leave the main sequence with masses below  $\sim 10M_{\odot}$  end up as white dwarfs (WEIDEMANN; KOESTER, 1983; SHAPIRO; TEUKOLSKY, 2004). These stars start their lives at high temperatures, which build them up as a core –usually composed of oxygen, helium, and carbon– surrounded by an envelope that could be rich in hydrogen (DUFOUR *et al.*, 2008).

One of the first theoretical studies about white dwarfs based on temperature was developed by (MARSHAK, 1940). Considering a star constituted by an isothermal core composed of degenerate matter and an envelope whose temperature distribution depends on energy generation rate and that is made-up by nondegenerate matter, he obtained an estimate of the quantity of hydrogen (in mass percentage) in the envelope of the stars Sirius B and Eridani B. At low densities, the change from degenerate to nondegenerate matter is a perfect environment in which to implement temperature distribution and energy transport (see, e.g., (KOESTER, 1972)), since this is associated with the effect of the electron temperature.

Usually, in the envelope, it is considered that the energy transport mechanism is realized by radiation or by convection. In the first case, the energy transport by radiation is produced by photons, and some models associate luminosity with small nuclear reactions in the envelope, such as p–p and CNO cycles (see e.g., (BETHE; CRITCHFIELD, 1938; BETHE, 1939; BETHE; MARSHAK, 1939)). In the second case, energy transport by convection appears to be due to the temperature difference between the core and the

envelope. This process has been considered in some white dwarf studies, for instance, those by (HORN, 1970; BÖHM, 1968; BÖHM, 1970; KOESTER, 1972; FONTAINE; HORN, 1976; HUBBARD; WAGNER, 1970). In both cases, energy transport provides a temperature distribution that affects the equilibrium configuration of white dwarfs.

The temperature influence on the structure of white dwarfs has been investigated under diverse conditions. For example, in the Newtonian framework, to optimize the temperature effects, (VAVRUKH; SMERECHYNSKYI, 2012) assumed the thermal energy is proportional to the kinetic energy of the electrons. Considering the Fermi-Dirac equation of state (EOS)–with the (SOMMERFELD, 1928) expansion–the authors found that the static equilibrium configurations derived from their model are within the results estimated by the observational data.

A generalization of the work developed in (VAVRUKH; SMERECHYNSKYI, 2012) was published by (CARVALHO *et al.*, 2014). Inspired in (ROTONDO *et al.*, 2011), who once generalized the Feynman–Metropolis–Teller treatment of compressed matter to the case of the finite temperature in a Fermi-Dirac EOS, de Carvalho *et al.* investigated the white dwarf equilibrium configurations at finite temperatures. They found that the correction in the lattice has more influence at low masses. The authors deduced that the onset of the inverse  $\beta$  – –decay instability is not altered for temperatures  $T \lesssim 10^8 K$ , however, higher temperatures could have significant influences on pycnonuclear reaction rates within white dwarfs. In addition, they also reported that the presence of temperature increases the electric field on the surface of the core of these objects. Based on the EOS derived in (CARVALHO *et al.*, 2014), (BOSHKAYEV *et al.*, 2016) analyzed the equilibrium configuration of rotating white dwarfs at finite temperatures. They reported that the impact of finite temperatures is relevant in low-mass white dwarfs, as in the estimation of the radii of these objects. Comparing their results with observational data from the Sloan Digital Sky Survey (SDSS) Data Release 4 (TREMBLAY *et al.*, 2011; NALEŻYTY; MADEJ, 2004; KOESTER; KEPLER, 2019; MADEJ *et al.*, 2004), the authors determined that their model can be used to illustrate some white dwarfs detected from the SDSS.

### 5.1.2 On the stability of white dwarfs

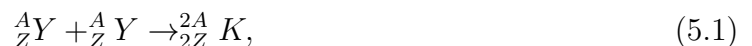
In the study of white dwarfs, an interesting physical property to analyze is their stability against some perturbations. In this sense, it is important to study and analyze how this aspect changes against small radial perturbations, pycnonuclear reactions, and inverse  $\beta$ -decay since it could give some information about the conditions that allow the existence of white dwarfs.

Since the analysis of the stability of compact objects against small radial perturbations developed in Chandrasekhar’s seminal works (CHANDRASEKHAR, 1964a; CHAN-

DRASEKHAR, 1964b), several articles have investigated the radial stability of white dwarfs at zero and nonzero temperatures, without. A few of them are described as follows. At zero temperature: In (MELTZER; THORNE, 1966) the periods and e-folding of the lowest three normal radial pulsations of white dwarf equilibrium configurations at the end point of thermonuclear evolution were investigated. The authors found that at mass densities of  $2.5 \times 10^8 < \rho < 1.3 \times 10^9 [\text{g cm}^{-3}]$ , there are metastable white dwarfs with e-folding time  $\gtrsim 10^{10}\text{yr}$ , which corresponds to Hubble time. The radial stability of zero-temperature white dwarfs was also investigated taking into account different values of the mean molecular weight per electron,  $\mu_e$ , in (WHEELER *et al.*, 1968) and accounting for two different adiabatic indices in (CHANMUGAM, 1977). These works were found a limit to the radial stability for completely degenerate white dwarfs at central mass densities  $\rho_c \lesssim 10^{10}[\text{g cm}^{-3}]$ . At nonzero temperature: White dwarfs were analyzed by using an analytical approximated EOS for the relativistic Fermi gas (BISNOVATYI-KOGAN, 1966). In that work, Bisnovatyi-Kogan found the critical mass of isothermal white dwarf depends on the central density. Using Chandrasekhar's equation for radial oscillations, (BAGLIN, 1966) reported that the relativistic effect can affect the stability of white dwarfs with low temperatures. Moreover, the author showed that radial instability is attained in lower energy densities compared to those obtained from the classical framework.

Since high-density matter in compact objects must be in chemical equilibrium against nuclear reactions, it is also important to investigate white dwarfs' stability against both pycnonuclear reactions and inverse  $\beta$ -reaction.

Pycnonuclear reactions, as schematically expressed by



have been studied for white dwarfs by (GASQUES *et al.*, 2005). The authors developed a phenomenological formalism for pycnonuclear reaction rates between identical nuclei and applied it to the carbon fusion reaction. They also found a limit for carbon burning importance of  $T \sim (4 - 15) \times 10^8 [\text{K}]$  for  $\rho \lesssim 3 \times 10^9 [\text{g cm}^{-3}]$ , and of mass density  $\rho \sim (3-50) \times 10^9 [\text{g cm}^{-3}]$  for  $T \lesssim 10^8 [\text{K}]$ . This type of reaction could be interpreted as an event preceding a Type Ia supernova explosion (NIEMEYER; WOOSLEY, 1997; HILLEBRANDT; NIEMEYER, 2000; HAN; PODSIADLOWSKI, 2004; LIU *et al.*, 2013; BARON, 2014).

An inverse  $\beta$ -reaction is an instability reached due to the decay of atom  $A(N, Z)$  into  $A(N, Z - 1)$ ,  $N$  being the mass number and  $Z$  the atomic number. This type of reaction has been investigated in the context of white dwarfs, e.g., by (ROTONDO *et al.*, 2011) and by (MATHEW; NANDY, 2017). In the first article, in the context of general relativity, the authors determined that the inverse  $\beta$ -reaction occurs above the threshold density estimated for white dwarfs. In the second work, it was found showing that the heavier

the atom element, the lower the instability threshold density.

### 5.1.3 Our aim

In this article, in the framework of general relativity, we study the static structure configuration and stability against small radial perturbations, pycnonuclear reactions and inverse  $\beta$ -decay of white dwarfs with finite temperature. Inspired by previous studies (TIMMES; ARNETT, 1999; CARVALHO *et al.*, 2014; BOSHKAYEV *et al.*, 2016), we model the EOS for hot white dwarfs taking into account a Wigner-Seitz cell composed of electrons and nucleons (SALPETER, 1961) surrounded by free photons. We consider that these stars are constituted by an isothermal core, made up of degenerate matter, and an envelope, made up of nondegenerate matter, whose temperature distribution depends on the mass density (see (BÖHM, 1968; SHAPIRO; TEUKOLSKY, 2004)). This consideration is reasonable since the energy transport occurs by conduction in the core, making the temperature almost constant, and the radiation and convection create a temperature distribution in the envelope. For this model, the static equilibrium configurations are investigated through the numerical integration of the (TOLMAN, 1939; OPPENHEIMER; VOLKOFF, 1939) (TOV) equation. We compare our results for the hot white dwarf structure with observable white dwarfs from the Extreme Ultraviolet Explorer (EUVE) and SDSS reported in (VENNES *et al.*, 1997; MADEJ *et al.*, 2004; NALEŻYTY; MADEJ, 2004; TREMBLAY *et al.*, 2011; KOESTER; KEPLER, 2019). We estimate the mass, radius and central temperature analyzing the effective temperature and gravity for massive stars with  $M/M_{\odot} \geq 1.33$  from (VENNES *et al.*, 1997). For some central temperatures and surface gravities  $\log(g/g_{\odot}) \geq 4.4$ , we obtain an equation that connects the mass with the surface gravity and effective temperature. Furthermore, we investigate the eigenfrequencies of radial oscillations using the (CHANDRASEKHAR, 1964a) pulsation equation. We correlate the behavior of radial eigenfrequency oscillations as a function of the star mass and central temperature with the existence of hot and massive white dwarfs. We also study the dependence of some physical white dwarf properties such as the fluid pressure, energy density, mass, radius, and the fundamental-mode eigenfrequency on the temperature.

This article is organized as follows: In section 5.2 the EOS is described. Section 5.3 describes both the stellar equilibrium equations and the radial stability equations and their boundary conditions. In section 5.4 is depicted the pycnonuclear reactions and inverse  $\beta$ -decay inside white dwarfs. The results are presented in section 5.5. Finally, we conclude in section 7. Throughout this article we consider the units  $c = 1 = G$ , where  $c$  and  $G$  represent the speed of light and the gravitational constant.

## 5.2 The EOS

The first assumption about the matter that makes up white dwarfs came from Chandrasekhar's works (CHANDRASEKHAR, 1931a; CHANDRASEKHAR, 1935) with the theory of the degenerate electron gas. These pioneering works have been extended to include the electrostatic energy by (AULUCK; MATHUR, 1959) and to insert Thomas–Fermi deviations from an uniform charge distribution of the electrons and the exchange energy and spin–spin interactions between the electrons (SALPETER, 1961), which were used to determine the white dwarf mass and radius in (HAMADA; SALPETER, 1961). According to (HAMADA; SALPETER, 1961), the electron density of stars is affected by these implementations, decreasing Chandrasekhar's mass limit. General relativity and temperature effects were investigated concerning the stability of white dwarfs in (BISNOVATYI-KOGAN, 1966), where a critical density and temperature as a function of the star mass were obtained. In that work, it was already concluded that the critical density for the electron capture reaction responsible for the neutralization of white dwarfs should appear before the threshold density of the general relativity instability.

The stability of white dwarfs with Salpeter's correction was studied by (WHEELER *et al.*, 1968) considering pycnonuclear reactions and electron capture reactions, thermonuclear processes, and radial oscillations. The effects of the magnetic field and rotation in white dwarfs were investigated by (OSTRIKER; HARTWICK, 1968), who found that moderated magnetic fields can increase the radius of white dwarfs. Another approach for the high-density matter EOS was proposed by (FEYNMAN *et al.*, 1949) and used to investigate the radial oscillation and stability of white dwarfs by (CHANMUGAM, 1977). (LAI; SHAPIRO, 1991) on the 1990s also investigated the effect of strong magnetic fields in the degenerate EOS, and in particular, in the Baym–Pethick–Sutherland EOS BPS used in the neutron star crust. An important review that takes into account all the progress made up to the 1990s concerning white dwarfs' structure and EOS and also the physical processes in the nondegenerate envelope was written by (KOESTER; CHANMUGAM, 1990).

A comprehensive review regarding the EOS of white dwarfs and neutron stars was done in (BALBERG; SHAPIRO, 2000) where condensed matter at extreme densities was discussed. Recently, the (FEYNMAN *et al.*, 1949) approximation has been applied in many works on white dwarfs, such as in investigations of white dwarf matter (RUFFINI, 2000; BERTONE; RUFFINI, 2000), relativistic corrections (ROTONDO *et al.*, 2011), and the inclusion of temperature in corrections (CARVALHO *et al.*, 2014). Inspired by (LAI; SHAPIRO, 1991) work on neutron stars, white dwarfs with magnetic fields have been investigated using the electron–ion interactions with a body-centered cubic lattice correction (OTONIEL *et al.*, 2019), and also with the addition of face-centered cubic, simple cubic, and hexagonal close-packed lattices (CHAMEL *et al.*, 2014). Since the EOS used by Salpeter allows

us to obtain white dwarf static equilibrium configurations similar to the ones obtained using the other EOSs reported in the previously mentioned works, we have decided to use Salpeter's approach. In such a way, the total pressure that supports the white dwarf against the collapse and the total energy density are, respectively, considered as follows:

$$P = P_L + P_R + P_i + P_e, \quad (5.2)$$

$$\varepsilon = \varepsilon_L + \varepsilon_R + \varepsilon_i + \varepsilon_e, \quad (5.3)$$

where  $P$  and  $\varepsilon$  with subscripts  $L$ ,  $R$ ,  $i$ , and  $e$  indicate, respectively, the pressure and density of the lattice (with (SALPETER, 1961) correction), radiation, nucleons, and electrons (TIMMES; ARNETT, 1999). The numerical method to obtain the energy density and pressure contributions of Eqs. (5.2) and (5.3) is explained in detail in subsection 5.5.1.

We consider that these stars to be constituted of an isothermal core, made up of degenerate matter, and an envelope, made up of nondegenerate matter, whose temperature distribution depends on the mass density of the form (BÖHM, 1968; SHAPIRO; TEUKOLSKY, 2004)

$$T/\rho^{2/3} = \text{constant}. \quad (5.4)$$

This temperature–density distribution is valid only for densities below the threshold of degeneracy. The temperature–density distribution obtained from the envelope models of carbon white dwarfs found by Kritcher and collaborators (KRITCHER, 2020) is different from the relation in Eq. (5.4). We test the temperature–density profiles of (KRITCHER, 2020) in our EOS and the results are very similar to the ones obtained in our work with Eq. (5.4). In fact, the sensitivity in the EOS of these temperature–density profiles is quite low since in the envelope the ranges of temperatures and densities are quite small compared to the core ones.

## 5.3 Stellar equilibrium equations and radial perturbation equations

### 5.3.1 The energy momentum tensor and the background line element

The fluid that makes up the white dwarfs is depicted by the perfect energy momentum tensor, which can be represented in the form

$$T_{\mu\nu} = (p_0 + \varepsilon_0) u_\mu u_\nu - p_0 g_{\mu\nu}. \quad (5.5)$$

$u_\mu$  and  $g_{\mu\nu}$  stand for fluid's four–velocity and the metric tensor, respectively.

The unperturbed line element employed to investigate the equilibrium configuration of hot white dwarfs is of the form

$$ds^2 = e^{\nu_0} dt^2 - e^{\lambda_0} dr^2 - r^2(d\theta^2 + \sin^2 \theta d\phi^2), \quad (5.6)$$

where  $(t, r, \theta, \phi)$  are the Schwarzschild-like coordinates.

The variables of the fluid  $P_0$  and  $\varepsilon_0$ , and of the metric  $\nu_0$  and  $\lambda_0$  are functions of the coordinates  $t$  and  $r$ . When radial stability against small radial perturbations is investigated, following the Chandrasekhar method, the functions aforementioned functions with subscript 0 can be divided into the form (CHANDRASEKHAR, 1964a):

$$f_0(t, r) = f(r) + \delta f(t, r). \quad (5.7)$$

$f(r)$  denotes the physical quantities of the fluid and the unperturbed metric functions.  $\delta f(t, r)$  represents the Eulerian perturbations that depend on the coordinates  $t$  and  $r$ .

### 5.3.2 Stellar equilibrium equations

The stellar equilibrium equations employed to investigate the configuration of white dwarfs in a static regime, i.e., in an unperturbed system,  $\delta f(t, r) = 0$ , are placed as follows

$$\frac{dm}{dr} = 4\pi\varepsilon r^2, \quad (5.8)$$

$$\frac{dp}{dr} = -(p + \varepsilon) \left( 4\pi r p + \frac{m}{r^2} \right) e^\lambda, \quad (5.9)$$

$$\frac{d\nu}{dr} = -\frac{2}{p + \varepsilon} \frac{dp}{dr}, \quad (5.10)$$

with

$$e^\lambda = \left( 1 - \frac{2m}{r} \right)^{-1}. \quad (5.11)$$

As usual, the function  $m$  represents the mass within a sphere of a radius  $r$ . Equation (5.9) is known as the hydrostatic equilibrium equation, also called the TOV equation.

After deriving the EOS, Eqs. (5.2) and (5.3), with the aim of looking for equilibrium solutions, we solve simultaneously the stellar equilibrium equations (Eqs. (5.8)-(5.10)). This set of equations is integrated from the center ( $r = 0$ ) to the star's surface ( $r = R$ ). The initial conditions at the center of the star are

$$m(0) = 0, \quad \varepsilon(0) = \varepsilon_c, \quad T(0) = T_c, \quad \text{and} \quad \nu(0) = \nu_c. \quad (5.12)$$

The star's surface is found when

$$P(R) = 0, \quad (5.13)$$

and consequently  $T(r = R) = 0$ . At this point, the interior solution connects smoothly to the spacetime outside the star. This indicates that the interior and exterior metric functions are related as follows:

$$e^{\nu(R)} = e^{-\lambda(R)} = 1 - \frac{2M}{R}, \quad (5.14)$$

where  $M$  represents the total mass of the star. In addition, this relation provides the boundary condition for the functions  $\nu$  and  $\lambda$  at the star's surface.

### 5.3.3 Radial perturbation equations

To investigate the stability of white dwarfs against small radial perturbations, it is necessary to determine the radial oscillation equations. For such an aim, firstly, the Eulerian perturbations must be derived. Once the nonzero four-velocity components are defined, the fluid and spacetime variables are decomposed into the form presented in Eq. (5.7). After replacing these definitions and decompositions in the field equations, the Eulerian perturbations are found just keeping the first-order terms.

The radial pulsation equation is derived taking into account the linearized form of the stress energy tensor conservation and the Eulerian perturbations, and considering that the perturbed quantities have a time dependence  $e^{i\omega t}$ , where  $\omega$  is the eigenfrequency. This constant parameter is determined through the equality (CHANDRASEKHAR, 1964a; BAGLIN, 1966)

$$\omega^2 = \frac{\mathcal{Z}}{\mathcal{D}}. \quad (5.15)$$

The functions  $\mathcal{Z}$  and  $\mathcal{D}$  are, respectively, determined by the equations

$$\begin{aligned} \mathcal{Z} = & 4 \int_0^R e^{\nu+\lambda/2} r^3 \frac{dp}{dr} dr + 8\pi \int_0^R e^{\nu+3\lambda/2} p(p+\varepsilon) r^4 dr + 9 \int_0^R e^{\nu+\lambda/2} r^2 \Gamma p dr \\ & - \int_0^R \frac{e^{\nu+\lambda/2} r^4}{(p+\varepsilon)} \left[ \frac{dp}{dr} \right]^2 dr, \end{aligned} \quad (5.16)$$

$$\mathcal{D} = \int_0^R e^{3\lambda/2} (p+\varepsilon) r^4 dr, \quad (5.17)$$

where  $\Gamma$  represents the adiabatic index and it is determined by the condition

$$\Gamma = \frac{d \log p}{d \log \varepsilon}. \quad (5.18)$$

Equation (5.15) helps us to discriminate stable equilibrium solutions from unstable

ones. This is made possible by analyzing the eigenfrequency values  $\omega$ .

## 5.4 Pycnonuclear reactions and inverse $\beta$ -decay

### 5.4.1 Pycnonuclear reactions

The possible occurrence of pycnonuclear reactions in dense stellar matter (YAKOVLEV *et al.*, 2005) creates a constraint in white dwarf's chemical composition. These reactions are almost independent of temperature and appear even at zero temperature. A rigorous approach to calculating these nuclear reactions was realized by (SALPETER; HORN, 1969), who established a ratio of the temperature-dependent pycnonuclear rate to the zero-temperature rate. For a pure-carbon core (OTONIEL *et al.*, 2019), where  $^{12}\text{C} + ^{12}\text{C} \rightarrow ^{24}\text{Mg}$ , this reaction rate can be written as (SALPETER; HORN, 1969):

$$\frac{R_{\text{pyc}}(T)}{R_{\text{pyc}}(0)} - 1 = a_1 \lambda^{-1/2} \left[ 1 + a_2 e^{b_1 \beta^{3/2}} \right]^{-1/2} \times \exp \left\{ b_2 \beta^{3/2} + \lambda^{-1/2} a_3 e^{b_1 \beta^{3/2}} \left[ 1 - a_4 e^{b_1 \beta^{3/2}} \right] \right\}, \quad (5.19)$$

where  $R_{\text{pyc}}(0)$  represents the pycnonuclear reaction at zero temperature, and  $a_1$ ,  $a_2$ ,  $a_3$ ,  $a_4$ ,  $b_1$ , and  $b_2$  are model-dependent dimensionless constants.

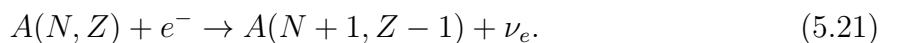
The time to complete the atomic nuclear fusion is obtained from previous studies (GASQUES *et al.*, 2005; BOSHKAYEV *et al.*, 2013; OTONIEL *et al.*, 2019)

$$\tau_{\text{pyc}} = \frac{n_N}{R_{\text{pyc}}}. \quad (5.20)$$

As considered in (OTONIEL *et al.*, 2019), we employ a pycnonuclear reaction time  $\tau_{\text{pyc}} = 10$  [Gyr], which corresponds to an upper limit where pycnonuclear reactions are extremely slow (CHUGUNOV *et al.*, 2007). For white dwarfs, a limit of  $\rho_{\text{pyc}}(10$  [Gyr]) corresponds to a maximum mass density for stable stars against pycnonuclear reactions. Through these times, we can estimate the mass density where these reactions appear,  $\rho_{\text{pyc}}(\tau_{\text{pyc}})$ . For white dwarfs, the limit of  $\rho_{\text{pyc}}(10$  [Gyr]) corresponds to a maximum density for stable stars, since from this point pycnonuclear reactions begin to appear.

### 5.4.2 Inverse $\beta$ -decay

It is known that the matter inside white dwarfs may experience instability against the inverse  $\beta$ -decay process,



Due to this process, atomic nuclei become more neutron-rich, and as a consequence, the electron energy density and pressure are reduced thus leading to a softer EOS (GAMOW, 1939; SHAPIRO; TEUKOLSKY, 2004). Since we are considering a nucleus of  $^{12}\text{C}$ , the instabilities are reached at energies higher than  $\epsilon_Z^\beta = 13.370$  [MeV] (see (ROTONDO *et al.*, 2011; CARVALHO *et al.*, 2014; OTONIEL *et al.*, 2019)).

## 5.5 Equilibrium and stability of hot white dwarfs

### 5.5.1 Numerical method

Due to the partial degeneracy considered in this model, the pressure and energy of electrons appearing on the EOS (Eqs. (5.2) and (5.3)) are solved numerically by means of the adaptive quadrature method. Through this numerical method, we reproduce the results reported in (VAVRUKH; SMERECHYNSKYI, 2012), which resolved the same EOS through the Sommerfeld approximation, and the results found in (CARVALHO *et al.*, 2014; BOSHKAYEV *et al.*, 2016), where the authors investigated the equilibrium of white dwarfs with a constant finite temperature.

Once the EOS is defined, both the stellar equilibrium equations, Equations. (5.8)-(5.10), and the radial stability equations, Equations (5.16) and (5.17), are integrated from the center ( $r = 0$ ) toward the surface of the spherical object ( $r = R$ ) through the Runge-Kutta fourth-order method for different values of  $\epsilon_c$  and  $T_c$  and a trial value for  $\nu_c$ .

The numerical solution of the stellar structure equations begins with the initial conditions (5.12) at  $r = 0$ . Once  $\epsilon_c$ ,  $T_c$ , and  $\nu_c$  are given, the integration proceeds from the center toward the star's surface where  $P(R) = 0$ . Nonetheless, if after the integration the condition of Equation (5.14) is not satisfied,  $\nu_c$  is corrected through a Newton-Raphson iteration scheme until it fulfills this condition. Thus, the zero fluid pressure determines the total radius  $r = R$  and total mass  $M = m(R)$ .

After the coefficients  $p$ ,  $\epsilon$ ,  $m$ ,  $\lambda$ , and  $\nu$  are determined for each  $\epsilon_c$ ,  $T_c$ , and correct  $\nu_c$ , the radial stability equations are integrated from the center to the surface of the star. After the integration, the eigenfrequency squared is found by Eq. (5.15).

### 5.5.2 Influence of temperature on the fluid pressure, energy density, and mass of the star

With the purpose of observing the EOS behavior, in Figure 5.1 plots the change of the fluid pressure against the energy density for different central temperatures. The energy

density employed goes from  $10^3$  [ $\text{g cm}^{-3}$ ] to  $10^{11}$  [ $\text{g cm}^{-3}$ ].

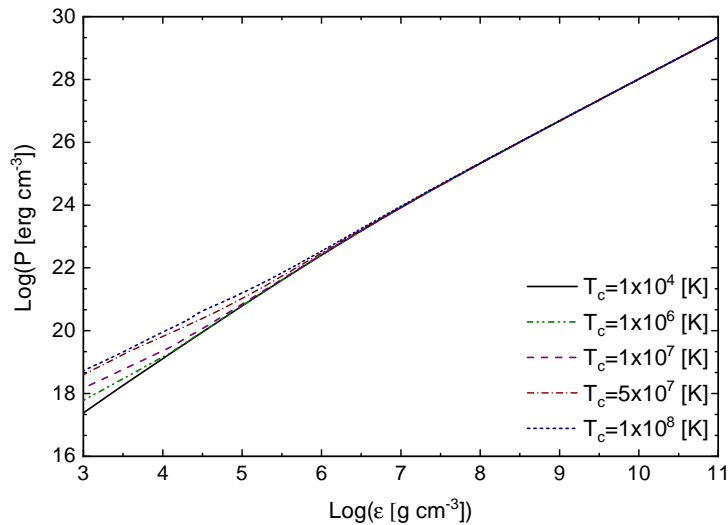


FIGURE 5.1 – Fluid pressure compared against the energy density for some different central temperatures.

In Figure 5.1, in all cases presented, it can be observed that the pressure decays monotonically with the energy density. Moreover, the effects of central temperature are noted in the graph. At low energy densities, the pressure has a slight growth with central temperature. This increment is associated with the increase of the radiation pressure, and the pressure of the nucleons.

At the central energy density  $10^4$  [ $\text{g cm}^{-3}$ ] and central temperature interval  $[10^4, 10^7]$  [K], we find fluid pressure similar to those ones reported by (CARVALHO *et al.*, 2014); namely, we derive  $p_c$  in the range  $[1 \times 10^{19}, 2 \times 10^{19}]$  [ $\text{erg/cm}^3$ ]. This result can be understood too be due to the fact that the temperature distribution is constant in the aforementioned range of  $\epsilon$  and  $T_c$ , and the treatment assumed in this work (Salpeter correction) and the one employed by (CARVALHO *et al.*, 2014) (Feynman–Metropolis–Teller treatment) are similar. In addition, the central pressures found are lower than the one derived by (BOSHKAYEV *et al.*, 2016). This could be associated with the fact that we are considering the Wigner–Seitz lattice correction.

The star mass as a function of the radial coordinate is presented in Fig. 5.2 for a white dwarf with a total mass of  $1.37M_\odot$  and several central temperatures. From this figure, we conclude that for a fixed star mass, the effect of the temperature is still important for very massive white dwarfs: when the temperature increases, the star radius increases, and this effect is more pronounced for central temperatures  $T_c \geq 10^8$  [K]. For the extreme case of a central temperature  $T_c = 10^8$  [K] the radius increases by 135% as compared to  $T_c = 10^4$  [K] due to the nucleons' pressure. This result was not observed for near–Chandrasekhar–mass white dwarfs with finite temperatures in a previous study (BOSHKAYEV *et al.*, 2016), since

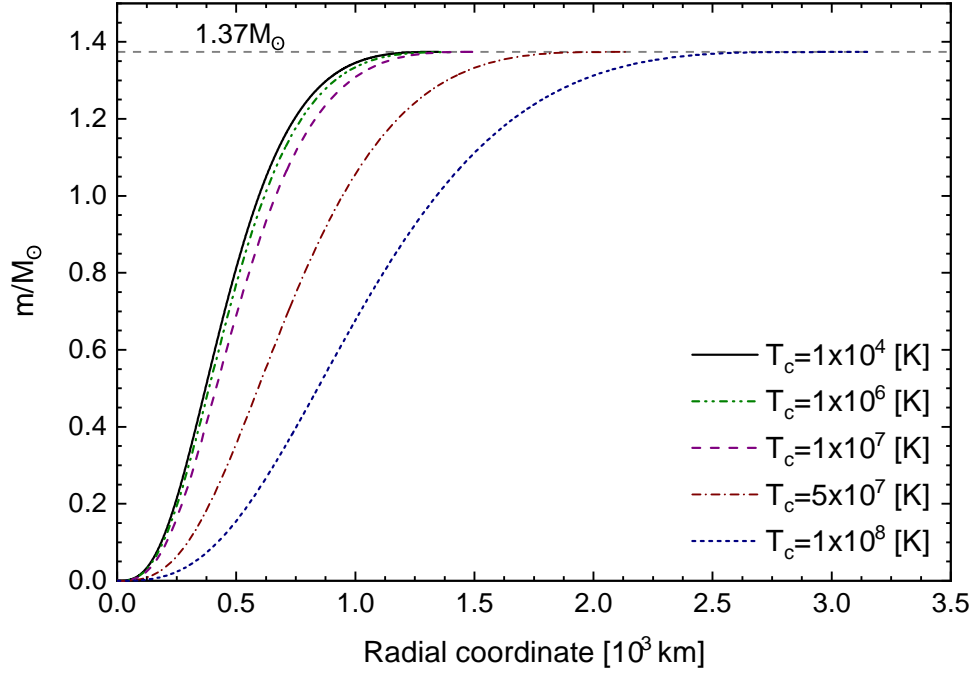


FIGURE 5.2 – Mass, normalized in solar masses  $M_{\odot}$ , as a function of the radial coordinate for five central temperature values and a total mass  $M = 1.37M_{\odot}$ .

this thermal pressure was not taken into account. This is an important observation since very massive white dwarfs, with larger radii than the ones derived for low temperatures ( $T_c \leq 10^4$ [K]), are an indication of lower surface gravity compared to the ones observed for cold white dwarfs (since  $g \sim 1/r$ ), and of high central temperature. In summary, it is important to consider the mass-radius relation obtained at finite temperature in the case of very massive white dwarfs, in order to obtain the correct mass and star radius from the observed surface gravity and effective temperature values.

### 5.5.3 Equilibrium configurations of hot white dwarfs

#### 5.5.3.1 Hot white dwarf equilibrium configuration sequence

The gravitational mass, in solar masses  $M_{\odot}$ , as a function of the central energy density is plotted in Fig. 5.3 for different central temperatures. It is considered at central energy densities within the interval  $10^5$  [g cm $^{-3}$ ]  $\leq \varepsilon_c \leq 10^{11}$  [g cm $^{-3}$ ]. The filled triangles placed over the curves mark the points where the maximum masses are attained.

In Fig. 5.3, in all central temperatures considered, we note that the curves present two branches. In the first one, the mass grows monotonically with  $\varepsilon_c$  until it reaches its maximum mass value ( $M_{\max}/M_{\odot}$ ); after this point, the curve turns downward for the mass starts to decay with the growth of  $\varepsilon_c$ . The central energy density used to determine the maximum-mass points coincide with the  $\varepsilon_c$  employed to find the eigenfrequency of the

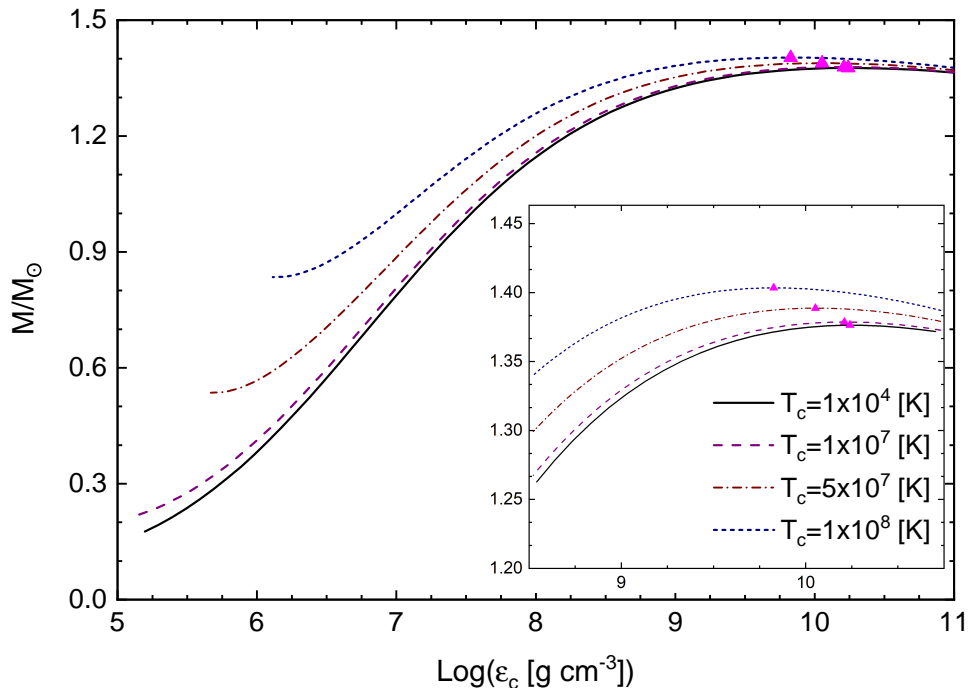


FIGURE 5.3 – Mass of the star, normalized to the Sun mass  $M_{\odot}$ , as a function of central energy density for four different central temperature values. The filled triangles over the curves represent the maximum-mass points. The box within the figure shows the region where the maximum mass values are found.

fundamental mode  $\omega = 0$ . This indicates that the maximum-mass point divides regions constituted by stable equilibrium configurations from regions established by the unstable ones. Thus, regions made up of stable and unstable equilibrium configurations against small radial perturbations are differentiated through the inequalities  $dM/d\varepsilon_c > 0$  and  $dM/d\varepsilon_c < 0$ , respectively. These conditions are necessary and sufficient to recognize a stable region from an unstable one.

Equilibrium configurations with energy densities lower than those considered in curves with  $T_c \gtrsim 5 \times 10^7$  [K] are also analyzed. As in previous references (CARVALHO *et al.*, 2014; BOSHKAYEV *et al.*, 2016), it is found that the total mass decreases with the increment of the central energy density. Moreover, these equilibrium configurations have an eigenfrequency of the fundamental mode close to zero ( $\omega \sim 0$ ).

The behavior of the total mass as a function of the radius is plotted in Figure 5.4 for a few different central temperatures. The filled triangles in pink over the curves indicate the maximum-mass points. The largest total radii shown in each curve are derived from the respective minimum central energy density value considered in each curve of Fig. 5.3. As already mentioned, for lower central energy densities than those mentioned, the eigenfrequency of the fundamental mode is close to zero. Moreover, in the figure, some observational results obtained from the catalogs in (TREMBLAY *et al.*, 2011),

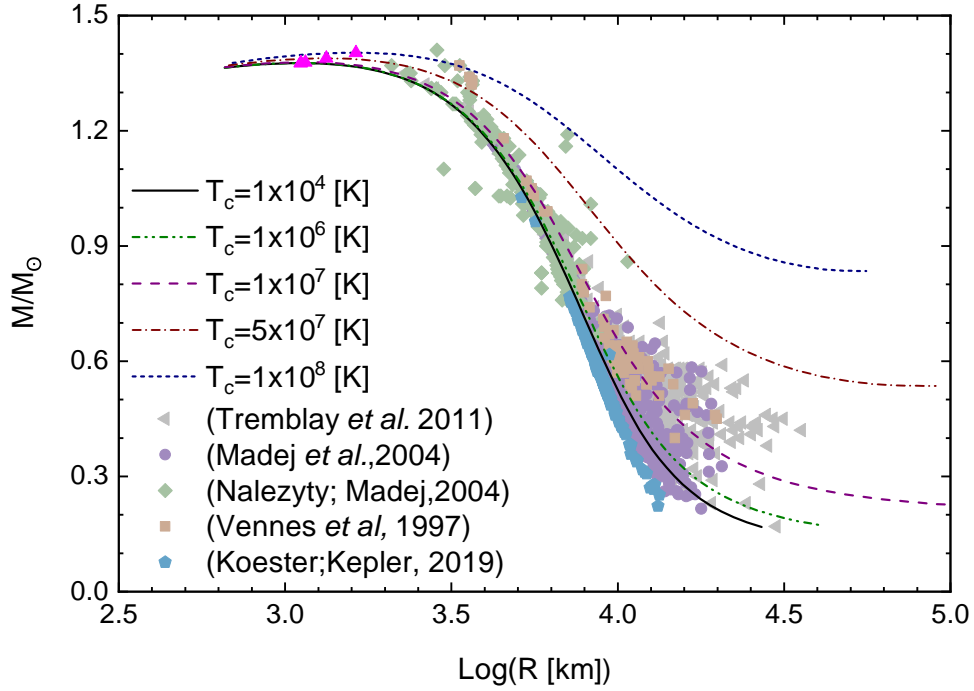


FIGURE 5.4 – Mass–radius curves for different central temperatures. The filled triangles represent maximum–mass points. Observational data extracted from the catalogs (TREMBLAY *et al.*, 2011), (NALEŻYTY; MADEJ, 2004), (KOESTER; KEPLER, 2019), (VENNES *et al.*, 1997) and (MADEJ *et al.*, 2004) are, respectively marked with gray triangles, purple circles, green diamonds, orange squares, and blue hexagons.

(NALEŻYTY; MADEJ, 2004), (KOESTER; KEPLER, 2019), (VENNES *et al.*, 1997) and (MADEJ *et al.*, 2004) are, respectively presented as gray triangles, purple circles, green diamonds, orange squares, and blue hexagons.

The central temperature’s influence on the total mass and radius is noted in Fig. 5.4. In all curves, the mass grows monotonically with the diminution of the total radius until it reaches  $M_{\text{max}}/M_{\odot}$ . After this point, the  $M(R)$  curves turn upward as to the masses start to decrease with the radii diminution. In the figure, a large group of white dwarfs detected is placed below  $M = 1.3 M_{\odot}$  and  $T_c = 10^7$  [K] and a small group is located in higher masses and central temperatures. These results could indicate that the mass of a white dwarf is associated with the central temperature in its cores, i.e., for higher central temperatures, more massive white dwarfs are found. The growth of the mass with the temperature could be understood by noting that some factors that compose the total fluid pressure—the pressures coming from the radiation, and nucleons—increase with  $T_c$ . This increment in the pressure helps to support more mass against collapse. Near the maximum–mass limit, we notice that some of the white dwarfs observed are within the range of masses with high central temperature. In particular, they present a small gravity value compared to the obtained for low-temperature white dwarfs.

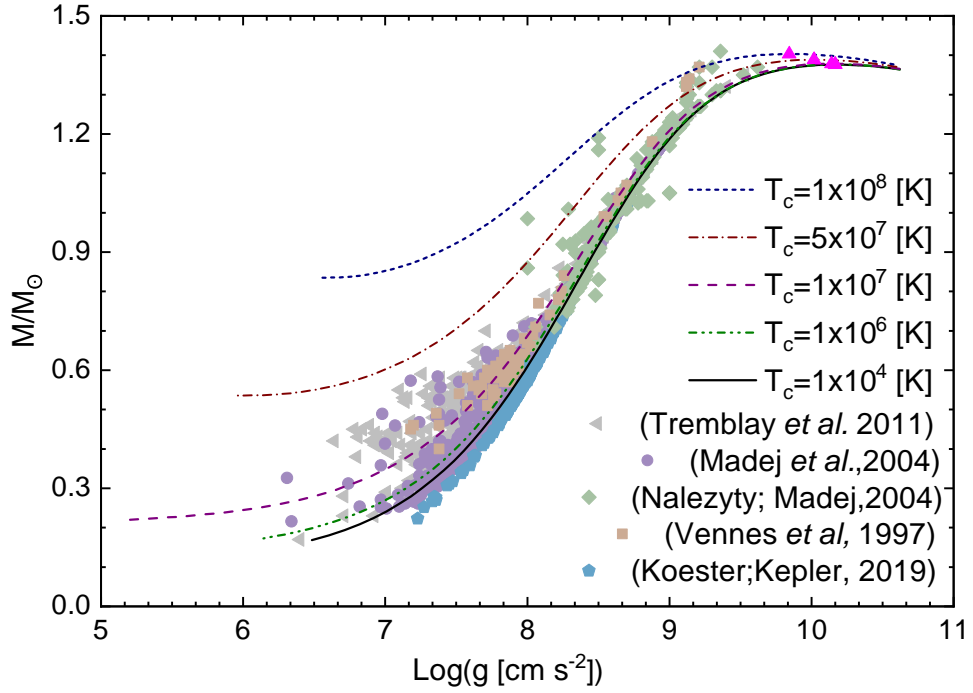


FIGURE 5.5 – The surface gravity of the white dwarf against its total gravitational mass, for some central temperatures. The filled triangles over the curves mark the maximum-mass points. Observational results obtained from the catalogs in (TREMBLAY *et al.*, 2011), (NALEŻYTY; MADEJ, 2004), (KOESTER; KEPLER, 2019), (VENNES *et al.*, 1997) and (MADEJ *et al.*, 2004) are, respectively indicated by gray triangles, purple circles, green diamonds, orange squares, and blue hexagons.

Comparing our results with the ones reported by (BOSHKAYEV *et al.*, 2016), for a star made up of  $^{12}\text{C}$  and having  $\mu_e = 2$ , with a central energy density of  $10^6$  [ $\text{g cm}^{-3}$ ] and temperature  $T = 10^6$  [K], we find that the mass of the star is smaller by 7% and the radius is larger by 23%, and for a temperature of  $T = 10^7$  [K], what is derived is nearly the same total mass and a radius greater by 34%. As can be seen, the mass derived in this work is in good agreement with the one reported by (BOSHKAYEV *et al.*, 2016), unlike the total radius, which differs significantly. The radii derived are larger due to the inclusion of the nucleon’s pressure, thermal energy, lattice corrections, and electron energy contributions in the EOS. In the maximum total mass range, we find that the white dwarfs’ masses depend on central temperature, unlike the ones published in (BOSHKAYEV *et al.*, 2016), where the total masses stay independent of the temperature. For instance, for  $T_c = 10^8$  [K], we find as maximum mass value of  $1.40M_\odot$  and a respective total radius of 1400 [km], while (BOSHKAYEV *et al.*, 2014) found a white dwarf with a mass of  $1.43M_\odot$  and a radius of 1000 [km]. This difference is associated with the nucleons’ pressure effects, which are still important for massive white dwarfs, and not only for the low-mass ones. It is the first time that the nucleons’ pressure is taken into account in a study of massive white dwarfs; it was previously considered in the analysis of low-mass

TABLE 5.1 – The central temperature employed with the maximum masses with their respective total radii and central energy density

$T_c$ (K)	$M_{\max}$ $M_{\odot}$	$R$ (km)	$\varepsilon_c$ ( $\text{g cm}^{-3}$ )
$1.0 \times 10^6$	1.3766	1114.9	$1.7440 \times 10^{10}$
$1.0 \times 10^7$	1.3787	1150.1	$1.6216 \times 10^{10}$
$5.0 \times 10^7$	1.3887	1334.6	$1.1181 \times 10^{10}$
$1.0 \times 10^8$	1.4034	1630.8	$6.7469 \times 10^9$

white dwarfs (CARVALHO *et al.*, 2014).

The gravity at the white dwarf surface versus the gravitational mass is shown in Figure 5.5 for different central temperatures. The filled triangles over the curves mark the maximum mass values. Some observational data taken from the catalogs (TREMBLAY *et al.*, 2011), (NALEŻYTY; MADEJ, 2004), (KOESTER; KEPLER, 2019), (VENNES *et al.*, 1997) and (MADEJ *et al.*, 2004) are, respectively, marked with gray triangles, purple circles, green diamonds, orange squares, and blue hexagons. In all cases, the total mass grows monotonically with the gravity until it attains a maximum mass value; after this point, the curve turns downward as the mass starts to decrease with the increment of gravity.

From Figure 5.5, we can note that for a fixed value of surface gravity, the total mass increases with the central temperature. The growth of the mass with the central temperature can be explained by noting that the central pressure increases with  $T_c$ ; from this, we understand that the central temperature acts as an effective pressure that helps the fluid pressure to support more mass against collapse.

The results reported in Figs. 5.4 and 5.5 are important in the cooling study of hot  $T_c > 10^7$  [K] and very massive white dwarfs  $M > 1.37M_{\odot}$ . In the common cooling process, these stars shrink, thus keeping constant the baryonic mass (ALTHAUS *et al.*, 2010) and increasing their densities. In our curves with constant gravitational mass, this would occasion them to run from a stable region to an unstable one (according to the threshold of instabilities due to radial oscillations, pycnonuclear reactions, and inverse  $\beta$ -decay; see Section 4.3). This evolutionary instability could explain the star collapse and justify an interesting mass limit for observable white dwarfs. Besides, as we consider the gravitational mass and not the baryonic one for this analysis, such collapse would not occur if they lose enough gravitational mass, thus allowing a stable cooling. To obtain a robust conclusion regarding this possible mechanism originating Type Ia supernova explosions further investigations are needed.

In Table 5.1, the central temperatures  $T_c$  used and the maximum white dwarf mass values and their respective radii and central energy densities are shown. It is found that for central temperatures in the range  $10^4 < T_c \lesssim 10^7$  [K], near the maximum total mass,

white dwarf masses remain nearly constant. At this range, the total pressure stays nearly constant with the increment of temperature, since the electron pressure decays with  $T$ , and the radiation pressure and the pressure of nucleons do not contribute considerably to the white dwarf's structure. In contrast, for  $T_c \gtrsim 10^7$  [K], an increase in total mass is observed. At this central temperature range, the contributions of  $P_R$  and  $P_N$  produce considerable effects on the white dwarf's structure. Thus, the white dwarf's mass at  $T_c \gtrsim 10^7$  [K] is larger than  $M/M_\odot$  at  $10^4 < T_c \lesssim 10^7$  [K]. On the other hand, in all cases analyzed here, at the maximum masses, it is found that the respective total radii and central energy densities increase and decrease with temperature, respectively.

### 5.5.3.2 The procedure to identify central temperatures in massive white dwarfs

The existence of some very massive white dwarfs has been shown by (VENNES *et al.*, 1997). According to their analysis, they obtained the effective temperature and gravity and used a fitting method to estimate the mass of such stars. In order to verify our model, we use the effective temperature and gravity reported in (VENNES *et al.*, 1997) to fit our curves. In our model, the effective temperature is obtained using the Stefan–Boltzmann law in the photons' luminosity, which depends on the elements' mass contributions (see (SHAPIRO; TEUKOLSKY, 2004)).

In Table 5.2, we report the data from (VENNES *et al.*, 1997) for some observational white dwarfs with  $M_{He} = 10^{-4}M_\odot$  and their mass, radius, central temperature, and  $\alpha$ , with  $\alpha$  being a dimensionless parameter that relates the effective temperature, gravity, and central temperature by means of the following relation (KOESTER, 1976)

$$\frac{T_{eff}^4}{g} = 2.05 \times 10^{-10} T_c^\alpha. \quad (5.22)$$

The index  $\alpha$  takes the value of 2.56 in (KOESTER, 1976).

From the results in Table 5.2, we can note that our mass presents values in the same range as the ones reported in (VENNES *et al.*, 1997), except for WD 1659 + 440 since (VENNES *et al.*, 1997) found a mass of  $1.41 \pm 0.04M_\odot$  for it and we obtain  $1.33 \pm 0.01M_\odot$ . This is due mainly to general relativity effects, which are more remarkable at large total masses. For all stars analyzed, we note that our radius results are within the same range as the ones reported in (VENNES *et al.*, 1997). Besides that, we find  $\alpha = 2.48 \pm 0.03$ . This result is within the range of the values reported in (KOESTER, 1972),  $\alpha = 2.50$ , and (KOESTER, 1976),  $\alpha = 2.56$ . The central temperature related to these massive white dwarfs suggests that some of them like EQ J0443 – 037, EQ J0916 – 197, and EUVE J1535 – 77.4 can have a high central temperature.

In Table 5.3, we analyze the same white dwarfs shown in Table 5.2 but considering

TABLE 5.2 – Comparison between the data reported by (VENNES *et al.*, 1997) and the results derived in this work for a helium surface.

Simbad Name	$T_{\text{eff}}$ $10^4$ (K)	$\log(g)$ ( $\text{cm/s}^2$ )	$M$ ( $M_{\odot}$ )	$R$ $10^3$ (km)	$M$ ( $M_{\odot}$ )	$R$ $10^3$ (km)	$T_c$ $10^7$ (K)	$\alpha$
EUVE J0003 + 43.6	4.24	$9.30 \pm 0.12$	$1.37 \pm 0.12$	$3.02 \pm 0.21$	$1.33 \pm 0.02$	$2.97 \pm 0.39$	$4.54 \pm 0.36$	$2.47 \pm 0.03$
WD 0136 + 251	3.94	$9.12 \pm 0.13$	$1.28 \pm 0.07$	$3.59 \pm 0.26$	$1.30 \pm 0.03$	$3.61 \pm 0.50$	$4.70 \pm 0.40$	$2.47 \pm 0.03$
WD 0346 – 011	4.32	$9.21 \pm 0.05$	$1.33 \pm 0.03$	$3.30 \pm 0.09$	$1.32 \pm 0.01$	$3.28 \pm 0.18$	$4.91 \pm 0.16$	$2.47 \pm 0.01$
EQ J0443 – 037	6.51	$9.12 \pm 0.12$	$1.29 \pm 0.06$	$3.60 \pm 0.24$	$1.33 \pm 0.02$	$3.65 \pm 0.48$	$8.36 \pm 0.67$	$2.50 \pm 0.03$
EQ J0916 – 197	5.64	$9.12 \pm 0.20$	$1.29 \pm 0.11$	$3.60 \pm 0.40$	$1.32 \pm 0.03$	$3.64 \pm 0.80$	$7.12 \pm 0.94$	$2.49 \pm 0.05$
WD 1659 + 440	3.05	$9.38 \pm 0.07$	$1.41 \pm 0.04$	$2.86 \pm 0.11$	$1.33 \pm 0.01$	$2.70 \pm 0.21$	$2.95 \pm 0.14$	$2.44 \pm 0.02$
EUVE J1535 – 77.4	5.80	$9.14 \pm 0.07$	$1.30 \pm 0.11$	$3.54 \pm 0.39$	$1.32 \pm 0.03$	$3.55 \pm 0.79$	$7.26 \pm 0.95$	$2.49 \pm 0.05$

Columns 2–5: Massive white dwarfs observed, with their respective effective temperatures and gravity on their surfaces. Columns 6–9: Mass, radius, central temperature and  $\alpha$  parameter for  $M_{\text{He}} = 10^{-4}M_{\odot}$  derived by using our numerical results. The mass, radius, and central temperature are obtained by fitting the effective temperature and gravity for  $M_{\text{He}} = 10^{-4}M_{\odot}$ .

**Reference.** (VENNES *et al.*, 1997).

 TABLE 5.3 – Comparison between the data reported by (VENNES *et al.*, 1997) and the results derived in this work for a helium surface.

Simbad Name	$T_{\text{eff}}$ $10^4$ (K)	$\log(g)$ ( $\text{cm/s}^2$ )	$M$ ( $M_{\odot}$ )	$R$ $10^3$ (km)	$M$ ( $M_{\odot}$ )	$R$ $10^3$ (km)	$T_c$ $10^7$ (K)	$\alpha$
EUVE J0003 + 43.6	4.24	$9.30 \pm 0.12$	$1.37 \pm 0.12$	$3.02 \pm 0.21$	$1.33 \pm 0.02$	$2.97 \pm 0.39$	$4.54 \pm 0.36$	$2.47 \pm 0.03$
WD 0136 + 251	3.94	$9.12 \pm 0.13$	$1.28 \pm 0.07$	$3.59 \pm 0.26$	$1.30 \pm 0.03$	$3.61 \pm 0.50$	$4.70 \pm 0.40$	$2.47 \pm 0.03$
WD 0346 – 011	4.32	$9.21 \pm 0.05$	$1.33 \pm 0.03$	$3.30 \pm 0.09$	$1.32 \pm 0.01$	$3.28 \pm 0.18$	$4.91 \pm 0.16$	$2.47 \pm 0.01$
EQ J0443 – 037	6.51	$9.12 \pm 0.12$	$1.29 \pm 0.06$	$3.60 \pm 0.24$	$1.33 \pm 0.02$	$3.65 \pm 0.48$	$8.36 \pm 0.67$	$2.50 \pm 0.03$
EQ J0916 – 197	5.64	$9.12 \pm 0.20$	$1.29 \pm 0.11$	$3.60 \pm 0.40$	$1.32 \pm 0.03$	$3.64 \pm 0.80$	$7.12 \pm 0.94$	$2.49 \pm 0.05$
WD 1659 + 440	3.05	$9.38 \pm 0.07$	$1.41 \pm 0.04$	$2.86 \pm 0.11$	$1.33 \pm 0.01$	$2.70 \pm 0.21$	$2.95 \pm 0.14$	$2.44 \pm 0.02$
EUVE J1535 – 77.4	5.80	$9.14 \pm 0.07$	$1.30 \pm 0.11$	$3.54 \pm 0.39$	$1.32 \pm 0.03$	$3.55 \pm 0.79$	$7.26 \pm 0.95$	$2.49 \pm 0.05$

Columns 2-5: Massive white dwarfs observed, with their respective effective temperatures and gravity on their surfaces. Columns 6–9: Mass, radius, central temperature and  $\alpha$  parameter for  $M_{\text{H}} = 10^{-4}M_{\odot}$  and  $M_{\text{He}} = 10^{-2}M_{\odot}$  derived by using our numerical results. The mass, radius, and central temperature are obtained by a fitting in the effective temperature and gravity for  $M_{\text{H}} = 10^{-4}M_{\odot}$  and  $M_{\text{He}} = 10^{-2}M_{\odot}$ .

**Reference.** (VENNES *et al.*, 1997).

$M_{\text{He}} = 10^{-2}$  and  $M_{\text{H}} = 10^{-4}$ . The results in mass and radius are very similar to the ones found in (VENNES *et al.*, 1997), except for WD 0346 – 011. This is due to the effects of general relativity being more remarkable at large total masses. For the stars in Table 5.3, we find  $\alpha = 2.54 \pm 0.02$ . This very similar to the one reported in (KOESTER, 1976) and used by (BOSHKAYEV *et al.*, 2016), i.e.,  $\alpha = 2.56$ . The central temperatures reported in this table are lower than the ones reported in Table 5.2, due to the photons' luminosity, which increases with the hydrogen contribution. In Tables 5.2 and 5.3, we find that all massive observable white dwarfs have masses below  $M \leq 1.35M_{\odot}$ . In the cooling process, these stars would not run from stable to unstable regions. On the contrary, they are likely to cool in the common white dwarf evolutionary track.

In Figure 5.6 we show the mass as a function of radius for some temperatures. The dashed curves are the same ones obtained in Figure 5.5 considering a TOV relativistic equation. The continuous curves are obtained using the Newtonian formulation (CARVALHO *et al.*, 2018a). The green points represent the source WD 1659 + 440 with a helium envelope and the pink ones represents WD 0346 – –011 with a helium and hydrogen envelope. The unfilled points are obtained according to (VENNES *et al.*, 1997) and the filled ones are obtained with our fitting.

From Fig. 5.6, as obtained in (CARVALHO *et al.*, 2018a) for cold white dwarfs, at the range of maximum white dwarf masses, for a fixed central temperature  $T_c \neq 0$ , we obtain smaller masses at the general relativity scope than in the Newtonian formulations. In addition, when the central temperature is increased, the total mass stays closer to the white dwarfs of WD 1659 + 440 and WD 0346 – –011 masses. On the other hand, at a fixed total mass, we find a smaller total radius in the relativistic case than in the classical one.

We propose an equation that relates mass and gravity values according to the central temperature. For such an equation, we fit the curves in Fig. 5.5 in Fourier second-order equations to obtain the relation

$$M(g) = \frac{k_0 \left[ \log \left( \frac{g}{g_{\odot}} \right) \right]^2 + k_1 \left[ \log \left( \frac{g}{g_{\odot}} \right) \right] + k_2}{\log \left( \frac{g}{g_{\odot}} \right) + k_3}, \quad (5.23)$$

where  $g_{\odot}$  is the Sun's surface gravity;  $k_0$ ,  $k_1$ , and  $k_2$  are parameters in solar masses  $M_{\odot}$ ; and  $k_3$  is a dimensionless constant. This relation is valid for surface gravity values  $\log \left( \frac{g}{g_{\odot}} \right) \geq 4.4$ . The fits implemented have a R – square = 1. As shown in Table 5.4, the parameters  $k_0$ ,  $k_1$ ,  $k_2$ , and  $k_3$  depend on the central temperature  $T_c$ . For different  $T_c$  than those ones reported in Table 5.4, new numerical values for the parameters from Eq. (5.23) can be obtained by interpolating the curves  $M(g)$  from Fig. 5.5.

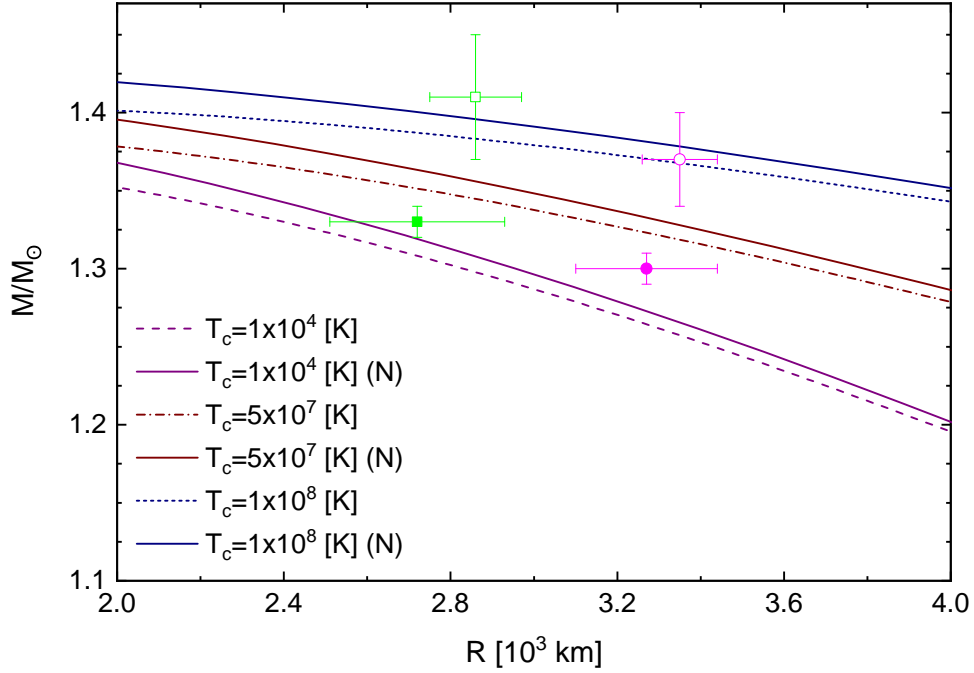


FIGURE 5.6 – The mass against the total radius for some temperatures according to general relativity (solid lines) and Newtonian formulations (full lines). The green points represent WD 1659 + 440 with a helium envelope and the pink ones represent WD 0346 – 011 with a helium and hydrogen envelope. The unfilled points are obtained according to (VENNES *et al.*, 1997) and the filled ones are obtained with our fitting.

TABLE 5.4 – Central temperatures and the parameter values appearing in Eq. (5.23).

$T_c$ (K)	Parameters			
	$k_0$ ( $M_\odot$ )	$k_1$ ( $M_\odot$ )	$k_2$ ( $10M_\odot$ )	$k_3$
$1.0 \times 10^6$	-0.355	5.400	-1.442	-2.187
$1.0 \times 10^7$	-0.347	5.293	-1.402	-2.162
$5.0 \times 10^7$	-0.333	5.076	-1.277	-1.845
$1.0 \times 10^8$	-0.324	4.894	-1.137	-1.414

## 5.5.4 Stability of hot white dwarfs

### 5.5.4.1 Stability of hot white dwarfs against small radial perturbations

The very massive white dwarfs reported in (VENNES *et al.*, 1997) have masses in the range of instabilities caused by radial oscillations, inverse  $\beta$ -decay, and pycnonuclear reactions. This, with their central temperatures that reach very high values, near  $10^8$  [K], made us realize the importance of investigating the stability of hot white dwarfs.

The behavior of the eigenfrequency squared with the central energy density  $\omega^2(\varepsilon_c)$  and with the total mass  $\omega^2(M/M_\odot)$  is plotted on the top and bottom panels of Fig. 5.7, respectively, for some central temperatures. All curves  $\omega^2(\varepsilon_c)$  and  $\omega^2(M/M_\odot)$  show Gaussian behavior, where the heights of the curves' peaks are, respectively, found in the

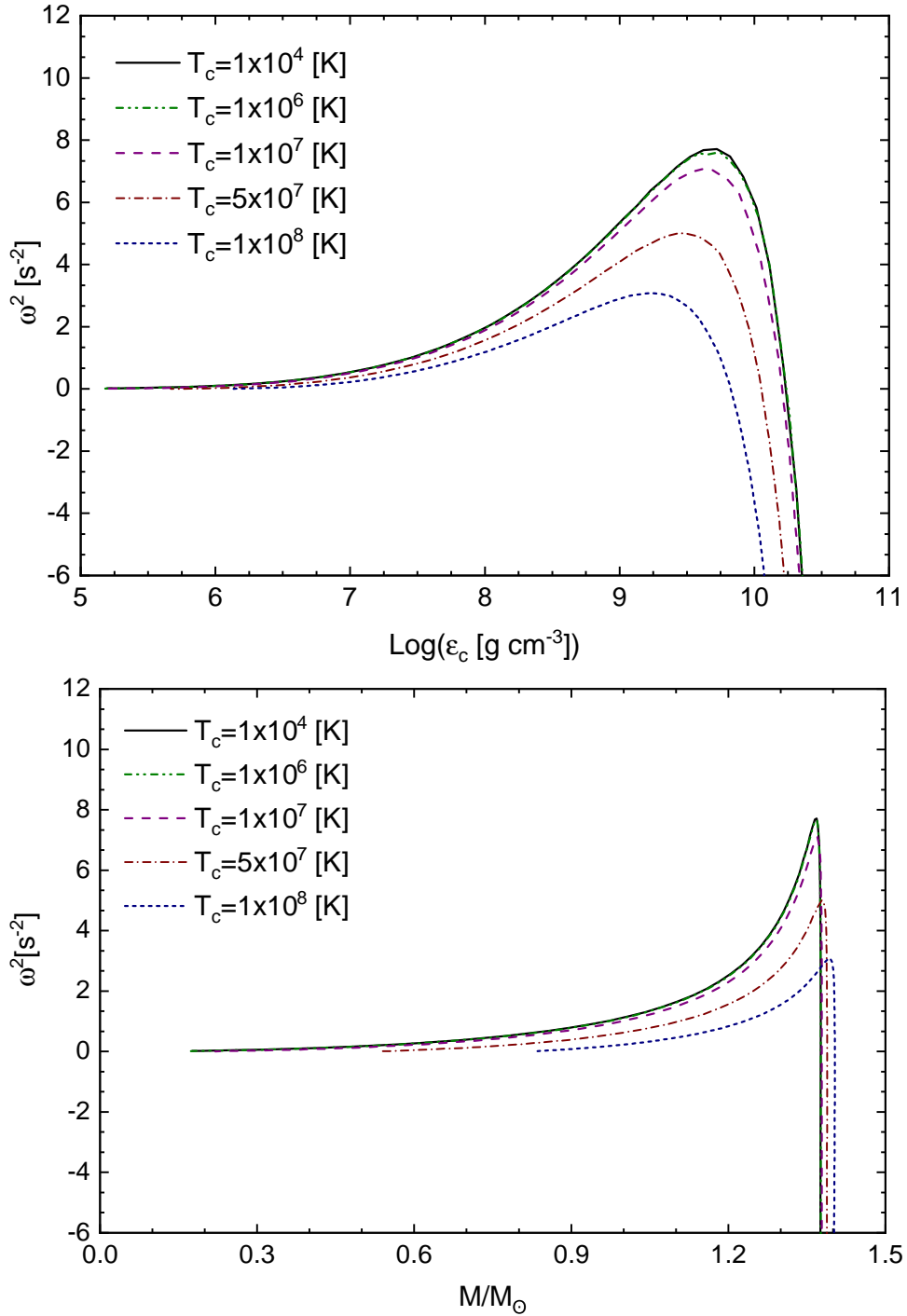


FIGURE 5.7 – Square of eigenfrequency  $\omega^2$  as a function of the central energy  $\varepsilon_c$  and of the total mass are shown on the panels on top and bottom, respectively, for some central temperatures.

range of central energy densities  $1.0 \times 10^8 \lesssim \varepsilon_c \lesssim 5.0 \times 10^{10} [\text{g cm}^{-3}]$  and total masses  $1.20 \lesssim M/M_\odot \lesssim 1.40$ . From the curves  $\omega(M/M_\odot)$ , it can be seen that the points of maximum mass are reached at  $\omega^2 = 0$ . In addition, it is important to say that the curve  $\omega^2(\varepsilon_c)$  derived for  $T_c \leq 10^6 [\text{K}]$  are similar to the ones reported by (WHEELER *et al.*, 1968) and (CHANMUGAM, 1977).

TABLE 5.5 – Threshold energy density values for instability against pycnonuclear reactions, inverse  $\beta$ -decay, and radial oscillations for some central temperature values.

$T$ $10^7(\text{K})$	$\varepsilon_{pyc}^*$ $10^{10}(\text{g cm}^{-3})$	$\varepsilon_{\beta}^*$ $10^{10}(\text{g cm}^{-3})$	$\varepsilon_{\omega}^*$ $10^{10}(\text{g cm}^{-3})$
0.1	0.878	3.515	1.744
1.0	0.878	3.515	1.622
5.0	0.876	3.515	1.118
10	0.874	3.515	0.675

The influence of temperature on the radial stability can also be observed in Fig. 5.7. In both panels of the figure, it can be noted that the increment of  $T_c$  decreases the squared eigenfrequency of the fundamental mode; this indicates that hotter white dwarfs will have lower stability. In fact, in our fitting for the stars reported in Tables 5.2 and 5.3 we also calculate their fundamental eigenfrequency. For white dwarfs composed of  $M_{\text{He}} = 10^{-4}M_{\odot}$  we found  $2.5 \leq \omega^2 \leq 4.4$  [ $\text{rad}^2 \text{s}^{-2}$ ] and for those ones made up of  $M_{\text{H}} = 10^{-4}M_{\odot}$  and  $M_{\text{He}} = 10^{-2}M_{\odot}$ , we find  $2.8 \leq \omega^2 \leq 4.6$  [ $\text{rad}^2 \text{s}^{-2}$ ]. Furthermore, most of the observable white dwarfs reported in previous studies (VENNES *et al.*, 1997; MADEJ *et al.*, 2004; NALEŻYTY; MADEJ, 2004; TREMBLAY *et al.*, 2011; KOESTER; KEPLER, 2019), i.e., white dwarfs with masses within  $0.3 \leq M/M_{\odot} \leq 1.3$ , have an eigenfrequency of oscillation in the interval  $0 < \omega^2 \leq 4.5$  [ $\text{rad}^2 \text{s}^{-2}$ ].

#### 5.5.4.2 Stability of hot white dwarfs against pycnonuclear reactions and inverse $\beta$ -decay

Recently, Otoniel and collaborators in (OTONIEL *et al.*, 2019) discussed the observation that the threshold central energy density, at which pycnonuclear reactions occur, is obtained by taking into account  $\tau_{\text{pyc}} = 10$  [Gyr]. In our model, at zero temperature, pycnonuclear reactions occur at the threshold density of  $9.56 \times 10^9$  [ $\text{g cm}^{-3}$ ], being a very close value to the one derived in (OTONIEL *et al.*, 2019). In contrast to that for pycnonuclear reactions, the threshold of central density for inverse  $\beta$ -decay instabilities is  $3.52 \times 10^{10}$  [ $\text{g cm}^{-3}$ ], close to the ones derived in (ROTONDO *et al.*, 2011; OTONIEL *et al.*, 2019).

The behavior of the total mass with the central energy density, at large total masses, is shown in Fig. 5.8 for some central temperatures. In the figure, we present the thresholds where instabilities occur against pycnonuclear reactions and inverse  $\beta$ -decay, in the gray shaded regions, and the places where the radial instability begins, marked by pink filled triangles.

Table 5.5 shows the threshold energy density values for instability against pycnonuclear reactions, inverse  $\beta$ -decay, and radial oscillations for four central temperature values.

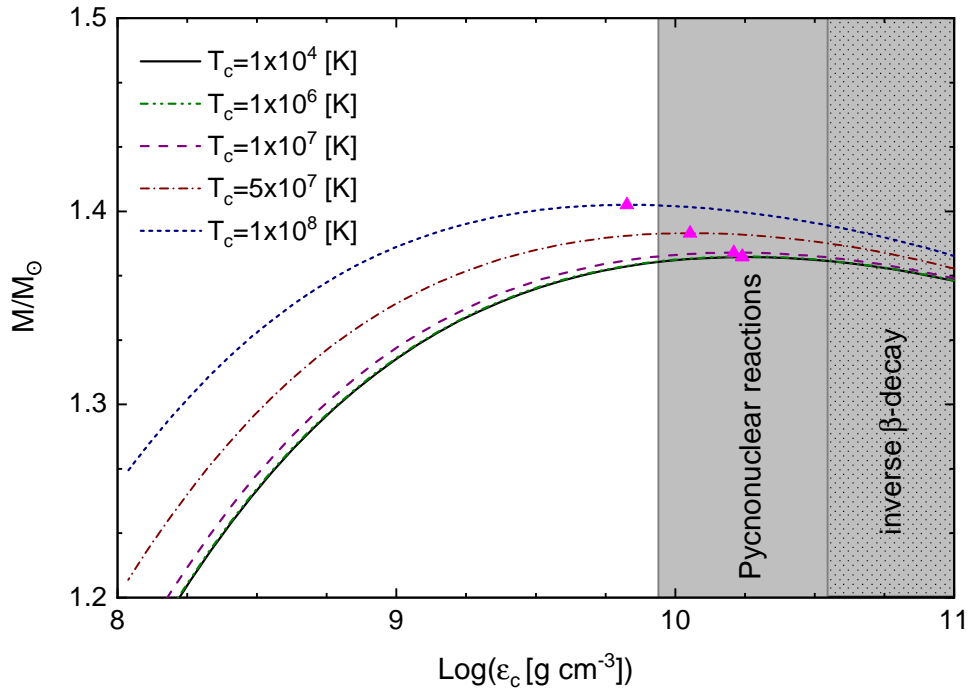


FIGURE 5.8 – Total mass against the central energy density for some central temperatures. The gray shaded regions indicate the places where the instabilities against pycnonuclear reactions and inverse  $\beta$ -decay take place, and the filled triangles in pink mark the onset of the radial instability.

From the results, we can note that the increase of temperature more remarkably affects stability against small radial perturbations. Moreover, for central temperature higher than  $1 \times 10^8$  [K], the radial stability is attained before the ones produced by pycnonuclear reactions and inverse  $\beta$ -decay.

# 6 Charge-Polarized Matter in Hot DQ White Dwarfs as a Possible Source of type Ia Supernovae

This chapter is an article in final revision to be submitted to a journal of astrophysics.

The super-Chandrasekhar mass white dwarfs (WDs) have been predicted as progenitors of super-luminous type Ia supernovae (SN Ia) (2003fg (HOWELL, 2006), 2009dc (TAUBENBERGER, 2011), 2006gz (HICKEN, 2007), and 2007if (SCALZO, 2010)). With the intent to justify the WDs increasing mass, there are some mechanisms to be associated. As an example, two white dwarfs merger (double degenerate scenario (WHELAN; IBEN ICKO, 1973; NOMOTO, 1982)) or an accreting material from a companion (single degenerate scenario (HOWELL, 2006; IBEN I.; TUTUKOV, 1984; WEBBINK, 1984)). Albeit these scenarios are commonly accepted, there are other mechanisms to increase the WD matter. Inspired in Schmidt and collaborators observational discovery (SCHMIDT, 2003), some authors associate the magnetic field (DAS; MUKHOPADHYAY, 2012; CHAMEL *et al.*, 2013; DAS *et al.*, 2013; DAS; MUKHOPADHYAY, 2014; FRANZON; SCHRAMM, 2015; OTONIEL *et al.*, 2019) as the responsible to the star's mass increase. This consideration makes authors to reach stars' masses values that can be more than  $\approx 3M_{\odot}$  (DAS; MUKHOPADHYAY, 2014). Alternatively, authors (BOSHKAYEV *et al.*, 2014; FRANZON; SCHRAMM, 2015; BERA; BHATTACHARYA, 2016; BECERRA *et al.*, 2018; BECERRA *et al.*, 2019) obtained values up to  $5M_{\odot}$  including very fast spin rotation in the calculations.

The super-Chandrasekhar white dwarfs have also been obtained as a consequence of strong electric fields presented in the star interior . Regarding the interstellar fluid of a white dwarf as nucleons and free electrons in a degenerate state, Liu and collaborators (LIU *et al.*, 2014) following (ROSSELAND, 1924) investigated charged white dwarfs as a possible source of super-luminous Type Ia Supernovae. The authors in this work considered the hydrostatic equilibrium using the Newtonian framework to describe the star structure and analyzed general relativity effects. The charge density was assumed to be proportional to the mass density in the entire star. They found that the mass of charged

white dwarfs increases when a strong electric field exists in the star interior, explaining the superluminous Type Ia supernovae explosions that seems to be originated from white dwarfs with masses above the Chandrasekhar limit. . They conclude that only a very strong electric field in the white dwarf can produce intrinsic observable effects in the star structure. It is important to mention that the charge density pointed by Liu is widely used in works considering a polytrope equation of state (RAY *et al.*, 2003; RAY *et al.*, 2004; ARBAÑIL *et al.*, 2013; AZAM; MARDAN, 2017; ARBAÑIL; ZANCHIN, 2018), anisotropic stars (MAURYA; GOVENDER, 2017), and in incompressible matter (ANNINOS; ROTHMAN, 2002; ARBAÑIL *et al.*, 2014; FELICE *et al.*, 1995; FELICE *et al.*, 1999; LEMOS *et al.*, 2015).

In a recent work, Carvalho, Arbañil, Marinho, and Malheiro (CARVALHO *et al.*, 2018a) implemented another charge density for cold white dwarfs. In this work, they follow the stellar fluid described in (LIU *et al.*, 2014) and a surface charge density already used in a charged strange star (NEGREIROS *et al.*, 2009). This model of a white dwarf, the conductor was never been proposed. Since very massive white dwarfs were the goal of this investigation, the authors used general relativity to describe stellar structure. As a consequence, they obtained larger and more massive white dwarfs with appreciate effects when the charge is at thpresente order of  $10^{20}[C]$ , with an electric field of  $10^{16}[V/cm]$ , below the Schwinger limit where the field has the energy to create an electron-positron pair that will neutralize the star charge. The maximum mass obtained in this work is around  $2M_{\odot}$ .

The prior studies of charged white dwarfs consider high charges to produce considerable effects in stellar structure. These charges, as a consequence, yield a high electric field outside the star. Under these conditions, a capture of negative particles could be responsible to create a dipole in the star's surface. Alternatively, when considering a white dwarf with temperature, in the non-degenerate envelope the binding energy is smaller compared to complete degenerate white dwarfs. This could cause, in the presence of a small rotation, the positive particles to be small displaced from electrons. In this circumstance, a dipole also is formed on the stellar surface. In this work, inspired in the charged strange star model in (NEGREIROS *et al.*, 2010), we propose a novel charge distribution that ensures a mass increasing in the white dwarfs remaining no electric field outside the star. We solve the Maxwell-Einstein equations by considering the stellar fluid composed of nucleons, electrons and photons (TIMMES; ARNETT, 1999; NUNES *et al.*, 2021). Due to the high central temperature, the lattice interaction is not necessary. We also investigate the instabilities due to pycnonuclear reactions and inverse  $\beta$ -decay in hot white dwarfs following the limits in (NUNES *et al.*, 2021). Finally, we suppose very small rotation periods, near the Kepler frequency of star break up, to investigate the maximum magnitude of an external stellar magnetic field in such configurations.

This article is organized as follows: In section 6.1 the equation of state (EoS) and the

charge distribution are described. Section 6.2 presents the stellar equilibrium equations for charged configurations, the boundary conditions, and the numerical technique we use. In section 6.3 we present the results. Finally, we conclude in section 7. Throughout this article is considered the units  $c = 1 = G$ , where  $c$  and  $G$  represent the speed of light and the gravitational constant.

## 6.1 The equation of state

The stellar fluid inside a white dwarf is widely investigated as composed of nucleons and electrons. This consideration, for low temperatures has to consider the electron-ion interaction (see, e.g., (CARVALHO *et al.*, 2014; OTONIEL *et al.*, 2019)). The consideration of these interactions due to crystallization depends on a property called Coulomb coupling parameter (GARCÍA-BERRO; OSWALT, 2016)

$$\Gamma = Z^{5/3}\Gamma_e, \tag{6.1}$$

where

$$\Gamma_e = \frac{e^2}{a_e k_B T}, \tag{6.2}$$

being  $Z$  the atomic number,  $e$  the electron charge,  $a_e$  the inter-electronic distance  $k_B$  the Boltzmann constant and  $T$  the temperature. The crystallization of a white dwarf is settled when  $\Gamma_e \approx 179$  (GARCÍA-BERRO; OSWALT, 2016). For carbon white dwarfs with temperatures of  $10^8$ [K], this occur for densities above  $\approx 10^{11}$ [g/cm<sup>3</sup>]. Therefore, we are neglecting lattice interactions in this work. The pressure and energy density of the interstellar fluid is described following (TIMMES; ARNETT, 1999; NUNES *et al.*, 2021)

$$P = P_n + P_e + P_\gamma, \tag{6.3}$$

$$\varepsilon = \varepsilon_n + \varepsilon_e + \varepsilon_\gamma, \tag{6.4}$$

being the subindex  $n$ ,  $e$ ,  $\gamma$  represent nucleons, electrons and photons contributions. Regarding the white dwarfs' temperature, the stellar interior is an isothermal core with constant temperature and a non-degenerate envelope, which has a temperature distribution due to the luminosity. In this work we follow the temperature-density relation used in (NUNES *et al.*, 2021).

## 6.2 Equilibrium Configuration

For the space-time remaining spherically symmetric the electric charge profile we considered needs to depend only on the radial coordinate. Thus, we can still use Schwarzschild-like coordinates, given as

$$ds^2 = e^\nu dt^2 - e^\lambda dr^2 - r^2 d\theta^2 - r^2 \sin^2 \theta d\phi^2, \quad (6.5)$$

being  $\nu$ , and  $\lambda$  only dependent on  $r$ . The inclusion of the electromagnetic tensor in the stress-momentum tensor leads to the Maxwell-Einstein equations that describe the stellar exterior structure (BEKENSTEIN, 1971)

$$\frac{dm}{dr} = 4\pi\varepsilon r^2 + \frac{q}{r} \frac{dq}{dr}, \quad (6.6)$$

$$\frac{dP}{dr} = -(P + \varepsilon) \left[ 4\pi r P + \frac{m}{r^2} - \frac{q^2}{r^3} \right] e^\lambda + \frac{q}{4\pi r^4} \frac{dq}{dr}, \quad (6.7)$$

$$\frac{d\nu}{dr} = -\frac{2}{(P + \varepsilon)} \left[ \frac{dP}{dr} - \frac{q}{4\pi r^4} \frac{dq}{dr} \right], \quad (6.8)$$

being  $q$  the local charge, and  $m$  the star mass inside a sphere of radius  $r$ . Besides, we approximate  $dq/dr \approx \delta q/\delta r$ . The metric function  $e^\lambda$  which is the solution of the Einstein equation for the charged star interior is

$$e^\lambda = \left[ 1 - \frac{2m}{r} + \frac{q^2}{r^2} \right]^{-1}. \quad (6.9)$$

### 6.2.1 The electric charge density

To obtain small electric fields outside the star, we follow (NEGREIROS *et al.*, 2009) to describe a charge-polarized matter in the white dwarf surface. Since electrons have a small mass comparing to protons, they tend to go far from the atomic nucleus that now are not in a lattice due to the high star temperature, and in the star surface this can create a polarized matter. As a result, there are two charges situated at the stellar envelope ( $R^+ \leq r \leq R$ ): a positive one at  $r = R^+$  due to the electrons deficiency and a negative one at  $r = R^- = R^+ + \Delta R$ , where they are accumulating. In Fig. 6.1 we illustrate the distances  $R^+$ ,  $R^-$ , and  $R$ . The polarization in the stellar envelope has to consider some aspects to ensure the global neutrality. One of them is to consider the two charge densities with the same local charge  $Q$ , i.e.,  $q(R^+) = -q(R^-) = Q$ . In our numeric calculations, we assume  $\Delta R = 5$  [km] and  $\delta R = 0.1\Delta R$ . The charge is located as in a spherical capacitor

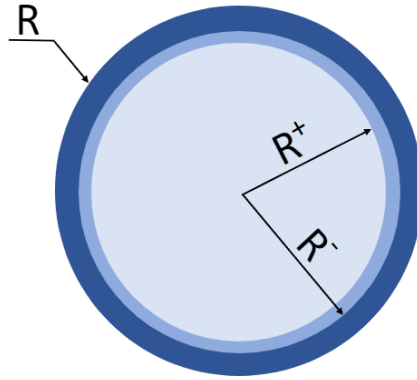


FIGURE 6.1 – A charge-polarized matter in a white dwarf star.

$$q(r) = \begin{cases} q(R^+) = -q(R^-) = Q, \\ 0, \end{cases} \quad \text{otherwise.} \quad (6.10)$$

We can obtain the electric field between the two charged shells using the Gauss's Law, and is given by

$$E(r) = \frac{Q}{r^2}, \quad (6.11)$$

where the conditions in Eq. 6.10 are satisfied. After  $R^-$  the electric field is zero and the white dwarf is globally neutral.

## 6.3 Equilibrium of charge-polarized matter in hot white dwarfs

### 6.3.1 Numerical method

In order to propose a structure which has the lattice dissolution, we propose a central temperature  $T_c = 10^8$ [K]. With this central temperature, the contributions from electrons in the EoS (Eqs. (6.3) and (6.4)) is found with integrals. We solve these integrals by using an adaptive quadrature method following (BOSHKAYEV *et al.*, 2016; NUNES *et al.*, 2021). Once these equations are solved, we begin the integration of Eqs. (6.6)-(6.8) using a fourth-order Runge-Kutta method for an uncharged star, (i.e.  $Q = 0$ ) considering as boundary conditions

$$m(0) = 0, \quad \varepsilon(0) = \varepsilon_0, \quad \text{and} \quad \nu(0) = \nu_0, \quad (6.12)$$

and the star surface is determined at  $P(r = R) = 0$ . The radius obtained for the uncharged integration is related to the positive radius as  $R(\rho_c) - 1$  [km] =  $R^+$ . Besides, for the

charged integration, we set the inputs

$$R^- = R^+ + \Delta R, \quad \text{and} \quad \Delta R = 10[\text{km}]. \quad (6.13)$$

## 6.4 Results

In Fig. 6.2, we show the electric field as a function of the radial coordinate for stars with  $\varepsilon_c = 5 \times 10^9 [\text{g}/\text{cm}^3]$  and charges  $Q = [0, 2, 3, 4, 5] \times 10^{19} [\text{C}]$ . Due to Gauss's Law, we can note that the electric field is zero for  $r < R^+$  and  $r \geq R^-$ . Besides, between  $R^+ \leq r \leq R^-$ , the electric field is expressed by the Eq. (6.11). We have to mention that the electric field increases with charge  $Q$ , and it is confined between  $R^+$  and  $R^-$  creating a spherical capacitor with a null electric field outside this region and, in particular, outside the star.

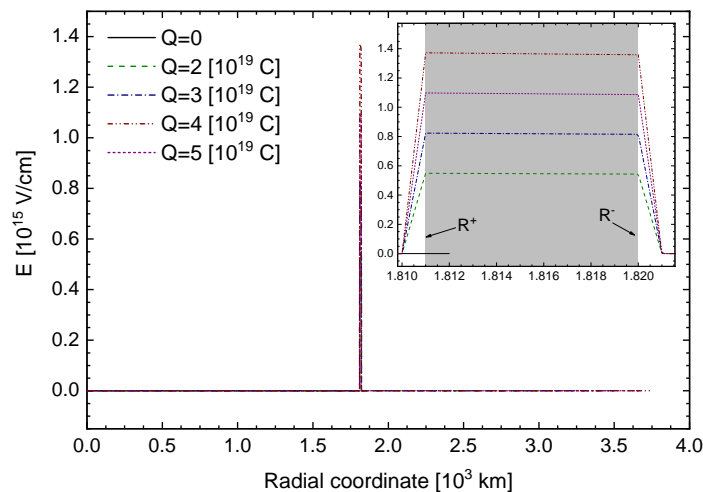


FIGURE 6.2 – The electric field as a function of radial coordinate for stars with  $\varepsilon_c = 5 \times 10^9 [\text{g}/\text{cm}^3]$  and several charges. The gray region represents the space between the two charges  $R^+$  and  $R^-$ .

We show the pressure as a function of the radial coordinate inside the star in Fig. 6.3. We can note that the pressure has a maximum value at the stellar center ( $r = 0$ ) and decays through its structure until the envelope. In the envelope, the charge-polarized matter at  $r = R^+$  increases abruptly the stellar pressure proportional to  $Q$ , in agreement with (CARVALHO *et al.*, 2018a) that also found this pressure behavior. Albeit we were expecting a different behavior for the pressure, due to the electric field confinement at  $R^+ \leq r < R^-$ , it does not influence the decay of the stellar pressure significantly.

In order to associate the charge due to the polarized matter of hot white dwarfs in the envelope with progenitors of type Ia Supernovae events, we show the mass as a function of the central energy density in Fig. 6.4. We restrict the interval for white dwarfs

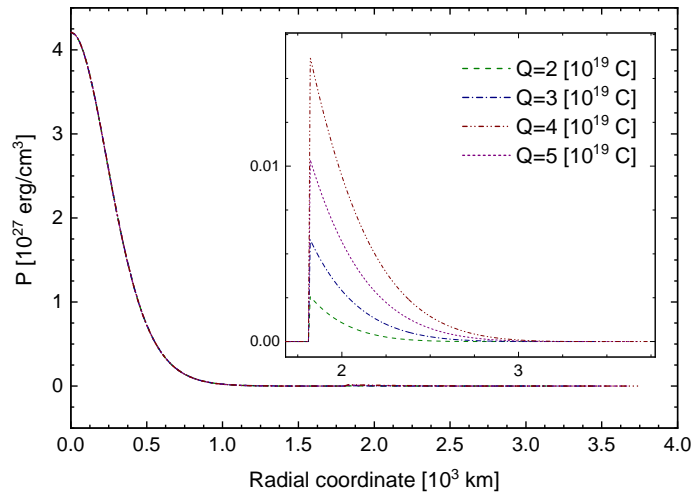


FIGURE 6.3 – The pressure as a function of radial coordinate for stars with  $\varepsilon_c = 5 \times 10^9$  [g/cm<sup>3</sup>] and several charges.

with central energy densities  $10^7 \leq \varepsilon_c \leq 10^{11}$  [g/cm<sup>3</sup>]. The mass increases with the central energy density to a maximum mass (pink triangles) and decays. We illustrate in this figure the threshold of density due to pycnonuclear reactions and inverse  $\beta$ -decay reported in (NUNES *et al.*, 2021). We can note that the increase in the charge makes the total mass increase and also it is corresponding central energy density as found also in (CARVALHO *et al.*, 2018b). In these charge-polarized matter stars, even for high central temperatures, the pycnonuclear reactions are the responsible for determining the threshold of instability, manifesting that the threshold density for these fusion reactions is almost independent of the temperature as expected. We highlight that due to the charge we implement, we obtain significant effects in the stellar structure for  $10^{19}$ [C] and no electric field outside the star.

We show the mass as a function of the radius in Fig. 6.5. We can note that the mass increases with the radius, reaching a maximum value (pink triangles) and after decreases. The radius for the maximum mass decrease with the increasing of the charge. This behavior shows that our model increases density, mass and radius proportionally, in contrast to (CARVALHO *et al.*, 2018a).

We can note that our curves are very similar to the ones obtained previously in (CARVALHO *et al.*, 2018a); the mass increases with mass, reaches a maximum value (pink triangles) and it decreases. Thus, we have significant effects for charge values of the order of  $10^{19}$ [C]. This value is smaller compared to the values found for different charge profile in white dwarfs (CARVALHO *et al.*, 2018a; LIU *et al.*, 2014), due to the two shells with opposite charges we used, and their positions. We report these values of maximum mass in the Table 6.1.

We present the values of radius and central energy density at the maximum mass

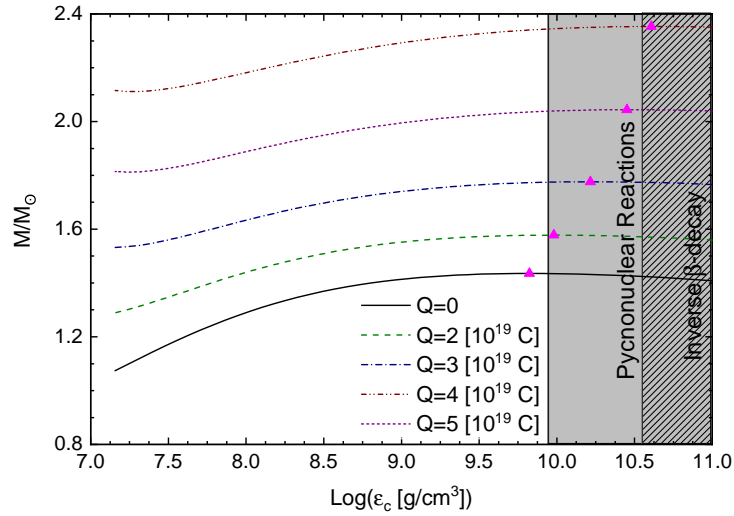


FIGURE 6.4 – Mass as a function of central energy density for several charges. The pink triangles represents the maximum mass.

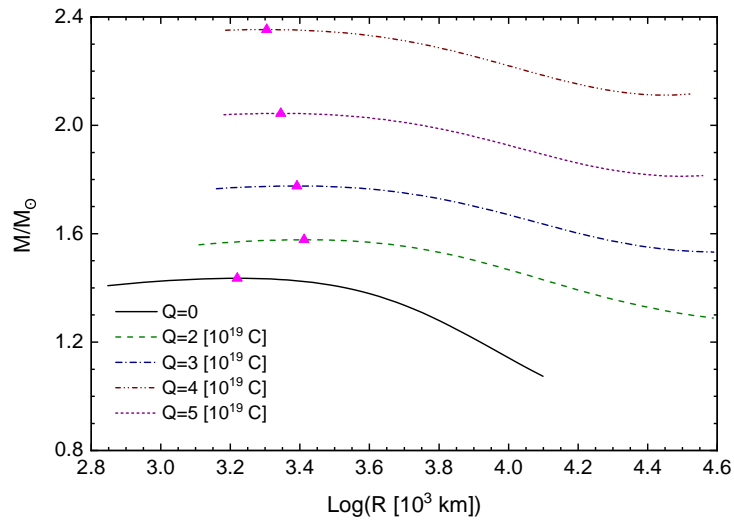


FIGURE 6.5 – Mass as a function of radius for several charges. The pink triangles represents the maximum mass.

in the Table 6.1. We can see the behavior we have mentioned before, that the mass increases with charge, accompanied by the radius and central energy density. Besides, it is important to mention a comparison between the results we find here and the reported in (NEGREIROS *et al.*, 2010). In our calculations, we find coherent results with the ones of Negreiros obtained for strange quark stars concerning the electrostatic mass contribution to the total star mass. This charge contribution for the star mass increase in our model, due to the weight and pressure of the charged-polarized matter, can become of the order of 63%, as seen in Fig. 6.5.

$Q [10^{19}C]$	0.00	2.00	3.00	4.00	5.00
$M^{\max}/M_{\odot}$	1.44	1.58	1.78	2.04	2.35
$\text{Log}(R [10^3\text{km}])$	3.22	3.41	3.39	3.34	3.30
$\varepsilon_c [10^9\text{g/cm}^3]$	0.66	0.95	1.64	2.82	4.05

TABLE 6.1 – The values of the maximum mass  $M^{\max}$  for radius and energy density for different values of a charge-polarized matter  $Q$ .

### 6.4.1 The magnetic field

In the last sections, we propose a static stellar configuration to calculate the electric field. Due to the global charge neutrality, it obeyed the charge stability limits. In this section, we suggest a small rotation in the star in order to analyze a possible magnetic field. Besides, this would clarify the limits to create the structures we propose.

The rotation in WDs distorts the star and creates a difference between equatorial and polar radius. The maximum frequency of rotation that the star could have before ejecting the mass and creates a rotational instability is the Keplerian frequency (BOSHKAYEV *et al.*, 2013)

$$\omega_{\text{Kep}} = \sqrt{\frac{M}{R^3}}. \quad (6.14)$$

Since we are going to consider sequences with constant axial rotation, we will use a fast rotational frequency of  $\omega = 2\pi\Omega \approx 1$  [rad Hz] to estimate the maximum external magnetic field generated by the electrical current due to the rotation of the two charged shells. It is worth mentioning that this rotation frequency, even higher for a white dwarf, is not sufficient to produce any considerable effects in the white dwarfs' structure (OTONIEL *et al.*, 2020). Therefore, the spherical symmetry is preserved.

In (NEGREIROS *et al.*, 2010), the magnetic field comes from the difference in velocity between the positive and the negative shells. We are going to consider this magnetic field only due to rotational effects of the two shell surface charge densities with opposite signs, and their different locations inside the star. The magnetic field at the star surface is a vectorial sum of the magnetic field due to the positive and negative shells. Following (NEGREIROS *et al.*, 2010), the dipole magnetic field at the star surface is

$$\vec{B} = \frac{1}{3}\mu_0 R^+ \omega \left( 2 \cos \theta \hat{r} + \sin \theta \hat{\theta} \right) \left[ \sigma^+ + \sigma^- \left( 1 + \frac{\Delta R}{R^+} \right) \right], \quad (6.15)$$

being  $\mu_0$  the magnetic permeability,  $\sigma^+$  and  $\sigma^-$  the positive and negative surface charge

distributions, respectively, and  $\omega$  the star angular frequency. The surface charges are

$$\sigma^+ = \frac{Q_0}{4\pi(R^+)^2}, \quad \sigma^- = -\frac{Q_0}{4\pi(R^-)^2}. \quad (6.16)$$

In Fig. 6.6, we show the magnetic field as a function of the total mass considering  $\omega = 1[\text{rad Hz}]$ . The red region in the curves represents the star instability region. We can note that the magnetic field increases with the mass, reaching a maximum value near  $\approx 10^8[\text{G}]$  for all the charge-polarized matter considered. We reached this since in Eq. (6.15) the magnetic field comes essentially from the different locations of the two charged shells inside the star. Due to our consideration of a possible magnetic fields in

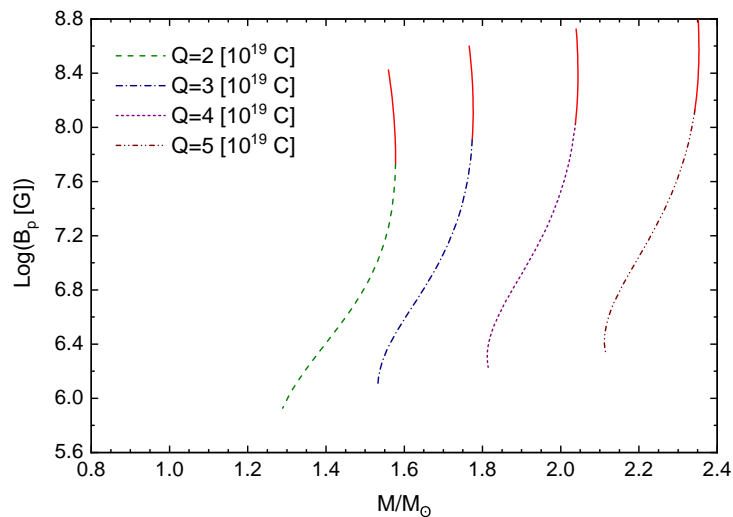


FIGURE 6.6 – Magnetic field as a function of mass for  $T_c = 10^8[\text{K}]$  and several charge-polarized matter. The red curves represents instabilities due to pycnonuclear reactions.

the star, the maximum magnetic field inside the star to guarantee dynamically stability is (COELHO *et al.*, 2014)

$$B_{\text{max}} = 2.24 \times 10^8 \frac{M}{M_\odot} \left( \frac{R_\odot}{R} \right)^2 [\text{G}], \quad (6.17)$$

for a massive white dwarf  $B \approx 10^{13}[\text{G}]$ . The values we find according to (6.15) even for a large rotational frequency of  $\omega = 1[\text{rad Hz}]$  are much smaller than the ones obtained by (6.17) (see Fig. 6.6). It is important to stress that the spin rotational frequencies of white dwarfs are usually much smaller,  $\omega \approx 10^{-4}[\text{Hz}]$  corresponding to periods of hours. Since from (6.15) the magnetic field is linear with the angular star frequency, we will expect - from these charge surface rotational effect - magnetic field more of the order of  $\approx 10^4[\text{G}]$  that are the usual surface fields observed at most white dwarfs. Therefore, the stars we are proposing can exist, even for a further collapse.

## 7 Conclusion

In this thesis, we first revisited the theory and observation of white dwarfs. In Chapter 2, we presented the white dwarfs' properties; revisiting their evolution, classification, history, and observations. In chapter 3 we described the equation of state we used in the entire work, deducing each term. In the chapter 4, we derived the Newtonian star hydrostatic equilibrium equation. Also in this chapter, we deduced the Tolman-Oppenheimer-Volkoff equations and the modifications with Maxwell-Einstein equations for charged stars. Besides, we also elucidate how to find the star instabilities due to pycnonuclear reaction, inverse  $\beta$ -decay and radial oscillations.

In the chapter 5, the static equilibrium configuration and stability against small radial perturbations, pycnonuclear reactions, and inverse  $\beta$ -decay in white dwarfs with a finite temperature are studied. Following previous studies (TOLMAN, 1939; TIMMES; ARNETT, 1999; ROTONDO *et al.*, 2011), with respect to the matter within white dwarfs, we take into account that it is made up nucleons and electrons confined in a Wigner-Seitz cell surrounded by free photons. Moreover, with the purpose of obtaining a null radiation pressure at the star's surface, a temperature distribution is considered in the nondegenerate envelope. We assume both that temperature dependence on the mass density and the existence of an isothermal degenerate core. The static configurations under analysis have spherical symmetry and are connected smoothly with the Schwarzschild exterior space-time. The hydrostatic configuration and stability are investigated for different central energy densities  $\varepsilon_c$  and central temperatures  $T_c$ .

We find that the necessary central temperature to influence the static structure and radial stability of very massive white dwarfs is approximately  $T_c = 10^7$  [K]. For a fixed central energy density, we find that white dwarfs' radius and total mass grow with the increase of the central temperature (for  $T_c > 10^7$  [K]). The temperature effects in the static equilibrium configurations are in concordance with the ones obtained in the study of white dwarfs with a finite temperature reported in (CARVALHO *et al.*, 2014) for low-mass white dwarfs but are different from the ones obtained in (BOSHKAYEV *et al.*, 2016) for the very massive ones.

For some massive white dwarfs, we derive the mass and radius by fitting both gravity

and effective temperature reported by the observation. This is done by assuming some white dwarfs are composed of  $M_{\text{He}} = 10^{-4}M_{\odot}$ , and other ones are made up of  $M_{\text{H}} = 10^{-4}M_{\odot}$  and  $M_{\text{He}} = 10^{-2}M_{\odot}$ . The results show that some white dwarfs could have central temperatures above  $5 \times 10^7$ [K]. Besides, from our results, we note that masses and radii are in the same range as those of the white dwarfs reported in (VENNES *et al.*, 1997), with the exception of EUVE J0003 + 43.6 and WD 1659 + 440. For these two stars, we find masses below the ones reported in (VENNES *et al.*, 1997). This is associated with the relativistic effects on these two massive stars. Furthermore, considering general relativity effects, we derive an equation that facilitates finding mass values from surface gravity and effective temperature values for observable massive white dwarfs with surface gravity  $\log\left(\frac{g}{g_{\odot}}\right) \geq 4.4$ .

We have conducted a novel study concerning the stability of white dwarfs with a finite temperature. For a central energy density interval, we find that the radial stability of the white dwarfs diminishes with the increment of the central temperature. Moreover, we also derived that the maximum mass and the zero eigenfrequencies of oscillation are attained at the same central energy density. This indicates that in a system of equilibrium star configurations at finite temperature, the regions formed by stable and unstable white dwarfs can be recognized by the inequalities  $dM/d\varepsilon_c > 0$  and  $dM/d\varepsilon_c < 0$ , respectively.

On the other hand, unlike the threshold energy density of instability for inverse  $\beta$ -decay, which does not change with temperature, the energy density threshold of instability for pycnonuclear fusion reactions show a small reduction when temperature in the stellar interior is present. Besides, for central temperatures higher than  $1 \times 10^8$  [K], we determine that instability due to small radial perturbations occurs before those produced by pycnonuclear reactions and inverse  $\beta$ -decay.

In the chapter 6, we presented for the first time super-Chandrasekhar charged white dwarfs with a null electric field outside (respecting global charge neutrality). To obtain these structures, we considered spherically charge-polarized matter in the envelope of white dwarfs solving the Einstein-Maxwell equations. We employed an equation of state following (TIMMES; ARNETT, 1999; NUNES *et al.*, 2021) to consider nucleons, electrons and photons contributions disregarding lattice interactions due to the high central temperature (GARCÍA-BERRO; OSWALT, 2016). In what concerns the stellar temperature, we considered a degenerate core and a temperature distribution in the stellar envelope, which depends on the density (NUNES *et al.*, 2021).

Inspired by (NEGREIROS *et al.*, 2010), we introduced a charge distribution for stellar interior by setting conditions, which allowed us to achieve global neutral white dwarfs. With the charge and the equation of state settle, we solved the hydrostatic equilibrium equation for charge stars. As a result, we found that for a certain central energy density, the increasing of charge in the stellar surface increases its mass and radius. In fact, we

obtained white dwarfs masses up to  $2.4M_{\odot}$  with a corresponding charge  $Q = 5 \times 10^{19}[\text{K}]$ . This very massive white dwarf, in particular, can have a maximum magnetic field at the order of  $10^8$  [G] when subjected to a very fast rotational angular frequency of  $\omega = 1$  [rad Hz].

Beyond the hydrostatic equilibrium, we analyzed the instabilities in the charged stars. Considering pycnonuclear reactions and inverse  $\beta$ -decay with temperature contributions (NUNES *et al.*, 2021), we found the threshold density for these reactions to settle in the star core creating instabilities. By considering radial oscillations coinciding to turning-point for stars sequences with a fixed charge, together with pycnonuclear reactions, we found the maximum star masses for white dwarfs with a charged-polarized matter in their envelope. Besides, as we estimated the magnetic field originated by the electrical current due to the rotation of the two charged shell, we compared our values with the maximum surface magnetic field allowed by the dynamical stability condition (COELHO *et al.*, 2014). We have to mention that this article is still in progress. Additionally, we may mention that the situation we are proposing may be a pre-collapse configuration.

In this work evolution, we have come across with some future perspectives. One of them is to investigate completely the influence of the charge-polarized matter with rotation using LORENE code. We also aim to investigate the cooling process of Chandrasekhar mass white dwarf to study possible collapses. Besides, we aim to include rotation in hot white dwarfs with realistic envelopes to start the comparison between observations and the theory of very fast, isolated, magnetic, and massive white dwarfs originated from white dwarf mergers, something recently started in (OTONIEL *et al.*, 2020).

# Bibliography

ALTHAUS, L. G.; CÓRSICO, A. H.; ISERN, J.; GARCÍA-BERRO, E. Evolutionary and pulsational properties of white dwarf stars. **Astron Astrophys Rev**, v. 18, n. 4, p. 471–566, out. 2010.

ALTHAUS, L. G.; Serenelli, A. M.; Panei, J. A.; Córscico, A. H.; García-Berro, E.; Scóccola, C. G. The formation and evolution of hydrogen-deficient post-AGB white dwarfs: The emerging chemical profile and the expectations for the PG 1159-DB-DQ evolutionary connection. **A&A**, v. 435, n. 2, p. 631–648, maio 2005.

ANNINOS, P.; ROTHMAN, T. Instability of extremal relativistic charged spheres. **Phys. Rev. D**, v. 65, n. 2, p. 024003, jan. 2002.

ARBAÑIL, J. D. V.; LEMOS, J. P. S.; ZANCHIN, V. T. Polytropic spheres with electric charge: Compact stars, the Oppenheimer-Volkoff and Buchdahl limits, and quasiblack holes. **Phys. Rev. D**, v. 88, n. 8, p. 084023, out. 2013.

ARBAÑIL, J. D. V.; LEMOS, J. P. S.; ZANCHIN, V. T. Incompressible relativistic spheres: Electrically charged stars, compactness bounds, and quasiblack hole configurations. **Phys. Rev. D**, v. 89, n. 10, p. 104054, maio 2014.

ARBAÑIL, J. D. V.; MALHEIRO, M. Equilibrium and stability of charged strange quark stars. **Phys. Rev. D**, v. 92, n. 8, p. 084009, out. 2015.

ARBAÑIL, J. D. V.; ZANCHIN, V. T. Relativistic polytropic spheres with electric charge: Compact stars, compactness and mass bounds, and quasiblack hole configurations. **Phys. Rev. D**, v. 97, n. 10, p. 104045, maio 2018.

AULUCK, F. C.; MATHUR, V. S. Electrostatic interactions in white Dwarfs. With 2 figures in the text. **Zeitschrift für Astrophysik**, v. 48, p. 28, jan. 1959.

AZAM, M.; MARDAN, S. A. Cracking of charged polytropes with generalized polytropic equation of state. **European Physical Journal C**, v. 77, n. 2, p. 113, fev. 2017.

BAGLIN, A. Dynamical instability of white dwarfs in the general relativity frame work. **Annales d’Astrophysique**, v. 29, p. 103, fev. 1966.

BALBERG, S.; SHAPIRO, S. L. The Properties of Matter in White Dwarfs and Neutron Stars. **arXiv e-prints**, p. astro-ph/0004317, abr. 2000.

BARON, E. SNe Ia: Can Chandrasekhar mass explosions reproduce the observed zoo? **Nuclear Physics A**, v. 928, p. 319–330, ago. 2014.

- BECERRA, L.; BOSHKAYEV, K.; RUEDA, J. A.; RUFFINI, R. Time evolution of rotating and magnetized white dwarf stars. **Mon. Not. R. Astr. Soc.**, v. 487, n. 1, p. 812–818, jul. 2019.
- BECERRA, L.; RUEDA, J. A.; LORÉN-AGUILAR, P.; E., G.-B. The Spin Evolution of Fast-rotating, Magnetized Super-Chandrasekhar White Dwarfs in the Aftermath of White Dwarf Mergers. **Astrophys. J.**, v. 857, n. 2, p. 134, abr. 2018.
- BEKENSTEIN, J. D. Hydrostatic Equilibrium and Gravitational Collapse of Relativistic Charged Fluid Balls. **Phys. Rev. D**, v. 4, n. 8, p. 2185–2190, out. 1971.
- BERA, P.; BHATTACHARYA, D. Mass-radius relation of strongly magnetized white dwarfs: dependence on field geometry, GR effects and electrostatic corrections to the EOS. **Mon. Not. R. Astr. Soc.**, v. 456, n. 3, p. 3375–3385, mar. 2016.
- BERGERON, P.; SAFFER, R. A.; LIEBERT, J. A Spectroscopic Determination of the Mass Distribution of DA White Dwarfs. **Astrophys. J.**, v. 394, p. 228, jul. 1992.
- BERTONE, G.; RUFFINI, R. Equilibrium configurations of relativistic white dwarfs. **Nuovo Cimento B Serie**, v. 115, n. 70809, p. 935, jul. 2000.
- BETHE, H. A. Energy Production in Stars. **Physical Review**, v. 55, n. 5, p. 434–456, mar. 1939.
- BETHE, H. A.; CRITCHFIELD, C. L. The Formation of Deuterons by Proton Combination. **Physical Review**, v. 54, n. 4, p. 248–254, ago. 1938.
- BETHE, H. A.; MARSHAK, R. E. The physics of stellar interiors and stellar evolution. **Reports on Progress in Physics**, v. 6, n. 1, p. 1–15, jan. 1939.
- BISNOVATYI-KOGAN, G. S. The Critical Mass of a Hot Isothermal White Dwarf with General Relativistic Effects Taken into Account. **Soviet Astronomy**, v. 10, p. 69, ago. 1966.
- BÖHM, K.-H. Outer Convection Zones and Internal Temperatures of Cool White Dwarfs. **Astrophysics and Space Science**, v. 2, n. 3, p. 375–383, nov. 1968.
- BÖHM, K. H. Pressure Ionization in White-Dwarf Convection Zones. **Astrophys. J.**, v. 162, p. 919, dez. 1970.
- BOSHKAYEV, K.; RUEDA, J. A.; RUFFINI, R.; SIUTSOU, I. On General Relativistic Uniformly Rotating White Dwarfs. **Astrophys. J.**, v. 762, n. 2, p. 117, jan. 2013.
- BOSHKAYEV, K.; RUEDA, J. A.; RUFFINI, R.; SIUTSOU, I. General relativistic white dwarfs and their astrophysical implications. **Journal of Korean Physical Society**, v. 65, n. 6, p. 855–860, set. 2014.
- BOSHKAYEV, K. A.; RUEDA, J. A.; ZHAMI, B. A.; KALYMOVA, Z. A.; BALGYMBEKOV, G. S. Equilibrium structure of white dwarfs at finite temperatures. In: **International Journal of Modern Physics Conference Series**. [S.l.: s.n.], 2016. (International Journal of Modern Physics Conference Series, v. 41), p. 1660129.

- CAMENZIND, M. **Compact Objects in Astrophysics - White Dwarfs, Neutron Stars and Black Holes**. 1. ed. [S.l.]: Springer, 2007. (Astronomy and Astrophysics Library, v. 1). ISBN 0792307798.
- CARROLL, S. **Spacetime and geometry: an introduction to General Relativity**. [S.l.]: Benjamin Cummings, 2004. ISBN 0805387323,9780805387322.
- CARVALHO, G. A.; ARBAÑIL, J. D. V.; MARINHO, R. M.; MALHEIRO, M. White dwarfs with a surface electrical charge distribution: equilibrium and stability. **European Physical Journal C**, v. 78, n. 5, p. 411, maio 2018.
- CARVALHO, G. A.; MARINHO, R. M.; MALHEIRO, M. General relativistic effects in the structure of massive white dwarfs. **General Relativity and Gravitation**, v. 50, n. 4, p. 38, abr. 2018.
- CARVALHO, S. M. de; ROTONDO, M.; RUEDA, J. A.; RUFFINI, R. Relativistic Feynman-Metropolis-Teller treatment at finite temperatures. **Phys. Rev. C**, v. 89, n. 1, p. 015801, jan. 2014.
- CHAMEL, N.; FANTINA, A. F.; DAVIS, P. J. Stability of super-Chandrasekhar magnetic white dwarfs. **Phys. Rev. D**, v. 88, n. 8, p. 081301, out. 2013.
- CHAMEL, N.; MOLTER, E.; FANTINA, A. F.; ARTEAGA, D. P. n. Maximum strength of the magnetic field in the core of the most massive white dwarfs. **Phys. Rev. D**, v. 90, n. 4, p. 043002, ago. 2014.
- CHANDRASEKHAR, S. **An introduction to the study of stellar structure**. [S.l.: s.n.], 1931.
- CHANDRASEKHAR, S. The Maximum Mass of Ideal White Dwarfs. **Astrophys. J.**, v. 74, p. 81, jul. 1931.
- CHANDRASEKHAR, S. The highly collapsed configurations of a stellar mass (Second paper). **Mon. Not. R. Astr. Soc.**, v. 95, p. 207–225, jan. 1935.
- CHANDRASEKHAR, S. Dynamical Instability of Gaseous Masses Approaching the Schwarzschild Limit in General Relativity. **Phys. Rev. Lett.**, v. 12, n. 4, p. 114–116, jan. 1964.
- CHANDRASEKHAR, S. The Dynamical Instability of Gaseous Masses Approaching the Schwarzschild Limit in General Relativity. **Astrophys. J.**, v. 140, p. 417, ago. 1964.
- CHANMUGAM, G. Radial oscillations of zero-temperature white dwarfs and neutron stars below nuclear densities. **Astrophys. J.**, v. 217, p. 799–808, nov. 1977.
- CHUGUNOV, A. I.; DEWITT, H. E.; YAKOVLEV, D. G. Coulomb tunneling for fusion reactions in dense matter: Path integral MonteCarlo versus mean field. **Phys. Rev. D**, v. 76, n. 2, p. 025028, jul. 2007.
- COELHO, J. G.; MARINHO, R. M.; MALHEIRO, M.; NEGREIROS, R.; CÁ CERES, D. L.; RUEDA, J. A.; RUFFINI, R. Dynamical Instability of White Dwarfs and Breaking of Spherical Symmetry Under the Presence of Extreme Magnetic Fields. **Astrophys. J.**, v. 794, n. 1, p. 86, out. 2014.

- DAS, U.; MUKHOPADHYAY, B. Strongly magnetized cold degenerate electron gas: Mass-radius relation of the magnetized white dwarf. **Phys. Rev. D**, v. 86, n. 4, p. 042001, ago. 2012.
- DAS, U.; MUKHOPADHYAY, B. Maximum mass of stable magnetized highly super-Chandrasekhar white dwarfs: stable solutions with varying magnetic fields. **JCAP**, v. 2014, n. 6, p. 050, jun. 2014.
- DAS, U.; MUKHOPADHYAY, B.; RAO, A. R. A Possible Evolutionary Scenario of Highly Magnetized Super-Chandrasekhar White Dwarfs: Progenitors of Peculiar Type Ia Supernovae. **Astrophys. J. Letters**, v. 767, n. 1, p. L14, abr. 2013.
- D'INVERNO, R. **Introducing Einstein's relativity**. 1. ed. [S.l.]: Clarendon Press; Oxford University Press, 1992. ISBN 0198596537,9780198596530,0198596863.
- DIRAC, P. A. M. On the theory of quantum mechanics. **Proceeding of Royal Society A: Mathematical, Physical and Engineering Sciences**, v. 112, p. 661, 1926.
- DUFOUR, P.; FONTAINE, G.; LIEBERT, J.; Schmidt, G. D.; Behara, N. Hot DQ White Dwarfs: Something Different. **Astrophys. J.**, v. 683, n. 2, p. 978–989, ago. 2008.
- DUFOUR, P.; LIEBERT, J.; FONTAINE, G.; BEHARA, N. White dwarf stars with carbon atmospheres. **Nature**, v. 450, n. 7169, p. 522–524, nov. 2007.
- FELICE, F. de; SIMING, L.; YUNQIANG, Y. Relativistic charged spheres: II. Regularity and stability. **Classical and Quantum Gravity**, v. 16, n. 8, p. 2669–2680, ago. 1999.
- FELICE, F. de; YU, Y.; FANG, J. Relativistic charged spheres. **Mon. Not. R. Astr. Soc.**, v. 277, n. 1, p. L17–L19, nov. 1995.
- FERMI, E. Zur quantelung des idealen einatomigen gases. **Zeitschrift Für Physik**, v. 36, p. 11, 1926.
- FEYNMAN, R. P.; METROPOLIS, N.; TELLER, E. Equations of State of Elements Based on the Generalized Fermi-Thomas Theory. **Physical Review**, v. 75, n. 10, p. 1561–1573, maio 1949.
- FONTAINE, G.; HORN, H. M. V. Convective white-dwarf envelope model grids for H-, He- and C-rich compositions. **Astrophysical Journal, Suppl. Ser.**, v. 31, p. 467, jul. 1976.
- FRANZON, B.; SCHRAMM, S. Effects of strong magnetic fields and rotation on white dwarf structure. **Phys. Rev. D**, v. 92, n. 8, p. 083006, out. 2015.
- GAMOW, G. Physical Possibilities of Stellar Evolution. **Physical Review**, v. 55, n. 8, p. 718–725, abr. 1939.
- GARCÍA-BERRO, E.; OSWALT, T. D. The white dwarf luminosity function. **New Astronomy Reviews**, v. 72, p. 1–22, jun. 2016.
- GASQUES, L. R.; AFANASJEV, A. V.; AGUILERA, E. F.; BEARD, M.; CHAMON, L. C.; RING, P.; WIESCHER, M.; YAKOVLEV, D. G. Nuclear fusion in dense matter: Reaction rate and carbon burning. **Phys. Rev. C**, v. 72, n. 2, p. 025806, ago. 2005.

- GLENDENNING, N. K. **Compact stars**. 2ed.. ed. [S.l.]: Springer, 2000. (Astronomy and Astrophysics Library). ISBN 9780387989778,0387989773.
- HAMADA, T.; SALPETER, E. E. Models for Zero-Temperature Stars. **Astrophys. J.**, v. 134, p. 683, nov. 1961.
- HAN, Z.; PODSIADLOWSKI, P. The single-degenerate channel for the progenitors of Type Ia supernovae. **Mon. Not. R. Astr. Soc.**, v. 350, n. 4, p. 1301–1309, jun. 2004.
- HICKEN, M. i. The Luminous and Carbon-rich Supernova 2006gz: A Double Degenerate Merger? **Astrophys. J. Letters**, v. 669, n. 1, p. L17–L20, nov. 2007.
- HILLEBRANDT, W.; NIEMEYER, J. C. Type IA Supernova Explosion Models. **Ann. Rev. Astron. Astrophys.**, v. 38, p. 191–230, jan. 2000.
- HORN, H. M. V. Convection in envelopes of white dwarfs. **Astrophysical Journal**, v. 160, p. L53, apr 1970.
- HORVATH, J. **Fundamentos da evolução estelar, supernovas e objetos compactos**. 1. ed. [S.l.]: Editora Livraria da Física, 2011. ISBN 978-85-7861-109-5.
- HOWELL, D. i. The type Ia supernova SNLS-03D3bb from a super-Chandrasekhar-mass white dwarf star. **Nature**, v. 443, n. 7109, p. 308–311, set. 2006.
- HOYNG, P. **Relativistic astrophysics and cosmology: a primer**. 1. ed. [S.l.]: Springer, 2006. (Astronomy and astrophysics library). ISBN 9781402045219,1-4020-4521-2.
- HUBBARD, W. B.; WAGNER, R. L. Hot White Dwarfs. **Astrophys. J.**, v. 159, p. 93, jan. 1970.
- IBEN I., J.; TUTUKOV, A. V. Supernovae of type I as end products of the evolution of binaries with components of moderate initial mass. **Astrophysical Journal, Suppl. Ser.**, v. 54, p. 335–372, fev. 1984.
- KAWALER, S. D.; NOVIKOV, I.; SRINIVASAN, G.; MEYNET, G.; SCHAEERER, D. **Stellar Remnants**. [S.l.: s.n.], 1996.
- KOESTER, D. Outer Envelopes and Cooling of White Dwarfs. **A&A**, v. 16, p. 459, fev. 1972.
- KOESTER, D. Convective Mixing and Accretion in White Dwarfs. **A&A**, v. 52, p. 415, nov. 1976.
- KOESTER, D.; CHANMUGAM, G. REVIEW: Physics of white dwarf stars. **Reports on Progress in Physics**, v. 53, n. 7, p. 837–915, jul. 1990.
- KOESTER, D.; KEPLER, S. O. Carbon-rich (DQ) white dwarfs in the Sloan Digital Sky Survey. **A&A**, v. 628, p. A102, ago. 2019.
- KRITCHER, A. L. i. A measurement of the equation of state of carbon envelopes of white dwarfs. **Nature**, v. 584, n. 7819, p. 51–54, ago. 2020.
- LAI, D.; SHAPIRO, S. L. Cold Equation of State in a Strong Magnetic Field: Effects of Inverse beta -Decay. **Astrophys. J.**, v. 383, p. 745, dez. 1991.

- LANG, K. R. **Essential Astrophysics**. 1. ed. [S.l.]: Springer Heidelberg New York Dordrecht London, 2013. ISBN 10.1007/978-3-642-35963-7.
- LEMOS, J. P. S.; LOPES, F. J.; Quinta, G.; ZANCHIN, V. T. Compact stars with a small electric charge: the limiting radius to mass relation and the maximum mass for incompressible matter. **European Physical Journal C**, v. 75, p. 76, fev. 2015.
- LIU, H.; ZHANG, X.; WEN, D. One possible solution of peculiar type Ia supernovae explosions caused by a charged white dwarf. **Phys. Rev. D**, v. 89, n. 10, p. 104043, maio 2014.
- LIU, Z.-W.; PAKMOR, R.; SEITENZAHL, I. R.; HILLEBRANDT, W.; KROMER, M.; RÖPKE, F. K.; EDELMANN, P.; TAUBENBERGER, S.; MAEDA, K.; WANG, B.; HAN, Z. W. The Impact of Type Ia Supernova Explosions on Helium Companions in the Chandrasekhar-mass Explosion Scenario. **Astrophys. J.**, v. 774, n. 1, p. 37, set. 2013.
- MACDONALD, J. **Structure and Evolution of Single Stars: An introduction**. 2. ed. [S.l.]: Morgan Claypool Publishers, 2015. ISBN 9781681741697,1681741695.
- MACIEL, W. J. **Introduction to Stellar Structure**. 1. ed. [S.l.]: Springer International Publishing, 2016. (Springer Praxis Books). ISBN 978-3-319-16141-9,978-3-319-16142-6.
- MADEJ, J.; NALEŻYTY, M.; ALTHAUS, L. G. Mass distribution of DA white dwarfs in the First Data Release of the Sloan Digital Sky Survey. **A&A**, v. 419, p. L5–L8, maio 2004.
- MARSHAK, R. E. The Internal Temperature of White Dwarf Stars. **Astrophys. J.**, v. 92, p. 321, nov. 1940.
- MATHEW, A.; NANDY, M. K. General relativistic calculations for white dwarfs. **Research in Astronomy and Astrophysics**, v. 17, n. 6, p. 061, maio 2017.
- MAURYA, S. K.; GOVENDER, M. A family of charged compact objects with anisotropic pressure. **European Physical Journal C**, v. 77, n. 6, p. 420, jun. 2017.
- MELTZER, D. W.; THORNE, K. S. Normal Modes of Radial Pulsation of Stars at the End Point of Thermonuclear Evolution. **Astrophys. J.**, v. 145, p. 514, ago. 1966.
- MESTEL, L.; RUDERMAN, M. A. The energy content of a white dwarf and its rate of cooling. **Mon. Not. R. astr. Soc.**, v. 136, p. 27, Jan 1967.
- MONTGOMERY, M. H.; KLUMPE, E. W.; WINGET, D. E.; WOOD, M. A. Evolutionary Calculations of Phase Separation in Crystallizing White Dwarf Stars. **Astrophys. J.**, v. 525, n. 1, p. 482–491, nov. 1999.
- NALEŻYTY, M.; MADEJ, J. A catalogue of isolated massive white dwarfs. Mass distribution of massive star. **A&A**, v. 420, p. 507–513, jun. 2004.
- NEGREIROS, R. P.; MISHUSTIN, I. N.; Schramm, S.; Weber, F. Properties of bare strange stars associated with surface electric fields. **Phys. Rev. D**, v. 82, n. 10, p. 103010, nov. 2010.
- NEGREIROS, R. P.; WEBER, F.; MALHEIRO, M.; USOV, V. Electrically charged strange quark stars. **Phys. Rev. D**, v. 80, n. 8, p. 083006, out. 2009.

- NIEMEYER, J. C.; WOOSLEY, S. E. The Thermonuclear Explosion of Chandrasekhar Mass White Dwarfs. **Astrophys. J.**, v. 475, n. 2, p. 740–753, fev. 1997.
- NOMOTO, K. Accreting white dwarf models for type I supernovae. I - Presupernova evolution and triggering mechanisms. **Astrophys. J.**, v. 253, p. 798–810, fev. 1982.
- NUNES, S. P.; ARBAÑIL, J. D. V.; MALHEIRO, M. The Structure and Stability of Massive Hot White Dwarfs. **Astrophys. J.**, v. 921, n. 2, p. 138, nov. 2021.
- OPPENHEIMER, J. R.; VOLKOFF, G. M. On Massive Neutron Cores. **Physical Review**, v. 55, n. 4, p. 374–381, fev. 1939.
- OSTRIKER, J. P.; HARTWICK, F. D. A. Rapidly Rotating Stars.IV. Magnetic White Dwarfs. **Astrophys. J.**, v. 153, p. 797, set. 1968.
- OTONIEL, E.; COELHO, J. G.; NUNES, S. P.; MALHEIRO, M.; WEBER, F. Mass limits of the extremely fast-spinning white dwarf CTCV J2056-3014. **arXiv e-prints**, p. arXiv:2010.12441, out. 2020.
- OTONIEL, E.; FRANZON, B.; CARVALHO, G. A.; MALHEIRO, M.; SCHRAMM, S.; WEBER, F. Strongly Magnetized White Dwarfs and Their Instability Due to Nuclear Processes. **Astrophys. J.**, v. 879, n. 1, p. 46, jul. 2019.
- POTEKHIN, A. Y.; CHABRIER, G. Equation of state of fully ionized electron-ion plasmas. II. Extension to relativistic densities and to the solid phase. **Phys. Rev. E Stat. Phys. Plasmas Fluids Relat. Interdiscip. Topics**, v. 62, n. 6, p. 8554–8563, dez. 2000.
- RAY, S.; ESPÍNDOLA, A. L.; MALHEIRO, M.; LEMOS, J. P.; ZANCHIN, V. T. Electrically charged compact stars and formation of charged black holes. **Phys. Rev. D**, v. 68, n. 8, p. 084004, out. 2003.
- RAY, S.; MALHEIRO, M.; LEMOS, J. P. S.; ZANCHIN, V. T. Charged Polytropic Compact Stars. **Brazilian Journal of Physics**, v. 34, p. 310–314, mar. 2004.
- ROSE, W. K. **Advanced Stellar Astrophysics**. 1. ed. [S.l.]: Cambridge University Press, 1998. ISBN 0521581885,9780521581882.
- ROSSELAND, S. Electrical state of a star. **Mon. Not. R. Astr. Soc.**, v. 84, p. 720–728, jun. 1924.
- ROTONDO, M.; RUEDA, J. A.; RUFFINI, R.; XUE, S.-S. Relativistic Feynman-Metropolis-Teller theory for white dwarfs in general relativity. **Phys. Rev. D**, v. 84, n. 8, p. 084007, out. 2011.
- RUFFINI, R. J. On the Critical Mass: the Case of White Dwarfs. In: **Exploring the Universe**. [S.l.: s.n.], 2000. p. 373–382.
- SALPETER, E. E. Energy and Pressure of a Zero-Temperature Plasma. **Astrophys. J.**, v. 134, p. 669, nov. 1961.
- SALPETER, E. E.; HORN, H. M. van. Nuclear Reaction Rates at High Densities. **Astrophys. J.**, v. 155, p. 183, jan. 1969.

- SCALZO, R. A. i. Nearby Supernova Factory Observations of SN 2007if: First Total Mass Measurement of a Super-Chandrasekhar-Mass Progenitor. **Astrophys. J.**, v. 713, n. 2, p. 1073–1094, abr. 2010.
- SCHATZMAN, E. Le spectre des naines blanches et leur debit d'energie. **Publikationer og mindre Meddelelser fra Kobenhavns Observatorium**, v. 149, p. 1–100, jan. 1950.
- SCHMIDT, G. D. i. Magnetic White Dwarfs from the Sloan Digital Sky Survey: The First Data Release. **Astrophys. J.**, v. 595, n. 2, p. 1101–1113, out. 2003.
- SHAPIRO, S. L.; TEUKOLSKY, S. A. **Black Holes, White Dwarfs, and Neutron Stars - The Physics of Compact Objects**. 2. ed. [S.l.]: Wiley-VCH, 2004. ISBN 9783527617661.
- SION, E. M. Hot white dwarfs. In: **White Dwarf Atmospheres and Circumstellar Environments**. Pasadena, USA: John Wiley Sons, Ltd, 2011. v. 1, cap. 1, p. 1–23. ISBN 9783527636570.
- SOMMERFELD, A. Zur Elektronentheorie der Metalle auf Grund der Fermischen Statistik. **Zeitschrift fur Physik**, v. 47, n. 1-2, p. 1–32, jan. 1928.
- SON, S.; FISCH, N. Pycnonuclear reaction and possible chain reactions in an ultra-dense dt plasma. **Physics Letters A**, v. 337, n. 4, p. 397–407, 2005. ISSN 0375-9601. Disponível em: <<https://www.sciencedirect.com/science/article/pii/S0375960105002331>>.
- TAUBENBERGER, S. i. High luminosity, slow ejecta and persistent carbon lines: SN 2009dc challenges thermonuclear explosion scenarios. **Mon. Not. R. Astr. Soc.**, v. 412, n. 4, p. 2735–2762, abr. 2011.
- TIMMES, F. X.; ARNETT, D. The Accuracy, Consistency, and Speed of Five Equations of State for Stellar Hydrodynamics. **Astrophysical Journal, Suppl. Ser.**, v. 125, n. 1, p. 277–294, nov. 1999.
- TOLMAN, R. C. Static Solutions of Einstein's Field Equations for Spheres of Fluid. **Physical Review**, v. 55, n. 4, p. 364–373, fev. 1939.
- TREMBLAY, P. E.; BERGERON, P.; GIANNINAS, A. An Improved Spectroscopic Analysis of DA White Dwarfs from the Sloan Digital Sky Survey Data Release 4. **Astrophys. J.**, v. 730, n. 2, p. 128, abr. 2011.
- TREMBLAY, P.-E. e. a. Core crystallization and pile-up in the cooling sequence of evolving white dwarfs. **Nature**, v. 564, p. 202–205, jan. 2019.
- VAVRUKH, M. V.; SMERECHYNSKYI, S. V. A finite temperature Chandrasekhar model: Determining the parameters and calculation of the characteristics of Degenerate Dwarfs. **Astrophys. J.**, v. 125, p. 277, nov. 2012.
- VENNES, S.; THEJLL, P. A.; GALVAN, R. G.; DUPUIS, J. Hot White Dwarfs in the Extreme Ultraviolet Explorer Survey. II. Mass Distribution, Space Density, and Population Age. **Astrophys. J.**, v. 480, n. 2, p. 714–734, maio 1997.
- WEBBINK, R. F. Double white dwarfs as progenitors of R Coronae Borealis stars and type I supernovae. **Astrophys. J.**, v. 277, p. 355–360, fev. 1984.

WEBER, F. **Pulsars as Astrophysical Laboratories for Nuclear and Particle Physics (Series in High Energy Physics, Cosmology and Gravitation)**. 1st. ed. [S.l.]: Taylor Francis, 1999. ISBN 0750303328,9780750303323.

WEIDEMANN, V.; KOESTER, D. The upper mass limit for white dwarf progenitors and the initial-final mass relation for low and intermediate mass stars. **A&A**, v. 121, p. 77–84, maio 1983.

WHEELER, J. C.; HANSEN, C. J.; COX, J. P. General Relativistic Instability in White Dwarfs. **Astrophysical Letters**, v. 2, p. 253, jan. 1968.

WHELAN, J.; IBEN ICKO, J. Binaries and Supernovae of Type I. **Astrophys. J.**, v. 186, p. 1007–1014, dez. 1973.

WOOD, M. A. Theoretical white dwarf luminosity functions: Da models. In: **Proceedings of the 9th European Workshop on White Dwarfs Held at Kiel**. [S.l.]: Lecture Notes in Physics, 1995. v. 443, p. 41.

YAKOVLEV, D. G.; LEVENFISH, K. P.; GNEDIN, O. Y. Pycnonuclear reactions in dense stellar matter. **European Physical Journal A Supplement**, v. 25, n. 1, p. 669–672, set. 2005.

## FOLHA DE REGISTRO DO DOCUMENTO

1. CLASSIFICAÇÃO/TIPO <p style="text-align: center;">TD</p>	2. DATA <p style="text-align: center;">25 de janeiro de 2022</p>	3. REGISTRO N° <p style="text-align: center;">DCTA/ITA/TD-037/2021</p>	4. N° DE PÁGINAS <p style="text-align: center;">94</p>
5. TÍTULO E SUBTÍTULO:  The structure and stability of massive hot white dwarfs: comparisons with observational data and charge-polarized matter effects			
6. AUTOR(ES):  <b>Sílvia Pereira Nunes</b>			
7. INSTITUIÇÃO(ÕES)/ÓRGÃO(S) INTERNO(S)/DIVISÃO(ÕES):  Instituto Tecnológico de Aeronáutica – ITA			
8. PALAVRAS-CHAVE SUGERIDAS PELO AUTOR:  Compact stars; White dwarfs; Astrophysics.			
9. PALAVRAS-CHAVE RESULTANTES DE INDEXAÇÃO:  Estrelas anãs; Campos magnéticos; Equações de estado; Densidade de energia; Relatividade; Astrofísica; Física nuclear.			
10. APRESENTAÇÃO: <span style="float: right;"><input checked="" type="checkbox"/> Nacional    <input type="checkbox"/> Internacional</span>  ITA, São José dos Campos. Curso de Doutorado. Programa de Pós-Graduação em Física. Área de Física Nuclear. Orientador: Prof. Dr. Manuel Máximo Bastos Malheiro de Oliveira; coorientador: Prof. Dr. José Domingo Arbañil Vela. Defesa em 08/12/2021. Publicada em 2021.			
11. RESUMO:  In this work, we analyze the structure and stability of white dwarfs at finite temperature, making comparisons with observational data and analyzing the insertion of a an electric charge due to a polarization of the matter on their envelopes. Regarding the stellar fluid, we define it as being a composition of electrons and nucleons in a Wigner-Seitz cell, as well as free photons. Because a hot degenerate lump with conductive transport forms these white dwarfs, the temperature is approximately constant in this region. In the non-degenerate envelope, however, there is energy transport due to convection and radiation, which creates a temperature distribution. As we only considered massive white dwarfs in all analyses, the determination of this envelope does not change the structure of the star (although it is necessary to guarantee hydrostatic balance). Using the Tolman-Oppenheimer-Volkoff (TOV) equations, we numerically obtain the structure of hot white dwarfs. Through some observational stars present in the Sloan Digital Sky Survey and Extreme Ultraviolet Sky Survey catalogs, we observed that some of them had masses and radii compatible with very high core temperature curves. We then fit the observational surface gravity and effective temperature data to find the core mass, radius and temperature of these stars. We find that due to general relativity, these stars with very high surface gravity have smaller masses and radii than those previously reported. In order to improve the next estimates of the mass and radius of these stars, we obtain an equation for these quantities as a function of the effective temperature and surface gravity. We also analyzed the stability of very massive hot white dwarfs by pycnonuclear reactions, $\beta$ -inverse and radial oscillations. We obtain that white dwarfs with core temperature from $10^8$ [K] have their stability analyzed according to radial oscillations. Additionally, we also study a possible electric charge due to a polarized matter in the envelope of hot white dwarfs. We investigate this polarization by introducing conditions to the charge location, which ensures a global charge neutralization. By analyzing extreme cases, we consider that the core temperature would be in the order of $10^8$ [K], in which lattice interaction effects can be neglected. We solve the Maxwell-Einstein equations obtaining bigger and more massive stars (masses of approximately $2.4M_{\odot}$ for polarized charge of $Q=1.5 \times 10^{19}$ [C]). When analyzing these stars stability, we found that pycnonuclear reactions may be use to settle a limit for the star central density. Considering effects due to the star rotation we found maximum magnetic fields of the order of $10^8$ [G]. For the first time we provide white dwarf structures with masses beyond the Chandrasekhar limit, with zero external electric field.			
12. GRAU DE SIGILO:  <p style="text-align: center;"><input checked="" type="checkbox"/> OSTENSIVO                      <input type="checkbox"/> RESERVADO                      <input type="checkbox"/> SECRETO</p>			